Studies on the mechanical properties and phase behaviour of lipid bilayers in the presence of some alcohols and oxysterols

by

Buti Suryabrahmam

A thesis submitted to
the Jawaharlal Nehru University for the degree of
Doctor of Philosophy

2021

Raman Research Institute
Banglore 560 080
India

DECLARATION

I hereby declare that this thesis is composed independently by me at Raman Research Institute, Bangalore under the supervision of Prof. Pramod Pullarkat and Prof. V. A. Raghunathan. The subject matter presented in this thesis has not previously formed the basis of the award of any degree, diploma, associateship, fellowship or any other similar title. I also declare that I have run it through the **Turnitin** plagiarism software.

Signature of the Student

(Buti Suryabrahmam)

Signature of the Supervisor

(Prof. Pramod Pullarkat)
Raman Research Institute
Bangalore 560080

Signature of the Co-supervisor

(Prof.V.A.Raghunathan)
Raman Research Institute
Bangalore 560080

CERTIFICATE

This is to certify that the thesis entitled **" Studies on the mechanical properties and phase behaviour of lipid bilayers in the presence of some alcohols and oxysterols "** submitted by Buti Suryabrahmam for the award of degree DOCTOR OF PHILOSOPHY of Jawaharlal Nehru University is his original work. This has not been published or submitted to any other university for any other degree or diploma.

Signature of the Supervisor

(Prof. Pramod Pullarkat)
Raman Research Institute
Bangalore 560080

Signature of the Co-supervisor

(Prof.V.A.Raghunathan)
Raman Research Institute
Bangalore 560080

Signature of the Director

(Prof. S. Sridhar)
Director
Raman Research Institute
Bangalore 560080

Acknowledgements

It was a pleasure working with Prof. V. A. Raghunathan. His support was immense, at every step, from giving projects to writing papers and thesis. He gave me freedom and let me take my own time to learn and do experiments. Every discussion with him taught me something new. I was always amazed by his personality.

My sincere thanks to Prof. Pramod Pullarkat for his support and discussions. Whenever I was struck with some experimental protocol issues, his suggestions showed me the way. I would like to thank my thesis advisory committee members Prof. Yashodhan Hatwalne, Prof. Arun Roy and Prof. Sadiq Rangwala, for their valuable suggestions to keep my thesis work on track. I am extremely thankful to Prof. Sandeep Kumar, Prof. Ranjini Bandyopadhyay, Prof. Prathibha, Prof. Gautam Soni for letting me use their instruments and for their support. During my initial years in LAMP, I have learned a lot from Late Prof. Hema Ramachandran, Prof. Sadiq Rangwala, Prof. Andal Narayanan, Prof. Reji Philip, and Prof. Urbasi Sinha. Thanks to them.
I would like to thank Vasudha, Mani, Dhasan, Yatheendran, and Serene for their timely support in setting up and conducting experiments.
I am grateful to have a lab mate like Ayush. Thanks for his support with experiments and discussions. He was always ready to help me professionally and personally. Thanks to Sreeja Sesidaran for all her help, support and discussions. She was a very helpful lab mate. I have learned protocols of x-ray scattering experiments from her. I have also learned a lot through discussions with my lab mates Shabeeb, Madhukar, Meera and Anindya. They have been cooperative and friendly. Thanks to them. Thanks to Jibing and Vineeta for their help in studies with Micropipette aspirations set up.

I would like to thank Meena for her support with experiments and the care she showed me. I am thankful to Radha Krishna, Amuda and Chaitanya for their support. Radha and Vidya are always ready to help. Thanks to them. I would like to thank all RRI bodies such as SAAC, Library, Workshop, Canteen, Sports, Security, Transport, E & B, and Administration for their support.

RRI gave me many friends who showed so much care for me. They have filled my journey with fun. I can't thank them enough. Thanks to all non-RRI friends for their immense support.

I feel blessed to have a guru like Kondepi Koteswara Rao sir. My sincere thanks for all his parental care and encouragement from childhood. I would like to thank my family for their love, care, and persistent support.

Synopsis

Thesis title: "Studies on the mechanical properties and phase behaviour of lipid bilayers in the presence of some alcohols and oxysterols"

This thesis deals with studies on phase transitions, mechanical properties and structure of lipid bilayers in the presence of shorter and longer chain alcohols and oxysterols. These systems are probed with a variety of experimental techniques, such as vesicle fluctuation analysis, small-angle x-ray scattering (SAXS), fluorescence and phase contrast microscopy, fluorescence recovery after photo bleaching (FRAP), differential scanning calorimetry (DSC) and micropipette aspiration.

Lipids are amphiphilic biomolecules that form bilayers in water above a critical micellar concentration (CMC). Lipid bilayers are present in different parts of a cell, such as the plasma membrane, nuclear membrane, endoplasmic reticulum, Golgi apparatus and vacuole. They are involved in a variety of process like endocytosis, exocytosis, cell fusion and fission. In order to understand their function, it is important to know their physical properties and their interaction with biologically relevant molecules. To reduce the complexity of the system, studies are often conducted on model membranes made up of a few lipids. Lipid bilayers can exist in different morphologies, such as flat bilayer stacks, unilamellar vesicles and multilamellar vesicles. Unilamellar vesicles with their radii or diameters in the range of tens of microns are called giant unilamellar vesicles (GUV). Each of these morphologies is best suited for a particular experimental technique.

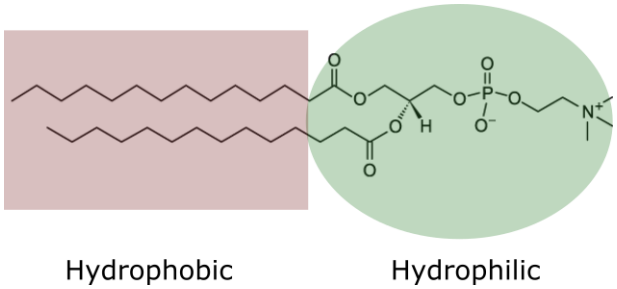

FIGURE 1: Chemical structure of 1,2-dimyristoyl-sn-glycero-3-phosphocholine (DMPC) lipid. Hydrophobic and hydrophilic parts of the molecule are highlighted.

Lipid bilayers broadly exhibit two phases, fluid and gel. The fluid phase occurs at temperatures above the chain melting transition temperature (T_m), and the gel phase at lower temperatures. In the fluid phase the in-plane order is liquid-like and the molecules are free to diffuse within the bilayer, whereas such molecular diffusion is highly restricted in the much more rigid gel phase. As a consequence, all biomembranes exist in the fluid phase.

During biologically important processes, such as endocytosis, exocytosis, cell fusion and fission, the membrane curvature changes dramatically. To understand these processes, therefore, a knowledge of the bending rigidity modulus (κ) of the membrane is needed. κ depends on many parameters, such as the surface charge density, membrane thickness and temperature. In the gel phase, it is about two orders of magnitude higher than the ambient thermal energy (K_BT, K_B being the Boltzmann constant). On the other hand, in the fluid phase κ is of the order of K_BT. As a result, thermal energy is sufficient to excite bending modes of the membrane in the fluid phase, giving rise to thermal shape fluctuations of giant unilamellar vesicles that can be observed under an optical microscope. One of the major objectives of this study is to determine the effect of different alcohols on the bending rigidity of the membrane from a quantitative analysis of such shape fluctuations of GUVs.

All biomembranes exist in the fluid phase. However, their composition need not be spatially uniform. According to the lipid raft hypothesis, cell membranes consist of coexisting ordered (l_o) and disordered (l_d) fluid phases, with the former being richer in cholesterol. Preference of membrane anchored proteins for one phase over the other is proposed to lead to membrane compartmentalization. Such $l_o - l_d$ phase coexistence is observed in ternary mixtures of cholesterol and two lipids with widely different values of T_m, leading to the formation of micron-sized domains. But in cell membranes in vivo, such large domains are not observed; instead experiments suggest the formation of nanometer-sized compositional heterogeneities. Another objective of this study is to explore the possibility of fluid-fluid coexistence in simpler two-component membranes.

In Chapter I, we present a brief introduction to the structure, phase transitions and mechanical properties of lipid bilayers.

In chapter II, we describe the implementation of vesicle fluctuation analysis. Using the Helfrich theory of membrane elasticity, bending rigidity (κ) and tension (σ) of membranes can be obtained from the vesicle shape fluctuation spectrum. Shape fluctuations of giant unilammelar vesicles (GUV) are visible under a phase contrast optical microscope as shown in figure 2. Measuring membrane fluctuations involve GUV preparation, image acquisition, contour detection, Fourier series expansion of contours and fitting the theoretical model to the observed spectrum.

TABLE 1: Values of the bending rigidity modulus (κ) of DMPC membranes obtained for different objective magnifications at T = 28 °C . The exposure time of the camera was 3 ms.

Objective	κ (10^{-20} J)
100X (N.A=1.35)	16.9±0.8
60X (N.A=0.70)	19.2±1.9

A sequence of images is acquired and contours are determined with sub pixel accuracy. Each contour is then expanded into a Fourier series. Mean square amplitudes of different modes are determined and fitted to the model, as shown in figure 3, thus obtaining the bending rigidity (κ) and tension (σ) of the membrane. In the literature, various possible artifacts related to this technique have been discussed. To understand these artifacts, we have studied the role of magnification of the microscope objective and camera exposure time in the estimation of κ. It is observed that lower

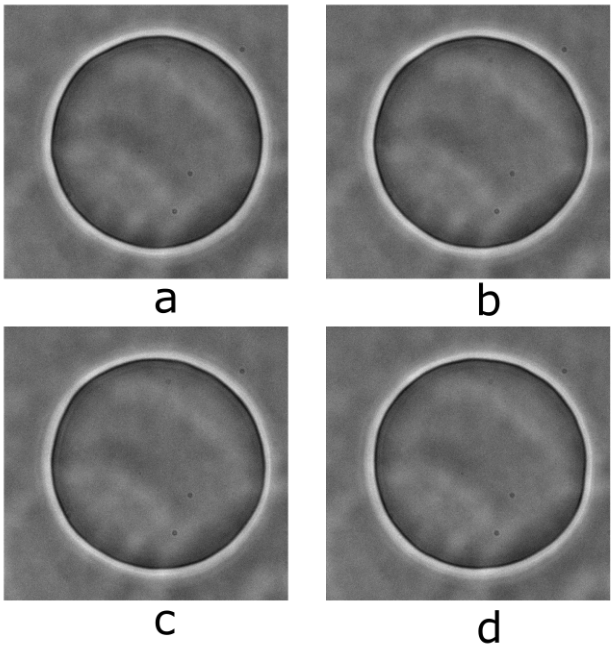

FIGURE 2: Series of images of a fluctuating GUV captured using phase contrast optical microscopy. Vesicle radius is around 18 µm. For video please click here

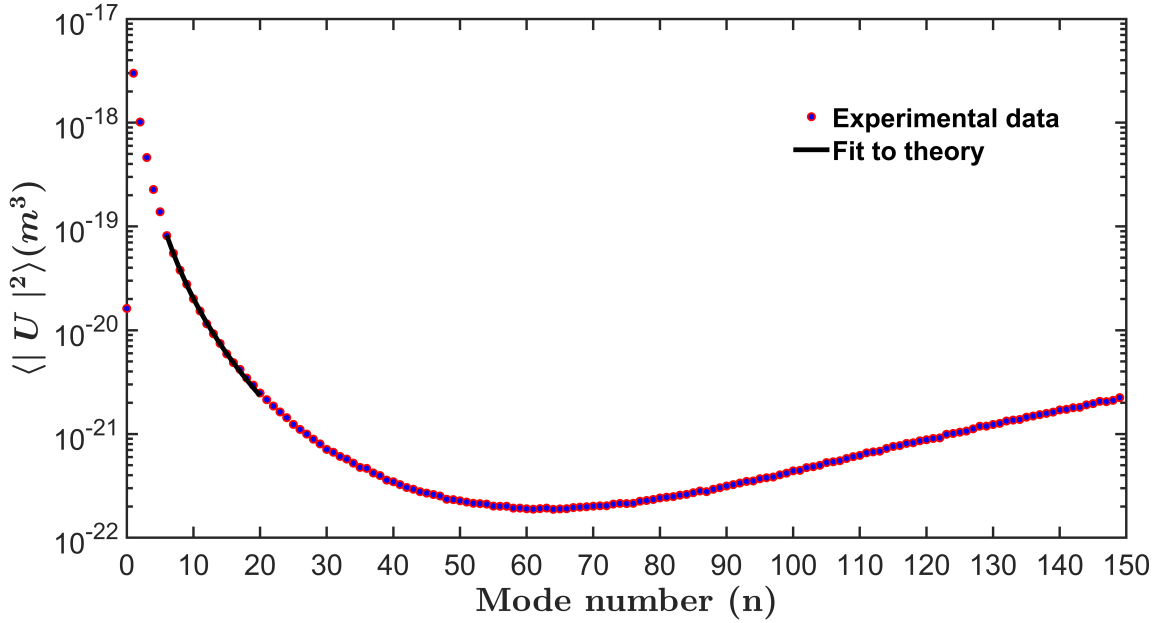

FIGURE 3: Typical fluctuation spectrum of a DMPC GUV. Variation of the mean square amplitude with mode number is shown. The solid line is the fit to the theory.

magnification systematically gives higher bending rigidity, whereas higher camera exposure time gives lower bending rigidity. The results are presented in tables 1 and 2. We have measured bending rigidity of 1,2-dimyristoyl-sn-glycero-3- phosphocholine (DMPC), 1-stearoyl-2-oleoyl-sn-glycero-3-phosphocholine (SOPC), SOPC+ cholesterol and 1-palmitoyl-2-oleoyl-glycero-3- phosphocholine (POPC) lipid bilayers. These are presented in table 3, and are found to be in very good agreement with values reported in the literature.

TABLE 2: Values of the bending rigidity modulus (κ) of DMPC membranes for different exposure times of the camera at T = 28 °C. The objective magnification was 100X.

Exposure time	κ (10^{-20} J)
3 ms	16.9±0.8
18 ms	14.3±0.8
33 ms	13.9±0.7

TABLE 3: Bending rigidity modulus (κ) of some lipids at 28 °C.

Lipid	κ (10^{-20} J)
SOPC	21.4±0.6
SOPC + Cholesterol (1:1)	44.0±2.0
DMPC	16.9±0.8
POPC	15.0±0.6

Alcohols influence cell growth, cell division and cell morphology. Their anesthetic and antimicrobial properties have been known for more than a century. Most of the studies on the interaction of alcohols with membranes have been focused on elucidating their anesthetic activity. Their anesthetic efficacy is found to depend on the chain length of the alcohol. Below some critical chain length, they act as anesthetics, whereas alcohols with longer chain length do not. This is called the cutoff effect. Short alcohols increase volume and area per lipid, lipid diffusivity, and reduce chain order, membrane thickness, and T_m. On the other hand, higher chain alcohols increase chain order, membrane thickness, T_m, and reduce lipid diffusivity.

There are very few studies on the influence of alcohols on the bending rigidity of lipid bilayers reported in the literature. It has been shown that alcohols from methanol to butanol lower bending rigidity of unsaturated lipid membranes. However, there have been no systematic studies by varying chain length of alcohols. We have, therefore, studied the influence of shorter and longer chain length alcohols on the bending rigidity of 1,2-dimyristoyl- sn-glycero-3- phosphocholine (DMPC) lipid bilayers in the fluid phase from the analysis of vesicle shape fluctuations. Since κ is known to depend on the thickness of the bilayer (d_{HH}), we have obtained d_{HH} from small-angle x-ray scattering experiments to understand the microscopic origin of the observed changes in κ.

In chapter III, we discuss the effect of shorter and longer chain alcohols, namely ethanol, pentanol, hexanol, octanol, decanol and dodecanol on the bending rigidity and thickness of DMPC bilayers. GUVs are prepared using the electro-formation method. Alcohols are introduced into the vesicle preparation and observation chambers by mixing them in the suspending aqueous solutions. In time, the alcohol is partitioned between the vesicles and water. Alcohol content in the membrane is tuned by varying the alcohol concentration in the suspending solution. Values of the bending rigidity obtained are shown in figure 4. Alcohols with chain length shorter than decanol reduce κ. On the other hand, decanol and dodecanol show no influence on κ. In order to understand changes caused by the alcohol in the structure of the bilayer, we have obtained the bilayer thickness from small-angle x-ray scattering experiments on dispersion of small unilamellar vesicles. In correlation with a reduction in κ, we have observed a reduction in the bilayer thickness

for all alcohols shorter than decanol. Decanol shows no influence on d_{HH} of DMPC bilayers.

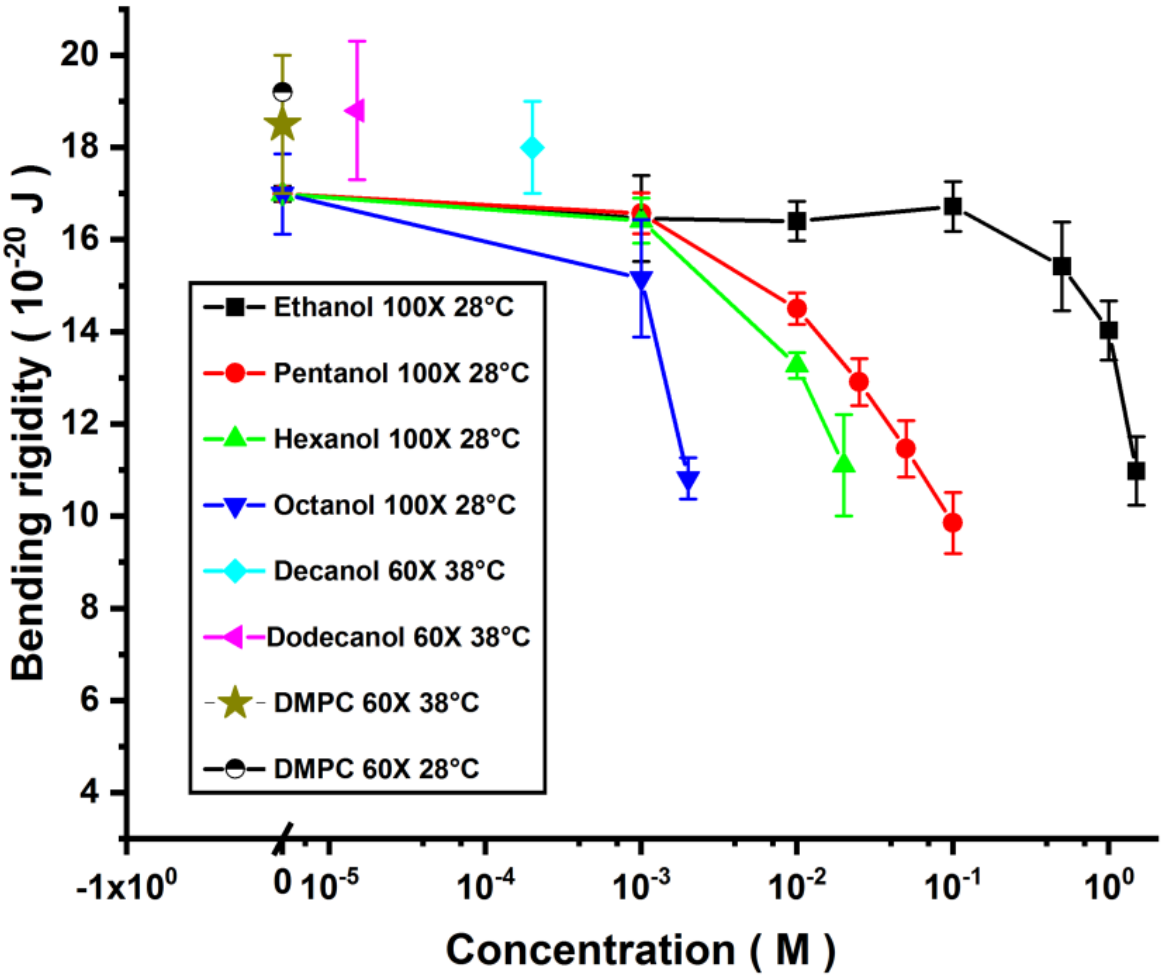

FIGURE 4: Variation of the bending rigidity modulus of DMPC bilayers with alcohol chain length and concentration in the suspending solution. Magnification of the objective used and the temperature at which data were collected are given in the legend.

Very few studies have been reported on the influence of longer chain alcohols on the phase behaviour of lipid bilayers. We have, therefore, studied the influence of 1-decanol on the phase behaviour of DMPC bilayers. These studies are summarized in chapter IV. The system is probed using fluorescence microscopy, fluorescence recovery after photo bleaching (FRAP), differential scanning calorimetry (DSC) and small angle x-ray scattering (SAXS) techniques. These bilayers show a transition from a uniform fluid phase to a gel phase on cooling, with a narrow fluid-fluid coexistence region in between as shown in figure 5. Occurrence of fluid-fluid coexistence was confirmed using a variety of membrane platforms such as giant unilamellar vesicles (GUVs), supported lipid bilayers (SLBs) and aligned bilayer stacks.

The decanol-rich fluid phase is found to have a higher bilayer thickness and lower lipid diffusivity compared to the decanol-poor fluid phase. On further cooling, the bilayers transitioned into a ripple phase with much higher wavelength ripples compared to the ripple phase of pure DMPC. Ripple to gel phase transition is observed on further cooling. All these transitions are reversible on heating. Although long-chain alcohols have been known to increase chain order in membranes,

their ability to induce fluid-fluid coexistence has not been anticipated.

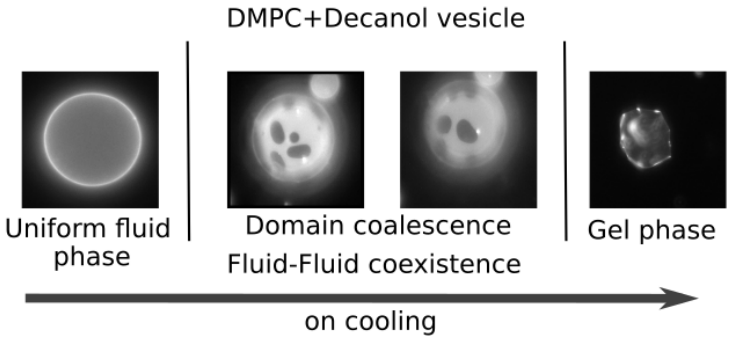

FIGURE 5: Fluorescence microscopy images of DMPC GUVs suspended in an aqueous solution containing 1-decanol at temperatures corresponding to the high-temperature fluid phase, intermediate fluid-fluid coexistence region and low-temperature gel phase.

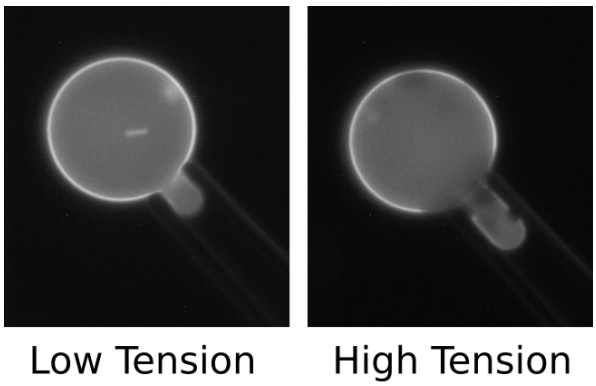

FIGURE 6: Fluorescence microscopy images of an aspirated GUV at lower tension exhibiting a uniform phase and at higher tension exhibiting dark domains indicating two-phase coexistence. The dark domains are found to diffuse and coalesce confirming that both phases are in the fluid state.

In chapter V, we report a novel tension-induced fluid-fluid coexistence region in an unsaturated lipid bilayer containing an oxysterol. Oxysterols are oxidized derivatives of cholesterol and are known to exhibit cytotoxic and pro-apoptotic activities. They are involved in biological processes such as cholesterol homeostasis and autophagy. Oxysterols interact with lipid bilayers and alter their physio-chemical properties differently compared to cholesterol. Although fluid-fluid coexistence has been observed earlier in our laboratory in binary lipid-oxysterol membranes, such a behaviour was confined to membranes composed of saturated lipids. We find that fluid-fluid coexistence can be induced in an unsaturated lipid bilayer containing an oxysterol on applying tension. The membrane tension is applied using the micropipette aspiration technique. A fluorescence microscopy image of a vesicle exhibiting fluid-fluid coexistence is shown in figure 6. We have observed a similar transition by applying tension in vesicles by changing the osmolarity of the solution. Membrane tension is known to play a crucial role in various cellular processes such as morphogenesis, endocytosis, exocytosis, fission and fusion. Hence the present observation of tension-induced fluid-fluid phase separation in a membrane made up of an unsaturated lipid is

of much interest.

In chapter VI, we present a brief summary of the main results of this thesis and indicate some directions for future research.

Signature of the Student

(Buti Suryabrahmam)

Signature of the Supervisor

(Prof. Pramod Pullarkat)
Raman Research Institute
Bangalore 560080

Signature of the Co-supervisor

(Prof.V.A.Raghunathan)
Raman Research Institute
Bangalore 560080

List of publications related to studies presented in this thesis

- "Fluid-fluid coexistence in phospholipid membranes induced by decanol", Buti Suryabrahmam, Ayush Agrawal, and V A Ragunathan,*Soft matter*,16,9002(2020).

- "Influence of alcohols on bending rigidity of saturated lipid bilayers", Buti Suryabrahmam, Ayush Agarwal, and V A Raghunathan. The manuscript is under preparation.

- "Tension induced phase separation in Unsaturated lipid bilayers in the presence of an Oxysterol", Buti Suryabrahmam and V A Raghunathan. The manuscript is under preparation.

List of other publications

- "Time-delayed intensity–interferometry of the emission from ultracold atoms in a steady-state magneto-optical trap", K Muhammed Shafi, Deepak Pandey, Buti Suryabrahmam, BS Girish and Hema Ramachandran, *J. Phys. B: At. Mol. Opt. Phys.*,49,025301(2016).

- "Classical light sources with tunable temporal coherence and tailored photon number distributions", Deepak Pandey, Nandan Satapathy, Buti Suryabrahmam, J. Solomon Ivan, Hema Ramachandran, *Eur. Phys. J. Plus*,129,115(2014).

Contents

Synopsis **ix**

1 Introduction **1**
1.1 Introduction . . . 1
1.2 Principles of self-assembly of amphiphiles . . . 1
1.3 Phase behaviour of lipid bilayers . . . 3
1.4 Mechanics of Lipid bilayers . . . 5

2 Vesicle Fluctuation Analysis **13**
2.1 Introduction and theory . . . 13
2.2 Materials . . . 15
2.3 Methods . . . 16
2.3.1 Vesicle preparation using Electro-formation method . . . 16
2.3.2 Vesicle observation . . . 16
2.3.3 Algorithm for detecting contour . . . 17
2.3.4 Fourier analysis of the contours . . . 20
2.3.5 Fitting the model spectrum to the experimental data . . . 22
2.4 Results and discussions . . . 23
2.4.1 Effect of the microscope objective and the magnification on vesicle fluctuation spectrum . . . 23
2.4.2 Effect of the camera exposure time on fluctuation spectrum . . . 25
2.4.3 Bending rigidity of some lipid bilayers . . . 25
2.5 Conclusions . . . 25

3 Influence of alcohols on bending rigidity of Phospholipid bilayers **31**
3.1 Introduction . . . 31
3.2 Materials and Methods . . . 32
3.2.1 Materials . . . 32
3.2.2 Differential scanning calorimetry (DSC) . . . 32
3.2.3 GUV preparation and observation . . . 32
3.2.4 Small angle x-ray scattering from small unilamellar vesicles (SUV) . . . 33
3.3 Results and discussions . . . 35
3.3.1 DSC studies . . . 35
3.3.2 Bending rigidity of DMPC membranes in the presence of alcohols . . . 37
3.3.3 Bilayer thickness in presence of the alcohols . . . 40
3.4 Conclusions . . . 42

4 Phase behaviour of DMPC-decanol membranes **47**
4.1 Introduction . . . 47
4.2 Materials and Methods . . . 48
4.2.1 Preparation of giant unilamellar vesicles (GUVs) . . . 48
4.2.2 Preparation of small unilamellar vesicles (SUVs) . . . 48
4.2.3 Preparation of supported lipid bilayers (SLBs) . . . 48
4.2.4 FRAP experiments . . . 48
4.2.5 X-ray diffraction on aligned bilayer stack . . . 49
4.2.6 Differential scanning calorimetry (DSC) . . . 49
4.3 Results . . . 49
4.3.1 Fluorescence microscopy . . . 49
4.3.2 FRAP . . . 50
4.3.3 SAXS and WAXS . . . 52
4.3.4 Differential scanning calorimetry (DSC) . . . 53
4.4 Discussions . . . 54
4.5 Conclusion . . . 58

5 Tension induced phase separation in an unsaturated lipid membrane containing hydroxycholesterol **63**
5.1 Introduction . . . 63
5.2 Materials . . . 64
5.3 Methods . . . 64
5.3.1 Vesicle preparation and observation . . . 64
5.3.2 Micro-pipette aspiration experiment . . . 64
5.4 Results . . . 66
5.4.1 Illumination induced fluid-fluid phase coexistence . . . 66
5.4.2 Osmotic pressure induced fluid-fluid coexistence . . . 67
5.4.3 Tension induced fluid-fluid coexistence . . . 68
5.5 Discussion . . . 69

6 Conclusions **77**

List of Figures

1 Chemical structure of 1,2-dimyristoyl-sn-glycero-3-phosphocholine (DMPC) lipid. Hydrophobic and hydrophilic parts of the molecule are highlighted. ix
2 Series of images of a fluctuating GUV captured using phase contrast optical microscopy. Vesicle radius is around 18 µm. For video please click here xi
3 Typical fluctuation spectrum of a DMPC GUV. Variation of the mean square amplitude with mode number is shown. The solid line is the fit to the theory. xi
4 Variation of the bending rigidity modulus of DMPC bilayers with alcohol chain length and concentration in the suspending solution. Magnification of the objective used and the temperature at which data were collected are given in the legend. . . . xiii
5 Fluorescence microscopy images of DMPC GUVs suspended in an aqueous solution containing 1-decanol at temperatures corresponding to the high-temperature fluid phase, intermediate fluid-fluid coexistence region and low-temperature gel phase. xiv
6 Fluorescence microscopy images of an aspirated GUV at lower tension exhibiting a uniform phase and at higher tension exhibiting dark domains indicating two-phase coexistence. The dark domains are found to diffuse and coalesce confirming that both phases are in the fluid state. xiv

1.1 Structure of various lipids, hydroxysterols and alcohols. This image is adopted from avantilipids.com. 2
1.2 The various interactions involved in self-assembly process. This image is adopted from ref 5. 3
1.3 Structure of lipid bilayer in various phases and corresponding x-ray scattering patterns from aligned bilayer stacks. This image is adopted from ref 7. 3
1.4 Partial phase diagram of DMPC lipid bilayers at different values of relative humidity. This image is adopted from ref 8. 4
1.5 Ordered and disordered fluid phase coexistence in DOPC: SM: cholesterol vesicles. This image is adopted from ref 11. 5
1.6 Morphologies of lipid bilayers and their methods of preparation. 7
1.7 List of techniques used on various lipid bilayer morphologies and the properties probed. 8

2.1 The vesicle fluctuation spectrum calculated using equation 2.5 with different values of camera exposure time (τ_c) for vesicle radius= 16.4 µm, tension= 1.85×10^{-8} N/m and bending rigidity= 14.5×10^{-20} J. Note that the spectrum is affected even if τ_c is as low as 3 ms. 14

2.2 Typical image of a vesicle in a) phase contrast and b) fluorescence microscopy. For video of vesicle shape fluctuations please click here. . . . 17
2.3 Intensity profile is taken along the line drawn across the image in order to determine the first contour point. . . . 17
2.4 The procedure followed to find the first contour point. Details are provided in the text. . . . 18
2.5 The total contour is divided into 8 regions.The probable sets of three neighboring pixels containing the next contour point are highlighted in red color. We identify the probable pixel coordinates in each region by using the signs of m_x, m_y, m_v, and m_w. . . . 19
2.6 The procedure followed to assign axes to the corresponding probable pixels. At each of the three probable pixels, slopes of the intensity profile is calculated along the appropriate directions. Both the axes and the corresponding pixels are shown in the same color. In the tangential direction of the contour, the slope sign fluctuates between positive and negative values of negligible magnitude. So, there are two probable pixels in that direction, which are highlighted in gray color. Here we show the procedure only for 1,2, and 8 regions, but a similar procedure is followed for the rest. . . . 20
2.7 Image of a vesicle with the detected contour superposed. . . . 21
2.8 Typical fluctuation spectrum of a DMPC vesicle of radius 15.5 µm. The solid line is the fit to equation 2.5. From the fit, values of σ and κ are found to be 1.1×10^{-8} N/m and 16.7×10^{-20} J, respectively. . . . 22
2.9 The effect of magnification on the spectrum of the same SOPC vesicle (R= 25.3 µm, $\tau_c = 3$ ms). The obtained values of κ and σ are listed in table 2.1. . . . 23
2.10 Shape fluctuation spectra of a vesicle. Each curve is obtained from a distinct data set consisting of 2500 images, captured sequentially. The overlap of the curves shows the stability of the vesicle during the observation time of around 15 minutes. . . . 24

3.1 Scattering from DMPC SUV dispersions of different concentrations at 30 °C. The curves are smoothed over 10 points. . . . 34
3.2 SAXS profiles of 5 w% DMPC SUV dispersions at a few different temperatures. The curves are smoothed over 10 points. . . . 35
3.3 Differential scanning calorimetry (DSC) cooling curves of DMPC with and without alcohols. a) DMPC b) DMPC:ethanol (1:30) c) DMPC: pentanol (1:3) d) DMPC: octanol (1:0.5) e) DMPC: decanol (1:0.5) f) DMPC: dodecanol (3:1). Alcohols with $C_n = 2 - 8$ reduce T_m and $C_n = 10 - 12$ increase T_m. . . . 36
3.4 Variation of the bending rigidity modulus of DMPC bilayers with alcohol concentration in the interior and exterior solutions of the vesicles. . . . 37
3.5 SAXS profiles of DMPC SUVs dispersion containing alcohols of different chain lengths. The solid lines are fits to equation 3.1. a) DMPC, 10 w/w %, 30 °C b) DMPC:ethanol (1:30 molar ratio), 10 w%, 30 °C c) DMPC:pentanol (1:3 molar ratio), 10 w%, 30 °C d) DMPC:octanol (1:0.5 molar ratio), 10 w%, 30 °C e) DMPC:decanol (1:0.5 molar ratio), 5 w%, 38 °C. Values of the model parameters obtained from the fit are listed in table 3.4 . . . 39

3.6 Variation of Bending rigidity with alcohol content of the membrane. Alcohol to lipid molar ratio in the GUV is obtained from the bulk alcohol concentration using values of partition coefficients taken from the literature and given in table 3.5. . . . 42

4.1 1 Left (top): A DMPC GUV suspended in a decanol saturated aqueous solution exhibiting a single fluid phase with thermal undulations at 30 °C. Middle (a)–(d): Time-lapse images showing the coalescence of dark domains at 28 °C, over a duration of 4 min. 2 Left (bottom): A cylindrical vesicle observed in the two-phase region at 24 °C. Fluorescence microscopy (3 right, top) and phase contrast microscopy (4 right, bottom) images of a GUV with faceted shape observed in the gel phase at 23.5 °C 50
4.2 Images of some non-spherical GUV shapes observed in the two-phase coexistence region at 28 °C. Note that the dark regions in all the GUVs have a smaller curvature compared to the bright region. The bright regions of the GUVs show thermal shape fluctuations, indicating that they are in the fluid phase. Magnification is the same in all the images. 51
4.3 (a) DMPC SLB in water exhibiting uniform fluorescence. The appearance of dark domains soon after the addition of decanol saturated PBS buffer at 30 °C (b) and after incubation for 2 hours at 45 °C (c). Magnification is the same in all the images. 51
4.4 Typical recovery curves in the dark and bright regions of a DMPC SLB in equilibrium with a decanol saturated PBS buffer solution at 40 °C (a) and at 30 °C (b) Solid lines are fits to a single exponential function. 52
4.5 Small-angle (a) and wide-angle (b) scattering profiles from 1:0.5 DMPC-decanol multilayers at different temperatures. 53
4.6 SAXS (a) and WAXS (b) patterns obtained from a 1:0.25 DMPC-decanol sample at a few temperatures on cycling the temperature from high to low and back to high, showing thermal reversibility of the phase behavior. 54
4.7 Transbilayer electron density profiles of 1:0.5 DMPC-decanol membranes in different phases determined from the SAXS data. The maxima correspond to the headgroup regions and the minimum to the midplane of the bilayer. The separation, d_{HH}, between the two maxima is a measure of the bilayer thickness. 54
4.8 Normalized DSC curves for pure DMPC and DMPC-decanol samples of 1:0.25 and 1:1 molar composition. Lipid concentration in all samples is 10 w%. 55

5.1 A typical differential interference contrast (DIC) image of SOPC vesicle. 50 mM sucrose and glucose solutions are used as interior and exterior media respectively, for vesicles. 65
5.2 a) Micro pipette puller b) Micro-forge c) Water column on 1-D movable stage d) Typical experimental set up for micro pipette aspiration. 66
5.3 POPC:27-hydroxysterol: rhodamine DHPE (79.5:20:0.5 molar ratio) vesicle showing an irreversible transition from a uniform phase to a fluid-fluid coexistence under illumination with a 100X objective. For the corresponding video, please click here . . 67

5.4 A POPC:27-hydroxysterol:DiI (79.5:20:0.5 molar ratio) vesicle showing an oscillatory behavior of tension-induced phase transition under a hypotonic environment from a uniform phase to fluid-fluid coexistence at 27 ± 2 °C. The vesicles are prepared in a 50 mM sucrose solution and then dropped in water. The magnification is the same for all the images. For the corresponding video, please click here 68
5.5 In the osmotic pressure induced fluid-fluid coexistence, domain diffusion and coalescence is observed. Figures (a,b,c), (d,e,f,g,h,i) correspond to two different domain merging events on the same vesicle. The scale bar is the same for all the images. These images and the images in 5.4 are part of the same video. 69
5.6 Fluorescence microscopy images of an aspirated POPC:27-hydroxysterol:DiI (79.5:20:0.5 molar ratio) GUV at lower tension exhibiting a uniform phase (a,b,c) and at higher tension exhibiting dark domains indicating two-phase coexistence (d,e). In image (e) top part of the vesicle is focused at same tension as in (d). The dark domains are found to diffuse and coalesce, confirming that both phases are in the fluid state. This phase transition is found to be reversible with tension, as shown in figure (f). The vesicle radius is 11.7 µm and the pipette radius is 3.4 µm. For the corresponding video, please click here 70
5.7 Histogram of the threshold tension in the membrane required to induce fluid-fluid coexistence in POPC:27- hydroxysterol:DiI vesicles. A total of 39 vesicles were considered to obtain this plot. 70
5.8 Vesicle diameter vs threshold tension needed to induce fluid-fluid coexistence. No correlation is found between them. 71

List of Tables

1 Values of the bending rigidity modulus (κ) of DMPC membranes obtained for different objective magnifications at T = 28 °C . The exposure time of the camera was 3 ms. x
2 Values of the bending rigidity modulus (κ) of DMPC membranes for different exposure times of the camera at T = 28 °C. The objective magnification was 100X. . . . xii
3 Bending rigidity modulus (κ) of some lipids at 28 °C. xii

2.1 Observed differences in σ and κ on using different magnifications. Observations are done on the same SOPC vesicle. 23
2.2 Average values of the bending rigidity modulus (κ) of DMPC membranes, for different magnifications at T = 28 °C. The exposure time of the camera is 3 ms. 24
2.3 Bending rigidity of DMPC membranes obtained with different camera exposure times (τ_c) at T = 28 °C. 25
2.4 κ of some lipid bilayers at 28 °C 25

3.1 Bending rigidity modulus (κ) of DMPC membranes obtained from VFA for different objective magnifications at T = 28$\pm$1 °C and 38$\pm$1 °C. A 3 ms camera exposure time is used. 33
3.2 Main phase transition temperature (T_m) of DMPC + alcohol systems obtained from DSC experiments. In case of DMPC T_m = 22.7 °C. 35
3.3 Bending rigidity values of DMPC membrane for different concentrations (m) and chain lengths of alcohols (C_n). 38
3.4 Membrane model parameters obtained from fitting the scattering data to 3.1. The alcohols used and their relative molar concentrations (lipid:alcohol) are mentioned. 40
3.5 Alcohol content in the membrane in GUV and SUV dispersion, estimated from the reported values of alcohol partition coefficients. Here K, K_m, K_c are partition coefficients defined in terms of mole fraction, molality ratio and molarity ratio, respectively. To make comparison easy, we have converted partition coefficients into mole fraction. C_A is the alcohol concentration in the solution used in GUV experiments. n_L is the lipid content in GUV or SUV samples. n_A is the total alcohol in the SUV dispersion. Alcohol content in the membrane is n'_A. 41

4.1 Values of diffusion coefficient obtained from FRAP experiments in the bright and dark phases of DMPC SLBs in the presence of decanol in the fluid state. 52

4.2 Observed relative magnitudes ($|F_h|$) and estimated phases (α_h) of different diffraction peaks used for the Fourier reconstruction of EDPs of different phases of 1:0.5 DMPC-decanol bilayers, and the corresponding values of lamellar periodicity (d) and bilayer thickness (d_{HH}). 55
4.3 The observed (d_o) and calculated (d_c) values of the spacings of the different reflections in the ripple phase of the 1:0.5 DMPC-decanol multilayers at 25.5°C are shown. The lattice parameters of the ripple phase are: d = 5.57 nm, ripple wave length (λ) = 38.72 nm and γ = 103.2°. 56

Chapter 1

Introduction

1.1 Introduction

Lipid bilayers are present in different parts of a cell, such as the plasma membrane, nuclear membrane, endoplasmic reticulum, Golgi apparatus and vacuole[1]. They are involved in a variety of processes like endocytosis, exocytosis, cell fusion and fission. In order to understand their function, it is essential to know their physical properties and their interaction with biologically relevant molecules[2]. To reduce the complexity of the system, studies are often conducted on model membranes made up of a few lipids. This thesis deals with the mechanical properties, structure and phase behaviour of lipid bilayers in the presence of shorter and longer chain length alcohols and oxysterols.

Lipids are amphiphilic biomolecules that form bilayers in water above a critical micellar concentration (CMC). Various types of lipids are present in the cell, such as phosphatidylcholine (PC), phosphatidylethanolamine (PE), phosphatidylserine (PS), phosphatidylinositol(PI), sphingolipids (SM) and cholesterol. Typical structures of some of them are shown in figure 1.1. Even though most of them consist of two hydrocarbon chains, single-chain ones also exist. Two chain lipids are classified based on their head groups, and the length and degree of saturation of the two chains.

This chapter discusses the self-assembly of lipids, the phase behaviour and mechanics of lipid bilayers.

1.2 Principles of self-assembly of amphiphiles

Amphiphilic molecules consist of hydrophilic (or polar) parts and hydrophobic (or non-polar) parts. Surfactants, lipids, sterols, fatty acids and alcohols are examples of amphiphilic molecules. At very low concentrations, amphiphilic molecules form molecular monolayers at the air-water interface, which is in equilibrium with monomers dispersed in the solution. Above a threshold concentration which is called the critical micellar concentration (CMC), they self-assemble into aggregates, called micelles. These spontaneously formed structures coexist with monolayers at the interface and monomers in the solution.

Tanford[3] and Israelachvilli et al[4] successfully modeled these systems. Here a dilute solution of the amphiphile is considered just above its CMC. It is assumed that aggregates of different sizes, including monomers, coexist in this solution. The aggregate size is defined in terms of the aggregation number N, which is the number of molecules present in the aggregate. Since the solution is at thermal equilibrium, the chemical potential per molecule should be the same in the aggregates of different sizes. Hence it follows that,

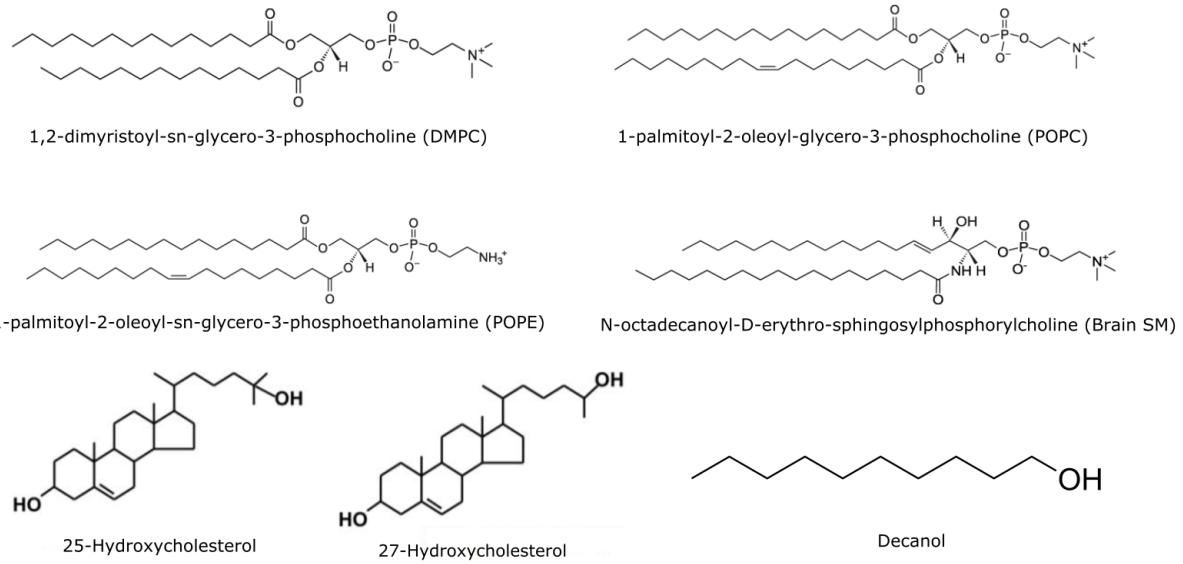

FIGURE 1.1: Structure of various lipids, hydroxysterols and alcohols. This image is adopted from avantilipids.com.

$$\mu_1^o + k_B T \ln(X_1) = \mu_2^o + \frac{1}{2} k_B T \ln(\frac{1}{2} X_2) = \mu_3^o + \frac{1}{3} k_B T \ln(\frac{1}{3} X_3) = \ldots\ldots\ldots\ldots = \mu_N^o + \frac{1}{N} k_B T \ln(\frac{1}{N} X_N) \tag{1.1}$$

where μ_N^o is the internal free energy of a molecule in an aggregate of N molecules, X_N is the mole fraction of the molecules present in all the aggregates of size N, $\alpha = \frac{\mu_1^o - \mu_N^o}{k_B T}$. The total concentration of the amphiphiles (C) is equal to $\sum_{N=1}^{\infty} X_N$. From the above equation, we get

$$X_N = N X_1^N \exp\left[\frac{N(\mu_1^o - \mu_N^o)}{k_B T}\right] = N\left(X_1 e^{\alpha}\right)^N \tag{1.2}$$

Since the concentration of the amphiphile is assumed to be low, the fraction of molecules in aggregates of size N (X_N) has to be small. From equation 1.2 it follows that $X_1 e^{\alpha}$ cannot exceed 1. Hence $X_1 \approx e^{-\alpha}$. This concentration is called CMC, above which aggregation starts and monomer concentration saturates.

$$CMC \approx \exp\left[-\frac{(\mu_1^o - \mu_N^o)}{k_B T}\right] \tag{1.3}$$

CMC of single-chain surfactants is in the order of millimolar concentration. In the case of double-chain lipids, it is in the nanomolar order.

Israelachvilli et al.[4] developed a molecular geometry based approach to predict the shapes of aggregates by including molecular packing considerations into the Tanford model[5,6].

The molecular packing parameter (P) is defined as follows

$$P = \frac{V}{a_o l_c} \tag{1.4}$$

where V= volume of hydrocarbon chains, a_0= surface area per molecule at equilibrium, l_c = chain length.

The packing parameter and shape of the aggregate are related as shown in figure 1.2. The amphiphiles with $P \leq \frac{1}{3}, \frac{1}{3} \leq P \leq \frac{1}{2}, P \approx 1$ form spherical micelles, cylindrical micelles and

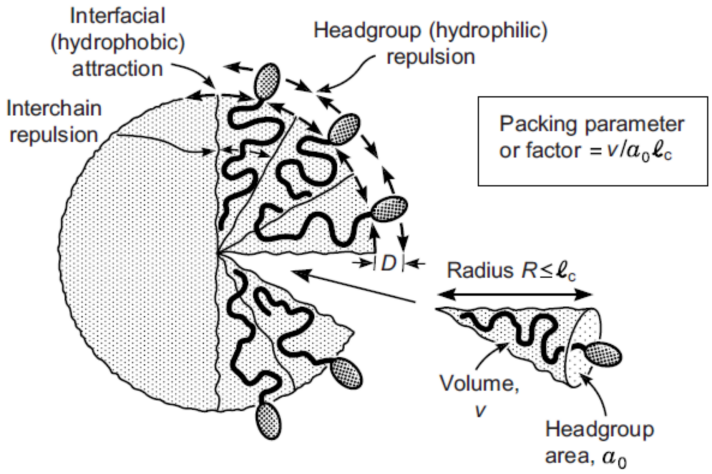

FIGURE 1.2: The various interactions involved in self-assembly process. This image is adopted from ref 5.

bilayers, respectively. In general, single chain surfactants forms micelles and double chain lipids form bilayers.

1.3 Phase behaviour of lipid bilayers

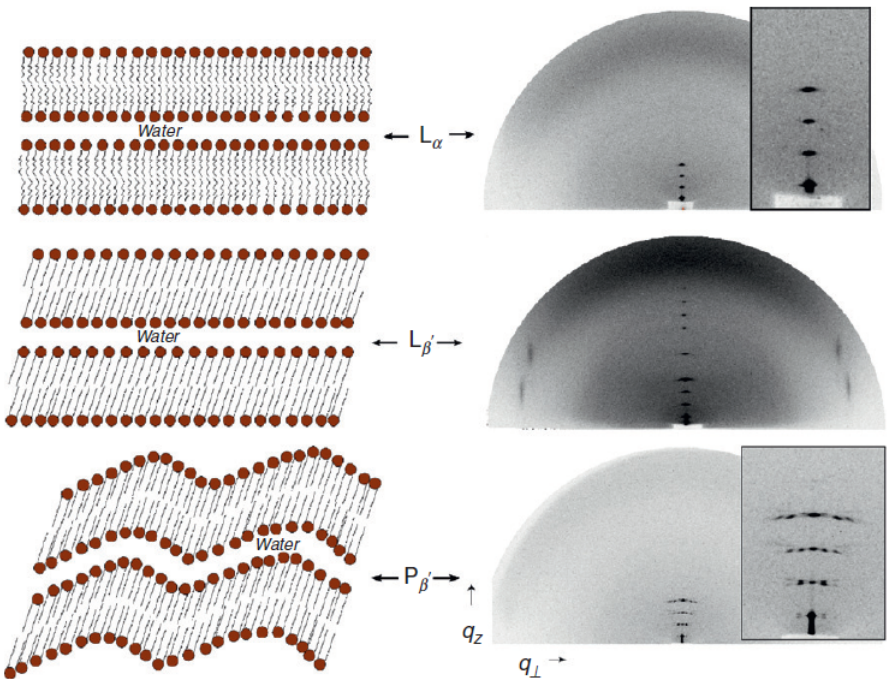

FIGURE 1.3: Structure of lipid bilayer in various phases and corresponding x-ray scattering patterns from aligned bilayer stacks. This image is adopted from ref 7.

Lipid bilayers broadly show the fluid and gel phases[8,9] as shown in figure 1.3. The transition from gel phase to fluid phase occurs at the main phase transition or chain melting transition temperature (T_m). In the fluid phase (L_α), the chains are disordered and the in-plane order is liquid-like. As a result, the fluid bilayers are very flexible and exhibit thermal undulations. In

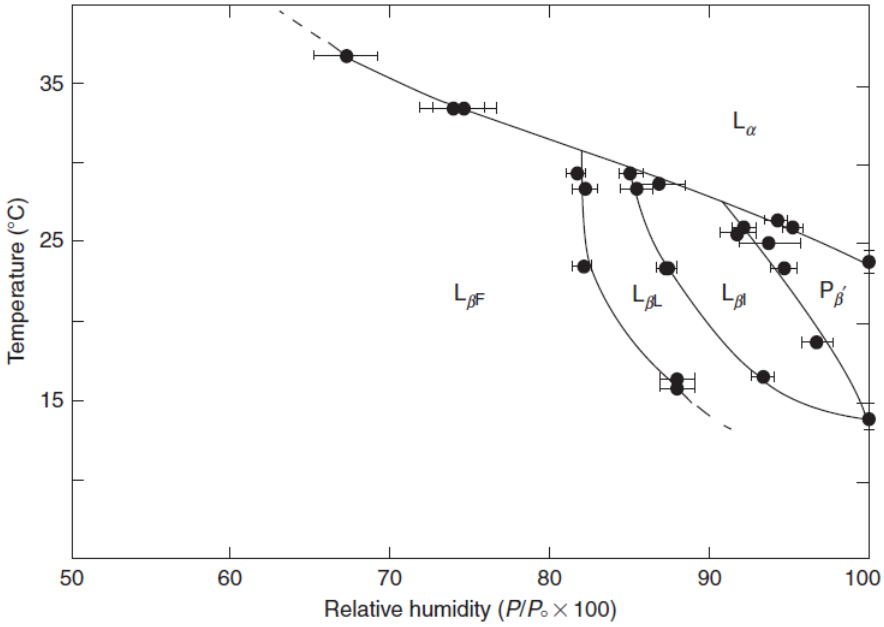

FIGURE 1.4: Partial phase diagram of DMPC lipid bilayers at different values of relative humidity. This image is adopted from ref 8.

the gel phase, on the other hand, the chains are ordered on a lattice and molecular diffusion is hindered. The bilayers in this phase are very rigid and do not show thermal undulations. Within the gel phase, various sub-phases can be seen, namely, ripple phase ($P_{\beta'}$), tilted gel phase ($L_{\beta'}$) and untilted gel phase (L_{β}). The phases shown by lipid bilayers depend on many factors, including size and charge of the head group, length of the hydrocarbon chains, degree of unsaturation of the chains, and hydration level. For example, various phases observed in DMPC lipid bilayers at different hydration levels are shown in figure 1.4. DMPC shows the L_{α} phase at high temperatures and on cooling, a transition to ripple phase ($P_{\beta'}$) appears at chain melting temperature (T_m). In this ripple phase, periodic height modulations of the bilayers exist. On further cooling, pre-transition occurs from ($P_{\beta'}$) to tilted gel phase ($L_{\beta'}$). In this phase, the chains take all trans confirmations and are tilted from bilayer normal. Single-component bilayers do not show areas of phase coexistence in the temperature-hydration plane, but in multi-component systems, two or more phases can coexist in equilibrium [10].

In some of the studies presented in this thesis, the x-ray scattering technique is used to obtain the bilayer structure and phase information. The structures and corresponding x-ray diffraction patterns of some of the phases are shown in figure 1.3. As shown in the figure, for a stack of bilayers in the fluid phase, aligned with the normal along the z-axis, a single set of lamellar Bragg peaks appear along q_z , in the small-angle region, and a diffused peak appears along $q_{\perp}$ in the wide-angle region. In the $L_{\beta'}$ phase, relatively larger number of lamellar peaks appear in the small-angle regions, and two or three sharp peaks appear in the wide-angle region. The number and position of the wide angle peaks is determined by the direction of the chain tilt with respect to the chain lattice. In the ripple phase additional "satellite" peaks appear in the small-angle region due to the periodic rippling of the bilayers.

All biomembranes exist in the fluid phase. However, their composition need not be spatially uniform. According to the lipid raft hypothesis, cell membranes consist of coexisting ordered

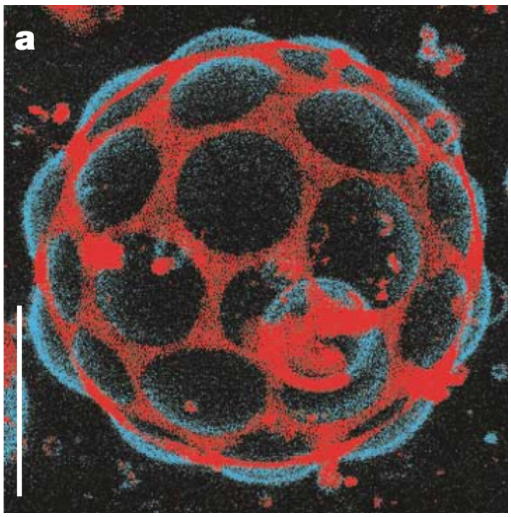

FIGURE 1.5: Ordered and disordered fluid phase coexistence in DOPC: SM: cholesterol vesicles. This image is adopted from ref 11.

(l_o) and disordered (l_d) fluid phases, with the former being richer in cholesterol[12]. Preference of membrane anchored proteins for one phase over the other is proposed to lead to membrane compartmentalization. Such $l_o - l_d$ phase coexistence is observed in ternary mixtures of cholesterol and two lipids with widely different values of T_m, leading to the formation of micron-sized domains[13,14]. A fluorescence image of a vesicle with $l_o - l_d$ phase coexistence is shown in figure 1.5[11]. In yeast vacuole[15] and in giant plasma membrane vesicles (GPMVs) or blebs formed from plasma membranes of cultured mammalian cells, micron-sized domains have been observed[16]. However, in cell membranes in vivo, such large domains are not observed; instead experiments suggest the formation of nanometer-sized compositional heterogeneities[17–19].

Hence it is important to find simple model systems that show fluid-fluid coexistence, in order to understand the mechanisms at play.

1.4 Mechanics of Lipid bilayers

During biologically important processes, such as cell migration, endocytosis, exocytosis, cell fusion and fission, the cell membrane experiences mechanical stress at various length scales[20–22]. To understand its response to the stress, knowledge of the elastic properties of the lipid bilayer is crucial[23].

According to the Helfrich theory[24,25], the curvature elastic energy or bending energy per unit area of lipid bilayer is defined as follows

$$E_{bend} = \frac{1}{2}\kappa\,(C_1 + C_2 - C_0)^2 \tag{1.5}$$

where $C_1 = \frac{1}{R_1}$ and $C_2 = \frac{1}{R_2}$ are principle curvatures, R_1 and R_2 are the principle radii of curvature. C_0 is spontaneous curvature which is zero for symmetric membranes and non-zero for asymmetric membranes. κ is the bending rigidity modulus, which for lipids such as DMPC is

around 10×10^{-20} J$\sim$ $20K_BT$ (K_BT is the thermal energy) in the fluid phase. As a result, thermal energy is sufficient to excite bending modes of the membrane in the fluid phase, giving rise to thermal shape fluctuations of giant unilamellar vesicles that can be observed under an optical microscope[25].

From Helfrich theory, the spectrum of thermal undulations of a planar bilayer, lying in the x-y plane, is given by[24,25]

$$\langle u(q_\perp)^2 \rangle = \frac{k_BT}{\sigma q_\perp^2 + \kappa q_\perp^4} \tag{1.6}$$

where $q_\perp = \sqrt{q_x^2 + q_y^2}$. $u(q_\perp)$ is the amplitude of undulations and σ is tension in the membrane. The procedure for experimentally obtaining the undulation spectrum is discussed in chapter 2. κ depends on many parameters, such as the surface charge density, membrane thickness and temperature. In the gel phase of the bilayer, it is about two orders of magnitude higher than the ambient thermal energy (k_BT, k_B being the Boltzmann constant). So thermal undulations are not visible in the gel phase.

The area of a lipid bilayer changes under tension and the corresponding energy is called the stretching energy, which is defined as follows[24].

$$E_{stretch} = \frac{1}{2}K\left(\frac{\Delta A}{A}\right)^2 \tag{1.7}$$

$$Tension(\sigma) = K\frac{\Delta A}{A} \tag{1.8}$$

where K is the elastic modulus of stretching or the area expansion modulus. A is the area of bilayer in the absence of tension, and ΔA is the change in area due to applied tension (σ). The area expansion modulus of lipid bilayers is in the order of 0.1 J/m^2. The direct stretching of the membrane is observed only at tensions of the order of mN m^{-1}. At lower tensions, smoothing of thermal undulations is observed[26]. From the measurement of area expansion versus tension in a micropipette aspiration experiment[26,27] both K and κ can be obtained by using equation 1.8 and the following equation, respectively[25,28,29].

$$\frac{\Delta A}{A} \simeq \frac{k_BT}{8\pi\kappa}\ln\sigma \tag{1.9}$$

Using both classical elastic theory or the polymer brush model, the bending rigidity and area expansion moduli can be related as follows[30–32]

$$\kappa = \beta K(2d_c)^2 \tag{1.10}$$

where β is a constant which depends on the coupling between the two leaflets of the bilayer and $2d_c$ is the thickness of the hydrophobic core of the bilayer. If the two leaflets are uncoupled and free to slide on one another $\beta = 1/48$. For the case of completely coupled leaflets $\beta = 1/12$. In polymer brush model $\beta = 1/24$. According to the classical elasticity theory, K depends linearly on the thickness of the bilayer. So effectively $\kappa \propto d_c^3$. If K is independent of bilayer thickness as in the polymer brush model $\kappa \propto d_c^2$. Rawicz et al.[30] independently measured K, κ and thickness of the lipid bilayer made up of different lipids and found good agreement with the polymer brush model.

Curvature of the bilayer-water interface at the bilayer edge leads to a contribution to the energy of the bilayer, called the edge energy. In the case of a flat circular bilayer with radius, l, edge energy is given as follows[33,34].

$$E_{edge} = 2\pi l\gamma \tag{1.11}$$

where γ is the edge line tension. Since the edge energy increases with the radius of the bilayer patch, beyond a critical value of the radius it is energetically favourable for it to form a spherical shell, called a vesicle. The elastic energy of a vesicle is independent of its radius. The threshold radius at which this happens is given by $2\kappa/\gamma$. The typical value of threshold radius is around 10 nm[35,36].

Vesicles can have various sizes from 10s of nano meters to 10s of microns. Vesicles with size in the range of 20 nm to 100 nm are called small unilammelar vesicles (SUV). Large unilammelar vesicles (LUV) typically have 100 nm to 1000 nm size. Vesicles with 1 µm to 200 µm size are called giant unilamellar vesicles (GUV)[37].

We have used various morphologies of bilayers, namely GUV, SUV, multilamellar vesicles(MLV), aligned bilayer stacks and supported bilayer as shown in figure 1.6. As mentioned in the figure, different experimental methods are used to obtain various morphologies of the bilayer.

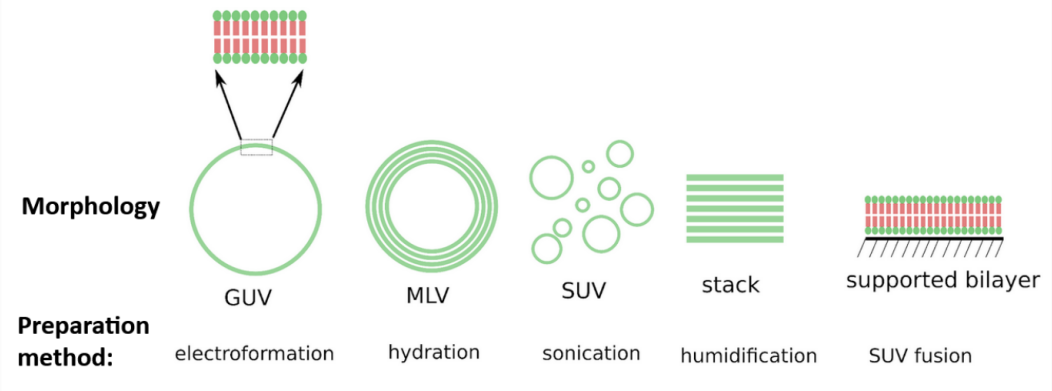

FIGURE 1.6: Morphologies of lipid bilayers and their methods of preparation.

In the studies described here, we have used various experimental methods, namely vesicle fluctuation analysis (VFA), micropipette aspiration, fluorescence and phase contrast microscopy, differential scanning calorimetry, x-ray scattering technique and Fluorescence recovery after photobleaching (FRAP). The details of these experimental methods are provided in the subsequent chapters.

By utilizing the above mentioned experimental techniques, we have probed various properties of bilayers such as phase behaviour, bending rigidity (κ), bilayer thickness (d_{HH}), electron density profile and diffusion coefficient. The experimental methods and the properties probed are summarized in figure 1.7

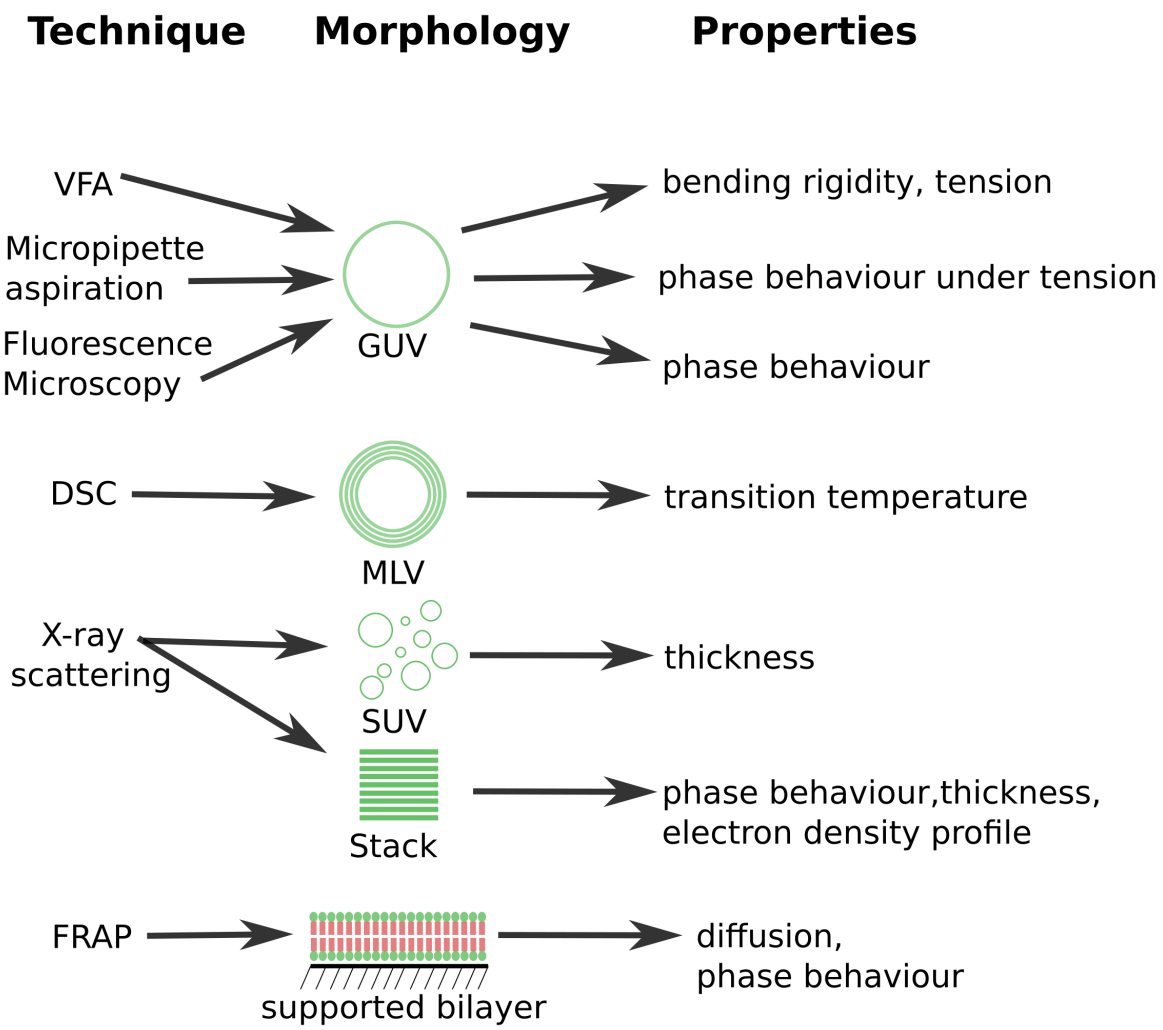

FIGURE 1.7: List of techniques used on various lipid bilayer morphologies and the properties probed.

Bibliography

[1] Bruce A, Alexander J, Julian L, Martin R, Keith R, Peter W. Molecular Biology of the Cell. Garland Science; 2002.

[2] Phillips R, Ursell T, Wiggins P, Sens P. Emerging roles for lipids in shaping membrane-protein function. Nature. 2009;459(7245):379–385.

[3] Tanford C. Theory of micelle formation in aqueous solutions. The Journal of Physical Chemistry. 1974;78(24):2469–2479.

[4] Israelachvili JN, Mitchell DJ, Ninham BW. Theory of self-assembly of hydrocarbon amphiphiles into micelles and bilayers. Journal of the Chemical Society, Faraday Transactions 2: Molecular and Chemical Physics. 1976;72:1525–1568.

[5] Israelachvili JN. Intermolecular and Surface Forces. Elsevier Science; 2011.

[6] Nagarajan R. Self-Assembly from Surfactants to Nanoparticles–Head vs. Tail. Self-Assembly: From Surfactants to Nanoparticles. 2019;.

[7] Liu AL. Advances in planar lipid bilayers and liposomes. Elsevier; 2011.

[8] Smith G, Sirota E, Safinya C, Plano R, Clark NA. X-ray structural studies of freely suspended ordered hydrated DMPC multimembrane films. The Journal of chemical physics. 1990;92(7):4519–4529.

[9] Chapman D. Phase transitions and fluidity characteristics of lipids and cell membranes. Q Rev Biophys. 1975;8(2):185–235.

[10] Karmakar S, Raghunathan V. Structure of phospholipid-cholesterol membranes: An x-ray diffraction study. Physical Review E. 2005;71(6):061924.

[11] Baumgart T, Hess ST, Webb WW. Imaging coexisting fluid domains in biomembrane models coupling curvature and line tension. Nature. 2003;425(6960):821–824.

[12] Simons K, Ikonen E. Functional rafts in cell membranes. Nature. 1997;387(6633):569–572.

[13] Dietrich C, Bagatolli L, Volovyk Z, Thompson N, Levi M, Jacobson K, et al. Lipid rafts reconstituted in model membranes. Biophys J. 2001;80(3):1417–1428.

[14] Veatch SL, Keller SL. Seeing spots: complex phase behavior in simple membranes. Biochim Biophys Acta Mol Cell Res. 2005;1746(3):172–185.

[15] Toulmay A, Prinz WA. Direct imaging reveals stable, micrometer-scale lipid domains that segregate proteins in live cells. Journal of Cell Biology. 2013;202(1):35–44.

[16] Levental I, Grzybek M, Simons K. Raft domains of variable properties and compositions in plasma membrane vesicles. Proceedings of the National Academy of Sciences. 2011;108(28):11411–11416.

[17] Kenworthy AK, Petranova N, Edidin M. High-resolution FRET microscopy of cholera toxin B-subunit and GPI-anchored proteins in cell plasma membranes. Mol Biol Cell. 2000;11(5):1645–1655.

[18] Sharma P, Varma R, Sarasij R, Gousset K, Krishnamoorthy G, Rao M, et al. Nanoscale organization of multiple GPI-anchored proteins in living cell membranes. Cell. 2004;116(4):577–589.

[19] Kusumi A, Koyama-Honda I, Suzuki K. Molecular dynamics and interactions for creation of stimulation-induced stabilized rafts from small unstable steady-state rafts. Traffic. 2004;5(4):213–230.

[20] McMahon HT, Gallop JL. Membrane curvature and mechanisms of dynamic cell membrane remodelling. Nature. 2005;438(7068):590–596.

[21] McMahon HT, Boucrot E. Membrane curvature at a glance. J Cell Sci. 2015;128(6):1065–1070.

[22] Makowski SL, Kuna RS, Field SJ. Induction of membrane curvature by proteins involved in Golgi trafficking. Advances in biological regulation. 2020;75:100661.

[23] Nussenzveig HM. Cell membrane biophysics with optical tweezers. European Biophysics Journal. 2018;47(5):499–514.

[24] Helfrich W. Elastic properties of lipid bilayers: theory and possible experiments. Z Naturforsch C. 1973;28(11-12):693–703.

[25] Helfrich W, Servuss RM. Undulations, steric interaction and cohesion of fluid membranes. Il Nuovo Cimento D. 1984;3(1):137–151.

[26] Evans E, Needham D. Physical properties of surfactant bilayer membranes: thermal transitions, elasticity, rigidity, cohesion and colloidal interactions. The Journal of Physical Chemistry. 1987;91(16):4219–4228. Available from: https://doi.org/10.1021/j100300a003.

[27] Evans E, Rawicz W. Entropy-driven tension and bending elasticity in condensed-fluid membranes. Phys Rev Lett. 1990;64(17):2094.

[28] Henriksen JR, Ipsen JH. Measurement of membrane elasticity by micro-pipette aspiration. Eur Phys J E Soft Matter. 2004;14(2):149–167.

[29] Bassereau P, Sorre B, Lévy A. Bending lipid membranes: experiments after W. Helfrich's model. Advances in colloid and interface science. 2014;208:47–57.

[30] Rawicz W, Olbrich KC, McIntosh T, Needham D, Evans E. Effect of chain length and unsaturation on elasticity of lipid bilayers. Biophysical journal. 2000;79(1):328–339.

[31] Bermudez H, Hammer D, Discher D. Effect of bilayer thickness on membrane bending rigidity. Langmuir. 2004;20(3):540–543.

[32] Nagle JF. Introductory lecture: basic quantities in model biomembranes. Faraday discussions. 2013;161:11–29.

[33] Huang C, Quinn D, Sadovsky Y, Suresh S, Hsia KJ. Formation and size distribution of self-assembled vesicles. Proceedings of the National Academy of Sciences. 2017;114(11):2910–2915.

[34] Li J, Pastor KA, Shi AC, Schmid F, Zhou J. Elastic properties and line tension of self-assembled bilayer membranes. Physical Review E. 2013;88(1):012718.

[35] Maulucci G, De Spirito M, Arcovito G, Boffi F, Castellano AC, Briganti G. Particle size distribution in DMPC vesicles solutions undergoing different sonication times. Biophysical journal. 2005;88(5):3545–3550.

[36] Israelachvili JN, Mitchell DJ, Ninham BW. Theory of self-assembly of lipid bilayers and vesicles. Biochimica et Biophysica Acta (BBA)-Biomembranes. 1977;470(2):185–201.

[37] Rideau E, Dimova R, Schwille P, Wurm FR, Landfester K. Liposomes and polymersomes: a comparative review towards cell mimicking. Chemical society reviews. 2018;47(23):8572–8610.

Chapter 2

Vesicle Fluctuation Analysis

2.1 Introduction and theory

Vesicle fluctuation analysis (VFA) is a popular technique to obtain bending rigidity (κ) of lipid bilayers. The theoretical description of thermal fluctuations of planar membranes is given by Helfrich[1] and for the spherical case by Milner and Safran[2]. Using this technique, the first estimate of bending rigidity of red blood cells (RBC) was obtained by Brochard and Lennon[3]. The technique has been extended to tubular vesicles[4] and then to quasi-spherical giant unilamellar vesicles (GUV)[5]. With technical advancement in the preparation of GUVs and image analysis, VFA has been used in recent times for more complex membranes, such as multi-component lipid membranes in the presence of proteins and peptides[6,7].

In this technique, a series of images of a vesicle is taken, and the contour of the vesicle in each image is extracted by image analysis. From the contours, bending rigidity can be obtained from time correlation function[8], angular correlation function[9], or Fourier spectrum of shape fluctuations[10]. In this study, we obtain bending rigidity (κ) and tension (σ) of membranes using the Fourier analysis method by following the procedure of Pécréaux et al[11].

In this method, each contour is expressed as a Fourier series in sine and cosine form. Fourier coefficients (a_n, b_n) are obtained for each mode (n). Variances of a_n, b_n over ensemble average are calculated. The experimental spectrum (u) is obtained by using the equation

$$\langle \mid u(q_x, y=0) \mid^2 \rangle = \frac{\pi \langle R \rangle^3}{2} \left[(\langle a_n^2 \rangle - \langle a_n \rangle^2) + (\langle b_n^2 \rangle - \langle b_n \rangle^2) \right] \tag{2.1}$$

where $\langle R \rangle$ is average radius of the vesicle.

From Helfrich theory, the spectrum of membrane fluctuations is given by

$$\langle u(q_\perp)^2 \rangle = \frac{k_B T}{\sigma q_\perp^2 + \kappa q_\perp^4} \tag{2.2}$$

where $q_\perp = \sqrt{q_x^2 + q_y^2}$. q_x, q_y are wave vectors in two principle directions of the surface. In an experiment, the equatorial plane of the vesicle is imaged. So the measured spectrum is as follows[11]

$$\langle \mid u(q_x, y=0) \mid^2 \rangle = \frac{k_B T}{2\sigma} \left[\frac{1}{q_x} - \frac{1}{\sqrt{\frac{\sigma}{\kappa} + q_x^2}} \right] \tag{2.3}$$

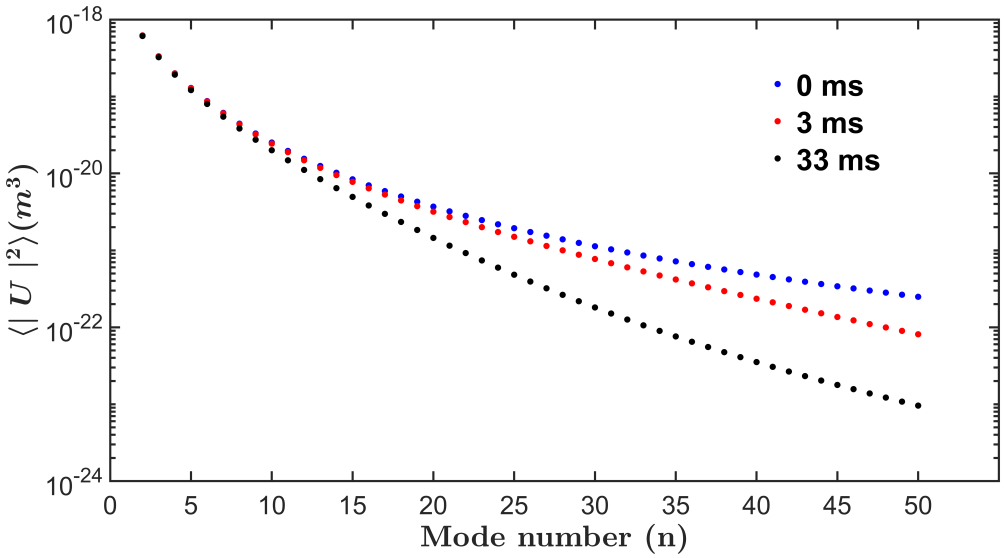

FIGURE 2.1: The vesicle fluctuation spectrum calculated using equation 2.5 with different values of camera exposure time (τ_c) for vesicle radius= 16.4 µm, tension= 1.85×10^{-8} N/m and bending rigidity= 14.5×10^{-20} J. Note that the spectrum is affected even if τ_c is as low as 3 ms.

The mode number (n) and wave vector q_x are related as $q_x = n/\langle R \rangle$. The relaxation time of the bending modes varies with mode number (n) from a fraction of a second to the order of a millisecond, and for planner geometry it is given by[11],

$$\tau_n(q_\perp)^{-1} = \frac{(\sigma q_\perp^2 + \kappa q_\perp^4)}{4\eta q_\perp} \tag{2.4}$$

where η is the coefficient of viscosity of the medium.

The exposure time of a camera (τ_c) is typically of the order of milliseconds. So the amplitude of modes, with decay times in the order of milliseconds, gets reduced due to smearing. To account for this, Faucon et al.[12] have given a correction factor to the spectrum which is highlighted in equation 2.5. Figure 2.1 shows the effect of the camera integration time on each mode. It is clear that with increasing exposure time, amplitude of each mode is further reduced. So a correction factor for τ_c is needed.

$$\begin{aligned} \langle |\, u(q_x, y=0)\, |^2 \rangle = \int_0^\infty \frac{2K_BT}{\pi} \frac{\tau_n(\zeta)}{4\eta q_x \sqrt{1+\zeta^2}} \times \\ \left[\frac{\tau_n^2(\zeta)}{\tau_c^2} \left(\frac{\tau_c}{\tau_n(\zeta)} + exp(\frac{-\tau_c}{\tau_n(\zeta)}) - 1 \right) \right] \quad q_x d\zeta \\ \zeta = \frac{q_y}{q_x} \end{aligned} \tag{2.5}$$

In the experiment, we measure fluctuations of spherical membranes, i.e., vesicles. In the literature, it is shown that amplitudes of modes above the sixth do not depend on the geometry of the membrane[11]. This approximation is valid due to the faster relaxation of the higher modes, so that they are more localized than the lower modes. We have fitted equations relevant to the planar geometry to experimental data by ignoring modes below the sixth.

Fluorescence[5], differential interference contrast (DIC)[9], and phase contrast microscopy[10,12] can be used to observe vesicles. Among these, phase contrast imaging is better as it provides a good contrast image of a vesicle with lower exposure time and without the use of a dye, which may affect κ[13]. A typical image of a vesicle is shown in figure 2.2 in both fluorescence and phase-contrast with sucrose inside and dextrose outside.

In the analysis of vesicle shape fluctuations, finding the contour of the vesicle is the first step. In initial studies, the pixel with the minimum intensity or with the highest slope in the intensity profile was taken as the membrane position[5,10,12]. So the accuracy in finding the contour is limited to pixel size. In time, various algorithms were reported to find the contour with sub-pixel accuracy[9,14,15]. Döbereiner et al.[16] followed an algorithm to obtain complete contour with accuracy of a sub-pixel by linear fitting the intensity profile around the steepest region and finding its intersection with the background intensity, as shown in figure 2.3 and 2.4. Some other procedures with slight variations are used in the literature to obtain the membrane position[11,14,15].

The accuracy in finding the contour depends on the contrast of the vesicle image. Sucrose and glucose solutions are used inside and outside to enhance the contrast of a vesicle in phase-contrast imaging. Due to the slightly higher density of sucrose, vesicles settle down to the bottom of the observation chamber, which enables us to capture images while they are in focus. Due to their weight, the vesicle can get deformed to non-spherical shapes[17], and these effects are dominant in vesicles with radius above a threshold (R_{max}) given by

$$R_{max} = \sqrt{\frac{\frac{\sigma}{\kappa} + \sqrt{(\frac{\sigma}{\kappa})^2 + \frac{4\Delta\rho g}{\kappa}12}}{\frac{2\Delta\rho g}{\kappa}}} \tag{2.6}$$

here $\Delta\rho$ is the density difference between the interior and exterior solutions of a vesicle. g is the acceleration due to gravity.

Another experimental parameter that needs to be taken care of is the depth of focus of the microscope objective. The effect of this on the spectrum has been recently studied by Rautu et al.[18]. It is observed that due to the finite depth of focus, membrane fluctuations get averaged out, which leads to lowering of the amplitudes and an increase in the bending rigidity. So correction for this is needed to get accurate values of κ. But analytical functional form for the case of planar membrane is not available. So, for the studies reported in this thesis, we have not included correction for depth of focus effects to the spectrum.

2.2 Materials

1,2-dimyristoyl-sn-glycero-3-phosphocholine (DMPC) and 1-stearoyl-2-oleoyl-sn-glycero-3- phospho choline (SOPC) were purchased from Avanti polar lipids. Rhodamine B 1,2-dihexadecanoyl-sn-glycero-3- phosphoethanolamine, triethylammonium salt (rhodamine DHPE) was obtained from Invitrogen bioservices. Sucrose and glucose were obtained from Sigma Aldrich. Indium tin oxide (ITO) coated glass plates with a sheet resistance of 10 Ω/sq were bought from Techinstro. Milli Q water is used for preparing the solutions. All chemicals are used as received.

2.3 Methods

The experimental and data analysis procedures consists of the following steps.

- Vesicle preparation
- Vesicle observation
- Contour detection
- Fourier analysis
- Fitting the theoretical model to the experimental spectrum

These are discussed in detail in the following sections.

2.3.1 Vesicle preparation using Electro-formation method

GUVs are prepared using the Electro-formation method described in the literature[19–21]. Stock solutions of lipid with 1 mg/ml concentration and Rhodamine DHPE dye with 0.1 mg/ml concentration are prepared by first dissolving them in chloroform and then mixing them appropriately to get a 0.1 molar relative concentration of dye in the final solution. The electro-formation or vesicle preparation chamber is made by pasting a Teflon ring of thickness 2 mm and diameter 18 mm on ITO plate. Around 10 - 15 µL of lipid solution is spread on the ITO plate and left for a minimum of 3 hours to let chloroform evaporate. During this process, we cover the ITO plate with aluminum foil to avoid bleaching of dye due to ambient light. Around 1.5 ml of 50 mM sucrose solution is introduced into the chamber and then covered with another ITO plate to make an electro-formation chamber. For electro-formation of vesicles, an alternating voltage of square waveform with 0.6 Vrms and 12 Hz frequency is applied between the ITO plates for 60 to 90 minutes. Subsequent to that, for 10 - 15 minutes, we reduce the frequency to 3 Hz and voltage to 0.3 Vrms to detach the vesicles from the surface. Vesicle formation happens only in the fluid phase of the bilayer. So the temperature of ITO plates is maintained above the main phase transition temperature (T_m) by keeping them on a hot plate. Once vesicles are formed, the vesicle solution is transferred into a 2 ml vial and stored above T_m.

2.3.2 Vesicle observation

For vesicle observation, a homemade chamber is used. Temperature of the chamber is controlled by circulating water with the help of a Julabo water circulating unit. The bottom cover-slip of the chamber where vesicles sediment is treated with (3-mercaptopropyl) trimethoxy silane, to avoid sticking of vesicles to the cover-slip. Glucose solution of 54 mM concentration is used as the external medium for vesicles. First, we bring the chamber to a set temperature, then the vesicle solution is injected gently into it, and then the glucose solution is added to the chamber. In about 15 minutes, vesicles sediment to the bottom due to the density difference between sucrose and glucose. Then images of vesicles are captured.

We use either a 100X oil objective or a 60X air objective for phase-contrast imaging on an IX-70 Olympus microscope. A 3 ms exposure time of the camera (cool snap ez) is used. Since sucrose

and glucose solutions have different refractive indices, vesicles appear with good contrast. Quasi-spherical, debris-free vesicles with a radius around 10-20 μm are selected for studies. We use ImageJ [22,23] software for image acquisition.

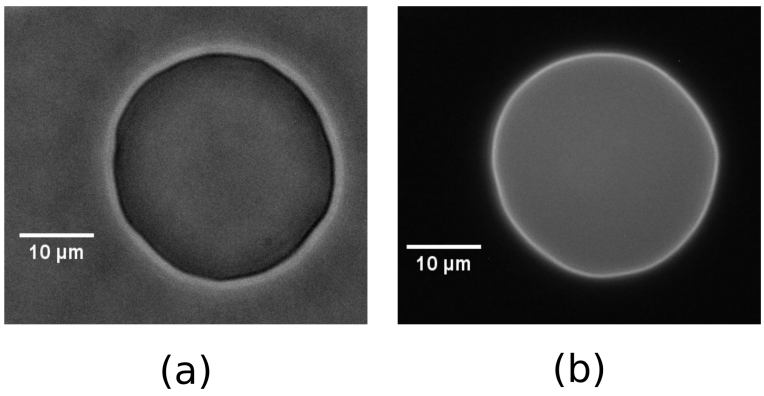

FIGURE 2.2: Typical image of a vesicle in a) phase contrast and b) fluorescence microscopy. For video of vesicle shape fluctuations please click here.

2.3.3 Algorithm for detecting contour

To carry out vesicle fluctuation analysis, we need to find the complete contour of the vesicle. For that, we use the halo effect around the vesicle as shown in figure 2.2. At the boundary of a vesicle, due to the halo, the intensity profile varies sharply as shown in figure 2.3 and 2.4, and it can be approximated as a linear curve in the high slope regime. The pixel, where the slope of the curve is maximum, contains the position of the membrane. To get the position of the membrane with sub-pixel accuracy, we consider the intersection point of the intensity profile with the local background intensity as shown in figure 2.4. This method gives an accurate value if the chosen direction is normal to the membrane. For this reason, we use four axes X, V, Y, and W, with V and W at 45 degrees to the X and Y axes, as shown in figure 2.5. This approach with multple axes and correction for the background has been described by Döbereiner et al. [16,24] and by Pécréaux et al. [11].

A global search is needed to find the first point of the contour. The intensity profile is obtained along a horizontal line drawn close to the diameter of the vesicle cross-section as shown in figure 2.3. The corresponding intensity varies as shown in figure 2.4.

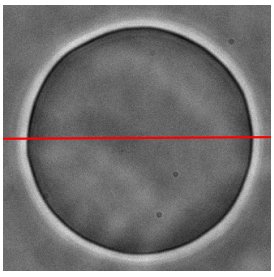

FIGURE 2.3: Intensity profile is taken along the line drawn across the image in order to determine the first contour point.

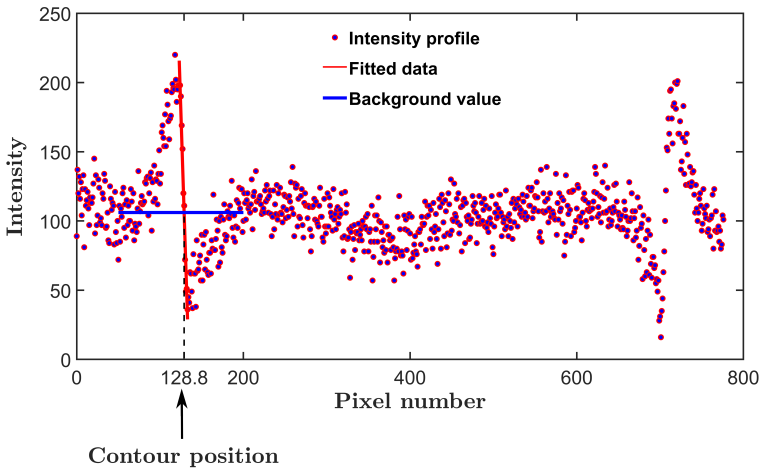

FIGURE 2.4: The procedure followed to find the first contour point. Details are provided in the text.

The algorithm used to find the first contour point with sub-pixel accuracy is described below. First, a window is defined with a width of 11 pixels from $x_i - 5$ to $x_i + 5$ pixels centered at x_i, where x_i is a point on the line drawn in figure 2.3. By fitting the intensity data to the linear equation $y = m_1 x + c_1$, the slope (m_1) and the intercept (c_1) are obtained. This procedure is repeated by moving the window pixel by pixel along the line and finding the maximum negative slope and the corresponding x_i. Here we choose negative slopes to start contour detection from the left part of the image. At the pixel with the maximum negative slope, the background intensity is obtained by averaging over a window of 14 pixels from $x_i - 7$ to $x_i + 7$. The intersection point of the fitted curve and the background is taken as the membrane position (x_0^c, y_0^c), and the integer parts or pixel coordinates are denoted as (x_0, y_0). Widths of the windows taken here are optimized by maximizing the number of closed contours that can be obtained for a given set of images, and depend on the magnification used to acquire images.

The procedure to find the next contour point should work everywhere along the contour. The algorithm used for this is summarised in figure 2.5. Contour is found in the clockwise direction. We divide the full contour into 8 regions. The next contour point exists in one of the 8 adjacent pixels of the first contour pixel (x_0, y_0). We consider the first contour point as the origin. Out of the 8 pixels, a set of three pixels is more probable, as shown in figure 2.5 and it varies from region to region.

As shown in figure 2.6, first the probable set of three pixels containing the next contour point is identified depending on the region of the contour. Taking each of these pixels to be at the centre of the window, the intensity profile is found along the appropriate direction, following the procedure used to find the first point on the contour. Then the slope of the intensity profile and the new contour position are obtained from each of the three pixels along the 4 axes as shown in figure 2.6. The final contour point is determined as the average of these four, weighted by the corresponding magnitude of the slope. Since one of the four chosen directions is always tangential to the contour, the slope along it has a small magnitude and random sign. The contour point calculated along this direction will also fluctuate. However, its contribution to the final value is negligible,

since the slope is very small.

A new contour point should satisfy a few conditions before getting accepted. To avoid artifacts like discontinuous contour and back traced contour, we apply the adjacent pixel test and direction test to the new contour point before accepting it. In the Adjacent pixel test, we check whether the new contour point is from among the adjacent pixels of the previous contour pixel or not. In the Direction test, two vectors are defined between (x^c_{i-1}, y^c_{i-1}) and (x^c_i, y^c_i), (x^c_i, y^c_i) and (x^c_{i+1}, y^c_{i+1}). When the contour is turning back or tracing back, the angle between these vectors is less than 90°. If it is the case, then that contour point is discarded. If the slope weighted contour point fails in the test, the contour point along the highest slope axis, second highest slope axis, and third-highest slope axis are preferred in that order. In case none of them pass the test, the program discards the current image and goes to the next image. If the new contour point is equal to the first contour point (x_0, y_0), we take it as a closed contour. Sometimes the program can go into a local loop. To avoid such cases, we keep a maximum limit of 5000 on the number of contour points. These algorithms are implemented in LabVIEW.

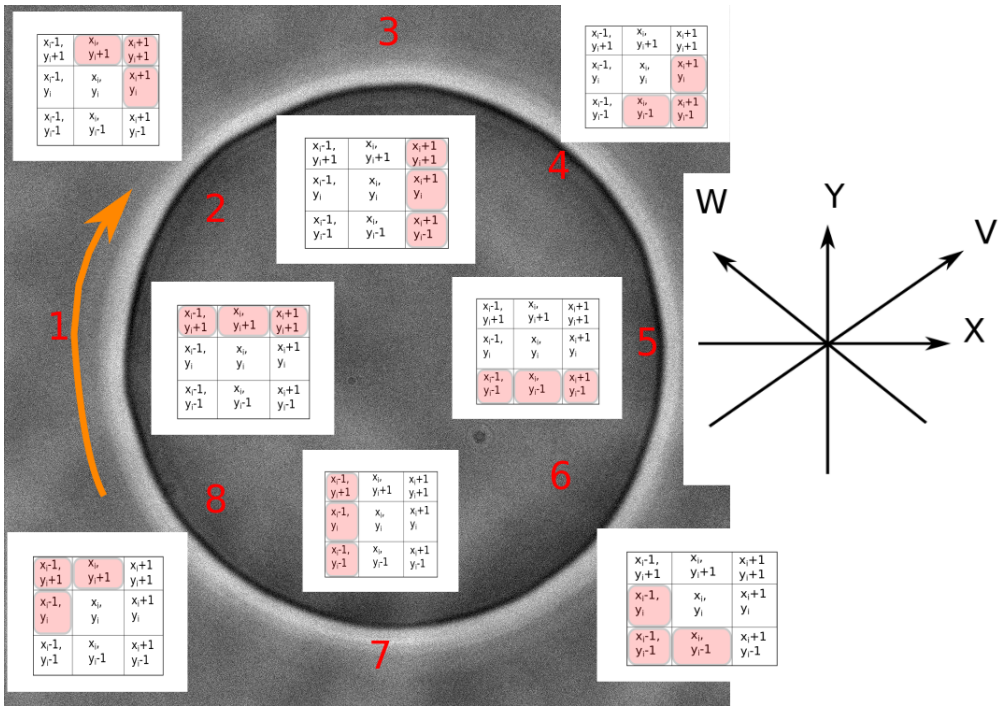

FIGURE 2.5: The total contour is divided into 8 regions.The probable sets of three neighboring pixels containing the next contour point are highlighted in red color. We identify the probable pixel coordinates in each region by using the signs of m_x, m_y, m_v, and m_w.

Sometimes during the acquisition of images, other vesicles can come into contact with the vesicle under observation. In the observation chamber, in time, bacteria can grow and come in contact with membranes. In these cases, the detected contour can have artifacts. To check for inhomogeneity in the contour, we conduct a Direction test and a Length test for each contour. In the Direction test, two sets of 30 consecutive contour points are taken with a separation of 20 points. Each set is fitted with a linear equation. The angle between the directions of the two lines is calculated. It is repeated along the contour by moving the sets point by point. If anywhere in

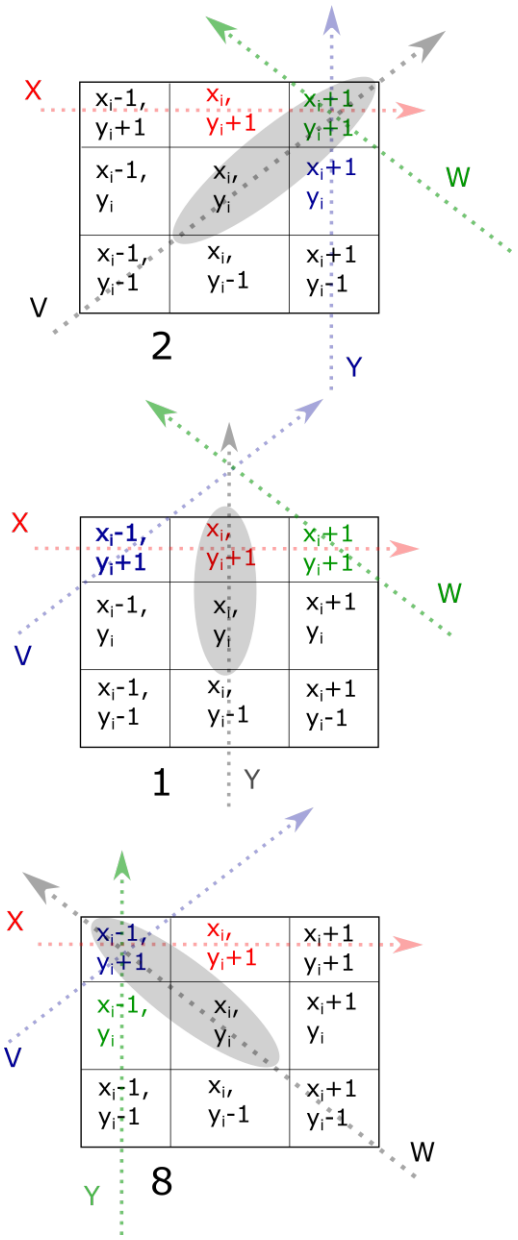

FIGURE 2.6: The procedure followed to assign axes to the corresponding probable pixels. At each of the three probable pixels, slopes of the intensity profile is calculated along the appropriate directions. Both the axes and the corresponding pixels are shown in the same color. In the tangential direction of the contour, the slope sign fluctuates between positive and negative values of negligible magnitude. So, there are two probable pixels in that direction, which are highlighted in gray color. Here we show the procedure only for 1,2, and 8 regions, but a similar procedure is followed for the rest.

the contour the angle between the two lines is more than 90°, those contours are discarded. In the Length test, contours whose length differ by more than 10% of the average contour length in a set, are discarded. We observe only a very few contours that get discarded for these reasons.

2.3.4 Fourier analysis of the contours

Since the vesicle shape in the image is quasi-circular, working in polar coordinates is a natural choice for Fourier analysis. The center of the vesicle (x_m, y_m) is needed for defining the polar

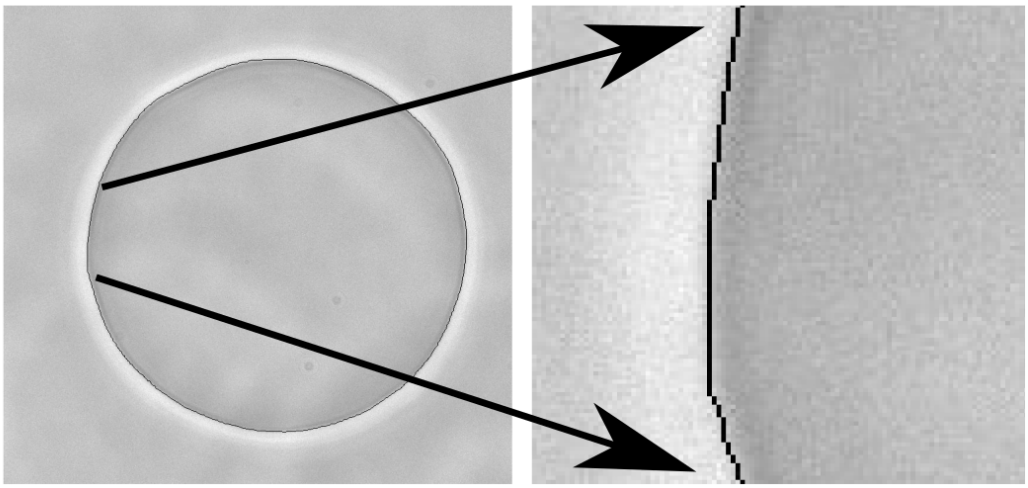

FIGURE 2.7: Image of a vesicle with the detected contour superposed.

coordinates. It is obtained by averaging x and y coordinates of the contour points weighted by the sum of distances from preceding and succeeding contour points as given in equations 2.7 and 2.8.

$$x_m = \frac{1}{2L}\sum_{i=1}^{N} x_i^c \times (s_{i-1} + s_i) \tag{2.7}$$

$$y_m = \frac{1}{2L}\sum_{i=1}^{N} y_i^c \times (s_{i-1} + s_i) \tag{2.8}$$

where

$$L = \sum_{i=1}^{N} s_i \quad and \quad s_i = \sqrt{(x_{i+1}^c - x_i^c)^2 + (y_{i+1}^c - y_i^c)^2}$$

N is total number of contour points.
Contour coordinates in Cartesian form are converted into polar coordinates (r, θ). Contour is expressed in Fourier series expansion with a_n and b_n as Fourier coefficients and n as mode number by using the following equations.

$$r(\theta) = R\big[1 + \sum_{n=1}^{\infty} \big(a_n cos(n\theta) + b_n sin(n\theta)\big)\big] \tag{2.9}$$

$$R = \frac{1}{2\pi}\sum_{i=1}^{N} \left(\frac{r_i + r_{i+1}}{2}\right)(\theta_{i+1} - \theta_i) \tag{2.10}$$

$$a_n = \frac{1}{\pi R}\sum_{i=1}^{N} (r_i cos(n\theta_i) + r_{i+1} cos(n\theta_{i+1}))\frac{(\theta_{i+1} - \theta_i)}{2} \tag{2.11}$$

$$b_n = \frac{1}{\pi R}\sum_{i=1}^{N} (r_i sin(n\theta_i) + r_{i+1} sin(n\theta_{i+1}))\frac{(\theta_{i+1} - \theta_i)}{2} \tag{2.12}$$

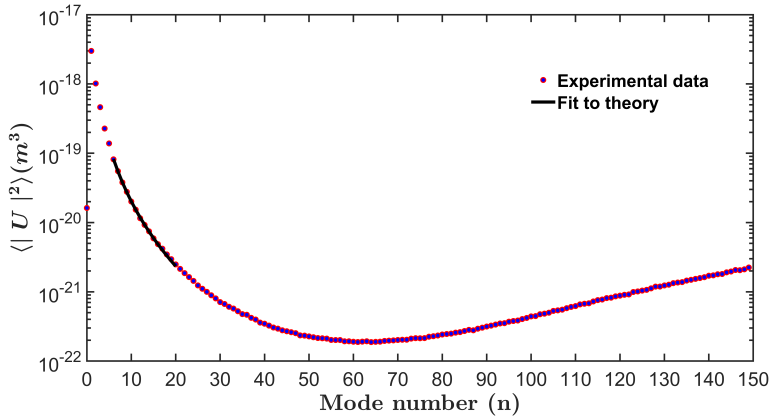

FIGURE 2.8: Typical fluctuation spectrum of a DMPC vesicle of radius 15.5 µm. The solid line is the fit to equation 2.5. From the fit, values of σ and κ are found to be 1.1×10^{-8} N/m and 16.7×10^{-20} J, respectively.

Values of average radius ($\langle$ R $\rangle$), a_n and b_n are inserted in equation 2.13 to obtain the spectrum as a function of n.

$$\langle | u(q_x, y = 0) |^2 \rangle = \frac{\pi \langle R \rangle^3}{2} \left[(\langle a_n^2 \rangle - \langle a_n \rangle^2) + (\langle b_n^2 \rangle - \langle b_n \rangle^2) \right] \tag{2.13}$$

We have implemented contour Fourier analysis in LabVIEW.

2.3.5 Fitting the model spectrum to the experimental data

A typical spectrum of vesicle fluctuations is shown in figure 2.8. The amplitudes are in the range of 10^{-18} m^3 to 10^{-22} m^3. Initially, the amplitude decreases with n and then increases. The reduction of amplitude as n increases is in accordance with Helfrich's theory, and it can be understood in terms of the higher curvature of higher modes. For the same amount of thermal energy, i.e., k_BT, lower modes with smaller curvature acquire higher amplitudes. As discussed in the earlier section, due to the approximation of quasi-spherical membrane as a planar membrane, the modes from 1^{st} to 5^{th} are not considered in the fitting procedure. The increase in the spectrum amplitude beyond the 60^{th} mode is due to the discreteness of the image. Gittes et al.[25] have provided a model to quantify noise due to discreetness of an image in Fourier spectrum for a one-dimensional case. But for the case of a vesicle, models are not available. So we could not subtract its contribution to the spectrum.

We calculate the spectrum from equation 2.5 by varying values of σ and κ in a step by step manner within fixed range and estimate the deviation from the experimental spectrum. Final values of σ and κ are obtained by minimizing the modulus of the deviation by giving higher weightage to the lower modes. A typical fit to the observed spectrum is shown in figure 2.8. Bending rigidities of a minimum of 10 to 20 vesicles are measured per lipid system. The inverse of fitting error is used as a weighting factor to obtain the final κ of the membrane. We use Mathematica for fitting the model to the observed spectrum.

Vesicles whose spectra fit well till the 20^{th} mode are only considered for calculating bending rigidity. We observe that the spectra of vesicles with parameters in the range $10 \leq$ R ≤ 25 µm, $10^{-8} \leq \sigma \leq 25 \times 10^{-8}$ N/m and $1 \times 10^{-20} \leq \kappa \leq 50 \times 10^{-20}$ J are fitted well to the theoretical model till a minimum of 20 modes.

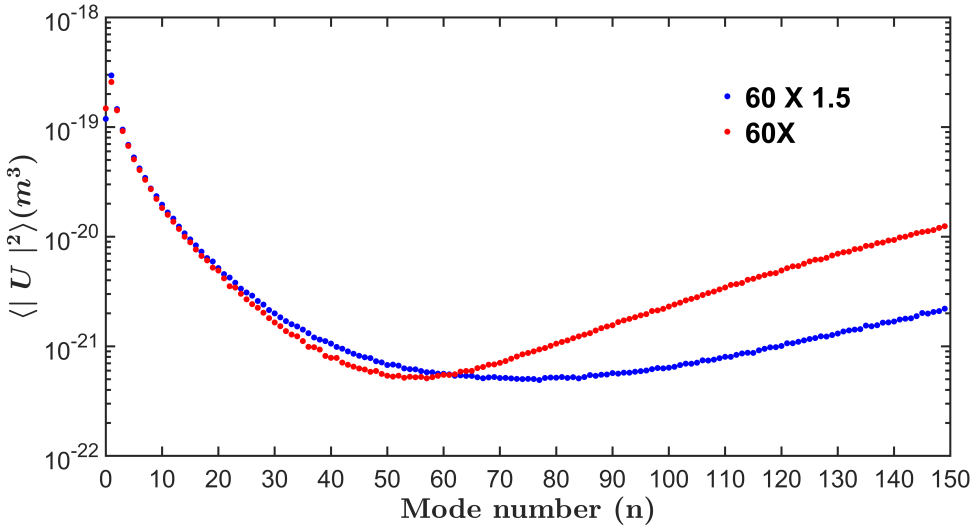

FIGURE 2.9: The effect of magnification on the spectrum of the same SOPC vesicle (R= 25.3 µm, τ_c = 3 ms). The obtained values of κ and σ are listed in table 2.1.

2.4 Results and discussions

In the literature, various possible artifacts related to the VFA technique, such as camera exposure time and depth of focus, are discussed [12,18]. While comparing the bending rigidities, which are measured with different experimental settings, we need to consider these artifacts. To understand these artifacts, we have studied the role of magnification of the microscope objective and the camera exposure time in the estimation of κ.

2.4.1 Effect of the microscope objective and the magnification on vesicle fluctuation spectrum

In the Olympus microscope (IX 71), there is a provision to insert a lens with 1.5X magnification into the optical path. So we can change the magnification without changing the objective. By using this, magnification effects are studied on the spectrum, and results are shown in figure 2.9. The two spectra are obtained for the same vesicle by using the 60X objective with two different magnifications. The spectrum in red color is obtained with bare 60X magnification, and the blue spectrum is obtained with the lens insert and hence at a magnification of 90X. In the spectrum, the amplitudes first decrease and then increase with increasing mode number. The cross over is at around the 50^{th} and the 70^{th} mode for 60X and 90X magnification, respectively. In the case of higher modes (> 70), amplitudes of the red spectrum are higher than the blue spectrum. As mentioned in the previous section, this part of the spectrum is affected by noise from the discreteness of the image.

TABLE 2.1: Observed differences in σ and κ on using different magnifications. Observations are done on the same SOPC vesicle.

Magnification	Tension (σ) (10^{-8} N/m)	Bending rigidity (10^{-20} J)
60X	15.3	23.2
60X1.5	15.1	20.2

For each vesicle, we acquire 3 sets of data with 2500 images per set. Only if the 3 spectra overlap as shown in figure 2.10 we consider them for further analysis. As can be seen from the figure, the error in each data point is typically comparable to the size of the symbol used. The two sets of data in figure 2.9, corresponding to two different magnifications, are clearly well separated. Hence the difference caused by the change in magnification is significant and not within the errors of measurement.

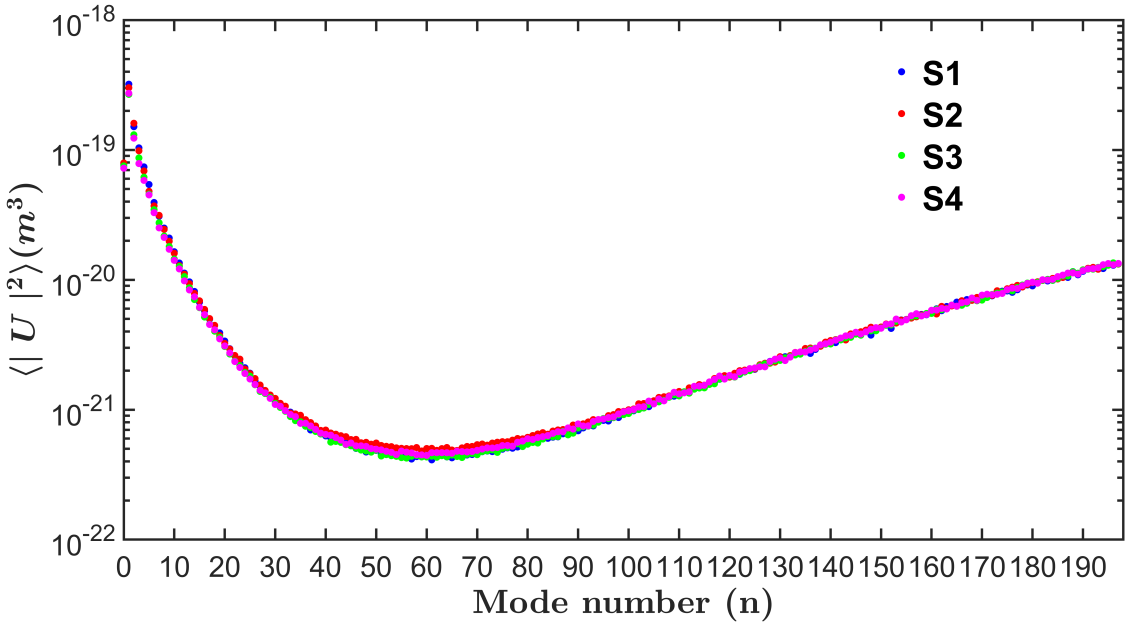

FIGURE 2.10: Shape fluctuation spectra of a vesicle. Each curve is obtained from a distinct data set consisting of 2500 images, captured sequentially. The overlap of the curves shows the stability of the vesicle during the observation time of around 15 minutes.

For studies at room temperature, a 100X oil immersion objective is used. Since oil is in contact with the observation chamber, convection currents are generated at higher temperatures. These currents make the vesicles move. To avoid the motion of vesicles, we use a 60X air objective for high-temperature studies. To compare the results from both room and high-temperature studies, we need to know the difference due to the different objectives. For this purpose, we measured fluctuations of DMPC vesicles by using both the objectives at room temperature. The results are summarized in table 2.2. As we lower the magnification (and numerical aperture (NA)) from 100X (NA=1.35) to 60X (NA=0.7) the average value of the bending rigidity increases slightly, but the difference is comparable to the error in the measurement. Hence we conclude that the variation in magnification from 100X to 60X has negligible effect on the value of κ.

TABLE 2.2: Average values of the bending rigidity modulus (κ) of DMPC membranes, for different magnifications at T = 28 °C. The exposure time of the camera is 3 ms.

Objective	κ (10^{-20} J)
100X (N.A=1.35)	16.9±0.8
60X (N.A=0.70)	19±2

2.4.2 Effect of the camera exposure time on fluctuation spectrum

We have systematically studied the effects of exposure time of the camera on the bending rigidity of DMPC lipid membrane. The results are summarized in table 2.3. Even after including correction for τ_c, with increasing exposure time (τ_c), the bending rigidity is systematically reduced.

TABLE 2.3: Bending rigidity of DMPC membranes obtained with different camera exposure times (τ_c) at T = 28 °C.

Objective	Exposure time of camera (τ_c)	Bending rigidity (10^{-20} J)
100X	3 ms	16.9±0.8
100X	18 ms	14.3±0.8
100X	33 ms	13.9±0.7

So when we compare results from two different studies, we should consider magnification, the numerical aperture of the objective, and the camera exposure time used in the studies.

2.4.3 Bending rigidity of some lipid bilayers

We have obtained bending rigidities of some standard lipid membranes, and the results are tabulated in table 2.4. In case of SOPC and SOPC:cholesterol membranes a 60X objective was used and τ_c=3 ms. For DMPC and POPC membranes a 100X objective was used and τ_c=3 ms. The values obtained are comparable to those reported in the literature[26–30]. As reported in the literature[11], a substantial enhancement of κ of SOPC membranes in the presence of cholesterol is observed.

TABLE 2.4: κ of some lipid bilayers at 28 °C

Lipids and Sterols	Bending rigidity (κ) (10^{-20} J)
SOPC	21.3±0.6
SOPC and Cholesterol (1:1)	44±2
DMPC	16.9±0.8
POPC	15.0±0.6

2.5 Conclusions

We have implemented the vesicle fluctuation analysis technique to estimate the tension and the bending rigidity of lipid bilayers in the form of vesicles. We have carried out some calibration measurements using different microscope objectives and camera exposure times. The bending rigidities of lipid bilayers made up of SOPC, DMPC, and POPC lipids are obtained and are found to agree very well with literature values.

Bibliography

[1] Helfrich W. Elastic properties of lipid bilayers: theory and possible experiments. Z Naturforsch C. 1973;28(11-12):693–703.

[2] Milner ST, Safran S. Dynamical fluctuations of droplet microemulsions and vesicles. Physical Review A. 1987;36(9):4371.

[3] Brochard, F , Lennon, J F . Frequency spectrum of the flicker phenomenon in erythrocytes. J Phys France. 1975;36(11):1035–1047. Available from: https://doi.org/10.1051/jphys:0197500360110103500.

[4] Beblik G, Servuss RM, Helfrich W. Bilayer bending rigidity of some synthetic lecithins. Journal de physique. 1985;46(10):1773–1778.

[5] Schneider M, Jenkins J, Webb W. Thermal fluctuations of large quasi-spherical bimolecular phospholipid vesicles. Journal de Physique. 1984;45(9):1457–1472.

[6] Méléard P, Pott T. Overview of a quest for bending elasticity measurement. In: Advances in planar lipid bilayers and liposomes. vol. 17. Elsevier; 2013. p. 55–75.

[7] Dimova R. Recent developments in the field of bending rigidity measurements on membranes. Advances in colloid and interface science. 2014;208:225–234.

[8] Schneider M, Jenkins J, Webb W. Thermal fluctuations of large quasi-spherical bimolecular phospholipid vesicles. Journal de Physique. 1984;45(9):1457–1472.

[9] Bivas I, Hanusse P, Bothorel P, Lalanne J, Aguerre-Chariol O. An application of the optical microscopy to the determination of the curvature elastic modulus of biological and model membranes. Journal de Physique. 1987;48:855–867.

[10] Engelhardt H, Duwe H, Sackmann E. Bilayer bending elasticity measured by Fourier analysis of thermally excited surface undulations of flaccid vesicles. Journal de Physique Lettres. 1985;46(8):395–400.

[11] Pécréaux J, Döbereiner HG, Prost J, Joanny JF, Bassereau P. Refined contour analysis of giant unilamellar vesicles. Eur Phys J E Soft Matter. 2004;13(3):277–290.

[12] Faucon J, Mitov M, Méléard P, Bivas I, Bothorel P. Bending elasticity and thermal fluctuations of lipid membranes. Theoretical and experimental requirements. J Phys France. 1989;50(17):2389–2414.

[13] Bouvrais H, Pott T, Bagatolli LA, Ipsen JH, Méléard P. Impact of membrane-anchored fluorescent probes on the mechanical properties of lipid bilayers. Biochimica et Biophysica Acta (BBA)-Biomembranes. 2010;1798:1333–1337.

[14] Gracia RS, Bezlyepkina N, Knorr RL, Lipowsky R, Dimova R. Effect of cholesterol on the rigidity of saturated and unsaturated membranes: fluctuation and electrodeformation analysis of giant vesicles. Soft Matter. 2010;6:1472–1482.

[15] Yoon YZ, Hale JP, Petrov PG, Cicuta P. Mechanical properties of ternary lipid membranes near a liquid–liquid phase separation boundary. Journal of Physics: Condensed Matter. 2010;22(6):062101.

[16] Döbereiner HG, Evans E, Kraus M, Seifert U, Wortis M. Mapping vesicle shapes into the phase diagram: A comparison of experiment and theory. Physical Review E. 1997;55(4):4458.

[17] Henriksen JR, Ipsen JH. Thermal undulations of quasi-spherical vesicles stabilized by gravity. The European Physical Journal E. 2002;9(4):365–374.

[18] Rautu SA, Orsi D, Di Michele L, Rowlands G, Cicuta P, Turner MS. The role of optical projection in the analysis of membrane fluctuations. Soft Matter. 2017;13:3480–3483. Available from: http://dx.doi.org/10.1039/C7SM00108H.

[19] Angelova MI, Dimitrov DS. Liposome electroformation. Faraday discussions of the Chemical Society. 1986;81:303–311.

[20] Bhatia T, Husen P, Brewer J, Bagatolli LA, Hansen PL, Ipsen JH, et al. Preparing giant unilamellar vesicles (GUVs) of complex lipid mixtures on demand: Mixing small unilamellar vesicles of compositionally heterogeneous mixtures. Biochimica et Biophysica Acta (BBA)-Biomembranes. 2015;1848(12):3175–3180.

[21] Meleard P, Bagatolli LA, Pott T. Giant unilamellar vesicle electroformation: From lipid mixtures to native membranes under physiological conditions. Methods in enzymology. 2009;465:161–176.

[22] Schneider CA, Rasband WS, Eliceiri KW. NIH Image to ImageJ: 25 years of image analysis. Nature methods. 2012;9(7):671–675.

[23] Schindelin J, Rueden CT, Hiner MC, Eliceiri KW. The ImageJ ecosystem: An open platform for biomedical image analysis. Molecular reproduction and development. 2015;82(7-8):518–529.

[24] Döbereiner HG, Gompper G, Haluska CK, Kroll DM, Petrov PG, Riske KA. Advanced flicker spectroscopy of fluid membranes. Physical review letters. 2003;91(4):048301.

[25] Gittes F, Mickey B, Nettleton J, Howard J. Flexural rigidity of microtubules and actin filaments measured from thermal fluctuations in shape. The Journal of cell biology. 1993;120(4):923–934.

[26] Faizi HA, Frey SL, Steinkühler J, Dimova R, Vlahovska PM. Bending rigidity of charged lipid bilayer membranes. Soft Matter. 2019;15:6006–6013. Available from: http://dx.doi.org/10.1039/C9SM00772E.

[27] Henriksen J, Rowat AC, Ipsen JH. Vesicle fluctuation analysis of the effects of sterols on membrane bending rigidity. European Biophysics Journal. 2004;33(8):732–741.

[28] Bouvrais H, Pott T, Bagatolli LA, Ipsen JH, Méléard P. Impact of membrane-anchored fluorescent probes on the mechanical properties of lipid bilayers. Biochimica et Biophysica Acta (BBA)-Biomembranes. 2010;1798(7):1333–1337.

[29] Meleard P, Gerbeaud C, Pott T, Fernandez-Puente L, Bivas I, Mitov MD, et al. Bending elasticities of model membranes: influences of temperature and sterol content. Biophysical journal. 1997;72(6):2616–2629.

[30] Mitkova D, Vitkova V. The aqueous surroundings alter the bending rigidity of lipid membranes. Russian Journal of Electrochemistry. 2016;52(12):1172–1178.

Chapter 3

Influence of alcohols on bending rigidity of Phospholipid bilayers

3.1 Introduction

Alcohols influence cell growth, cell division, and cell morphology[1]. Their anesthetic and antimicrobial properties have been known for more than a century[2]. Most of the studies on the interaction of alcohols with membranes have been focused on elucidating their anesthetic activity. Their anesthetic efficacy is found to depend on the chain length of the alcohol (C_n). They act as anesthetics below some critical chain length, whereas alcohols with longer chain length do not; this is called the cutoff effect[3]. Shorter chain alcohols increase volume per lipid, area per lipid, lipid diffusivity, and reduce chain order, membrane thickness, and main phase transition temperature (T_m). On the other hand, longer chain alcohols increase the chain order, membrane thickness, T_m, and reduce lipid diffusivity[4–12].

Very few experimental studies on the influence of alcohols on the bending rigidity (κ) of lipid bilayers were reported in the literature. It has been shown that alcohols from methanol to butanol lower κ of unsaturated lipid membranes[13]. Safinya et al.[14] indirectly obtained κ of surfactant - alcohol membranes, made up of sodium dodecyl sulphate (SDS) and alcohols of varying chain length, and a discontinuity in κ was observed at a chain length of 8. Foret et al.[15] have given a model to explain this observation. However, to our knowledge, in spite of their biological relevance, there are no systematic studies probing the influence of alcohols on lipid bilayer bending rigidity. So, we have studied the influence of alcohols on κ of 1,2-dimyristoyl-sn-glycero-3- phosphocholine (DMPC) lipid bilayers in the fluid phase by using the vesicle shape fluctuations analysis technique. We have measured alterations in κ as the alcohol concentration (m) and the chain length (C_n) are varied. The bending rigidity is known to depend on the thickness of the bilayer (d_{HH}). So, we have obtained d_{HH} from small-angle x-ray scattering experiments to understand the microscopic origin of the observed changes in κ.

This chapter discusses the effect of alcohols, namely ethanol, pentanol, hexanol, octanol, decanol, and dodecanol, on the bending rigidity and thickness of DMPC bilayers. GUVs are prepared using the electro-formation method[16]. Alcohols are introduced into the vesicle preparation and observation chambers by mixing them in the suspending aqueous solutions. In time, the alcohol is partitioned between the vesicles and water. The alcohol content in the membrane is tuned

by varying the alcohol concentration in the suspending solution. A reduction in κ is observed in the presence of ethanol to octanol, and no change is observed in the case of decanol and dodecanol. The observation of a sudden change in the trend from octanol to decanol is in agreement with the observations of Safinya et al.[14] on surfactant membranes.

To understand alterations caused by the alcohols in the bilayer structure, we have obtained the bilayer thickness from small-angle x-ray scattering experiments on dispersions of small unilamellar vesicles[17]. In correlation with a reduction in the bending rigidity, we have observed a reduction in the bilayer thickness from ethanol to octanol, and no thickness change is observed in the case of decanol.

3.2 Materials and Methods

3.2.1 Materials

1,2-dimyristoyl-sn-glycero-3- phosphocholine (DMPC) is purchased from Avanti polar lipids. Rhodamine b 1, 2-dihexadecanoyl-sn-glycero-3- phosphoethanolamine, triethylammonium salt (rhodamine DHPE) are obtained from Invitrogen bioservices. 1- pentanol, 1- hexanol, 1- octanol, 1-decanol, 1- dodecanol, 3-mercaptopropyl trimethoxy silane, sucrose, and glucose are obtained from Sigma Aldrich. Ethanol is obtained from Jebsen & Jessen. Indium tin oxide (ITO) glass plates with a sheet resistance of 10 Ω/sq are bought from Techinstro. Milli-Q water is used for preparing the solutions. All chemicals are used as received.

3.2.2 Differential scanning calorimetry (DSC)

Appropriate amounts of DMPC and alcohol are dissolved in deionized water to obtain a 10 w% lipid solution. A homogeneous solution is obtained by following the protocol described in the literature[18], which consists of repeated vortexing of the solution followed by temperature cycling between 4 °C and 45 °C. Samples are stored at 45 °C for 1 or 2 days prior to the experiments. The experiment is conducted on a Mettler Toledo (DSC-3 model) machine at 3 °C/minute scan rate with an initial 15 minutes of equilibration at 50 °C. The transition temperature is obtained from the cooling curves.

3.2.3 GUV preparation and observation

The procedure followed for vesicle preparation and observation is similar to that described in chapter 2, with small differences arising from the presence of alcohols. Alcohols are mixed with interior sucrose (50 mM) and exterior glucose (54 mM) water solutions. Decanol and dodecanol, at saturation concentration, increase T_m of DMPC from 24 °C to 28 °C and 35 °C, respectively, whereas ethanol to octanol reduces T_m. So, the temperature of vesicles is maintained at 30 °C in case of C_n= 2 to 8 and 38 °C for C_n=10 and 12 to keep them in the fluid phase. When a 100X oil immersion microscope objective is used to observe vesicles at 38 °C, convection currents appear and cause the motion of vesicles. To avoid this problem, we have used 60X air objective. When we use 100X and 60X objectives for VFA, slightly different bending rigidities are obtained for DMPC vesicles as shown in table 3.1. So, we have compared results obtained with the same objective at

the same temperature. The concentration limits used in this study are listed in table 3.3. If we increase the concentration further in the case of ethanol-octanol, in time, build up of tension in the vesicles is observed. Both decanol and dodecanol are used at the saturation concentration limit. Images are processed using the ImageJ software[19,20].

TABLE 3.1: Bending rigidity modulus (κ) of DMPC membranes obtained from VFA for different objective magnifications at T = 28±1 °C and 38±1 °C. A 3 ms camera exposure time is used.

Objective	κ (10^{-20} J)
100X (N.A=1.35), T=28 °C	16.9±0.8
60X (N.A=0.70), T=28 °C	19.2±1.9
60X (N.A=0.70), T=38 °C	18.5±1.5

3.2.4 Small angle x-ray scattering from small unilamellar vesicles (SUV)

We have obtained the form factor and the bilayer thickness of the membrane by measuring the scattering of x-rays from dispersions of SUVs. The ultrasonication method is used for the preparation of small unilamellar vesicles[21]. Appropriate amounts of water and alcohol are added to 10 to 15 mg of DMPC powder to obtain a 10 w% lipid solution. It is vortexed for 4-5 min and subsequently sonicated for 2 hours to obtain a clear SUV dispersion. The SUV dispersion is loaded into capillaries of 0.7 mm inner diameter and then flame sealed. Data is acquired for 3 - 5 hours. In the case of decanol 10 w% SUV dispersion showed a quick transition from transparent to turbid solution which is a signature of multilamellar vesicles. So, we reduced the lipid concentration to 5 w% to get a stable SUV dispersion. In the dodecanol case, even at 2.5 w% concentration, we did not get stable SUV dispersions. So, we could not collect data in this case.

Small Angle X-ray Scattering (SAXS) experiments are conducted on a HECUS S3 Microsystem with a Cu anode (Genix) and 1D position-sensitive detector. The temperature of the sample is controlled with the help of a Peltier element. Data is acquired at 30 °C for C_n= 2 - 8 and at 38 °C for C_n= 10 over a range of the magnitude of the scattering vector (q) from 0.02 to 0.6 $Å^{-1}$. The relationship between scattered intensity and form factor is given by equation 3.1 for uncorrelated vesicles. To test the correctness of the assumption of uncorrelated vesicles, we have measured the form factor from dispersions with different SUV concentrations. The results after smoothing over 10 points are shown in figure 3.1. For all the studied concentrations, diffraction curves overlap within the noise level. We have used the model for the electron density profile of lipid bilayer given by Pabst et al.[17,22]. The scattered intensity $I(q)$, form factor $F(q)$ and electron density profile $\rho(z)$ are given by the following equations.

$$I(q) = B + A\frac{|\ F(q)\ |^2}{q^2} \tag{3.1}$$

$$F(q) = \sqrt{2\pi}\left[2\sigma_H \exp\left(\frac{-\sigma_H^2 q^2}{2}\right)\cos\left(qZ_H\right) + \sigma_C\bar{\rho}\exp\left(\frac{-\sigma_C^2 q^2}{2}\right)\right] \tag{3.2}$$

$$\rho(Z) = \rho_{CH_2} + \bar{\rho}_H\left[\exp\left(-\frac{(Z-Z_H)^2}{2\sigma_H^2}\right) + \exp\left(-\frac{(Z+Z_H)^2}{2\sigma_H^2}\right)\right] + \bar{\rho}_C \exp\left(-\frac{Z^2}{2\sigma_C^2}\right) \tag{3.3}$$

Here, head group (ρ_H) and hydrocarbon chain (ρ_C) electron densities are defined relative to methylene electron density (ρ_{CH_2}).

$$\bar{\rho} = \frac{\bar{\rho}_C}{\bar{\rho}_H} = \frac{\rho_C - \rho_{CH_2}}{\rho_H - \rho_{CH_2}} \tag{3.4}$$

σ_H, σ_C are standard deviation of lipid head group position and center of bilayer respectively. Z_H is the position of head group center. A and B are constants.

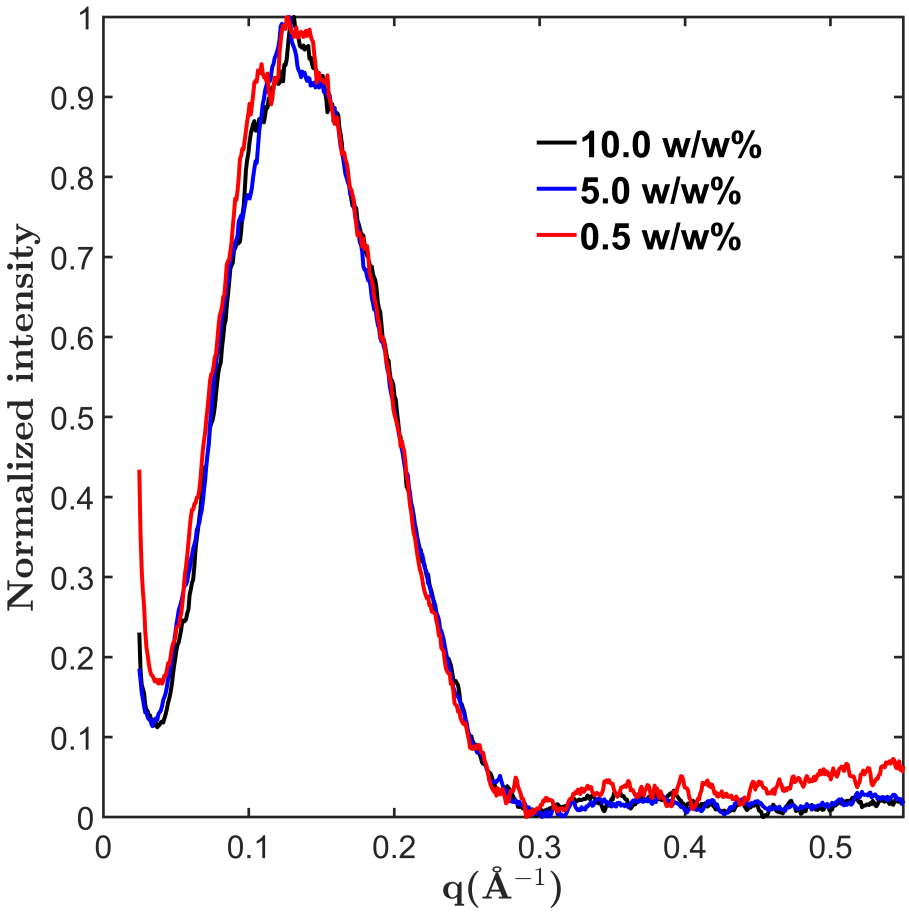

FIGURE 3.1: Scattering from DMPC SUV dispersions of different concentrations at 30 °C. The curves are smoothed over 10 points.

To find the sensitivity of our form factor measurement, we have measured DMPC bilayer form factor at different temperatures. Results are plotted in figure 3.2 and the values of the model parameters obtained are given in table 3.4. The lipid bilayer thickness increases as temperature decreases. The width of the broad peak in the form factor is inversely proportional to the thickness of the bilayer. We have obtained d_{HH} of 31.4 Å at 50 °C, 33.6 Å at 30 °C and 38.8 Å at 8 °C. These values are comparable to the literature values[18,23].

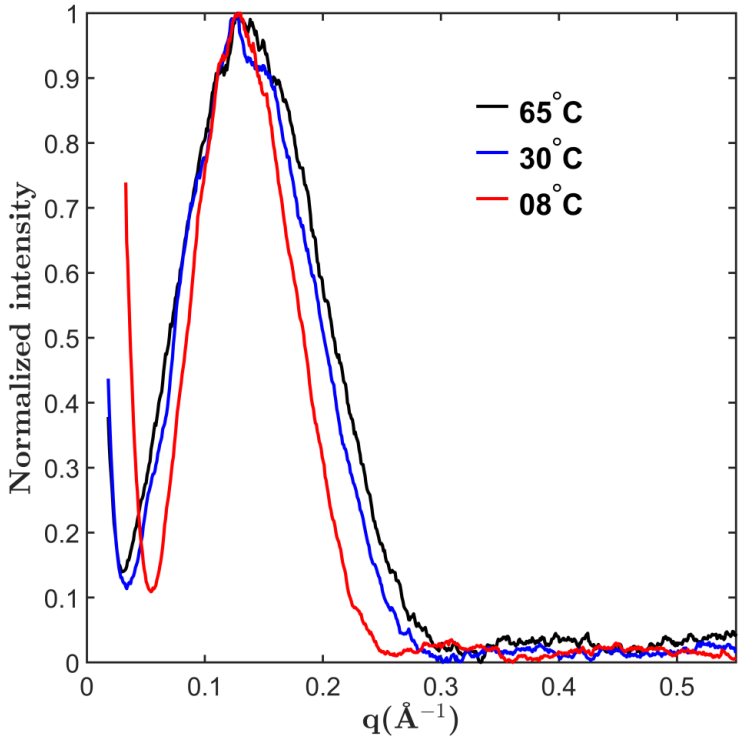

FIGURE 3.2: SAXS profiles of 5 w% DMPC SUV dispersions at a few different temperatures. The curves are smoothed over 10 points.

3.3 Results and discussions

3.3.1 DSC studies

The transition temperatures of DMPC+alcohol multi-lameller vesicle solutions are obtained from DSC cooling curves which are shown in figure 3.3 and table 3.2. Ethanol, pentanol and octanol reduced main phase transition temperature (T_m) of DMPC from 22.7 °C to 21.3 °C, 13.0 °C and 15.7 °C, respectively. Decanol and dodecanol increased T_m to 27.3 °C and 32.0 °C, respectively. These observations are in agreement with reports in the literature[24,25].

Alcohol	Molar ratio of DMPC:alcohol	T_m °C
Ethanol	1:30	21.3
Pentanol	1:3	13.0
Octanol	1:0.5	15.7
Decanol	1:0.5	27.3
Dodecanol	3:1	32.0

TABLE 3.2: Main phase transition temperature (T_m) of DMPC + alcohol systems obtained from DSC experiments. In case of DMPC T_m = 22.7 °C.

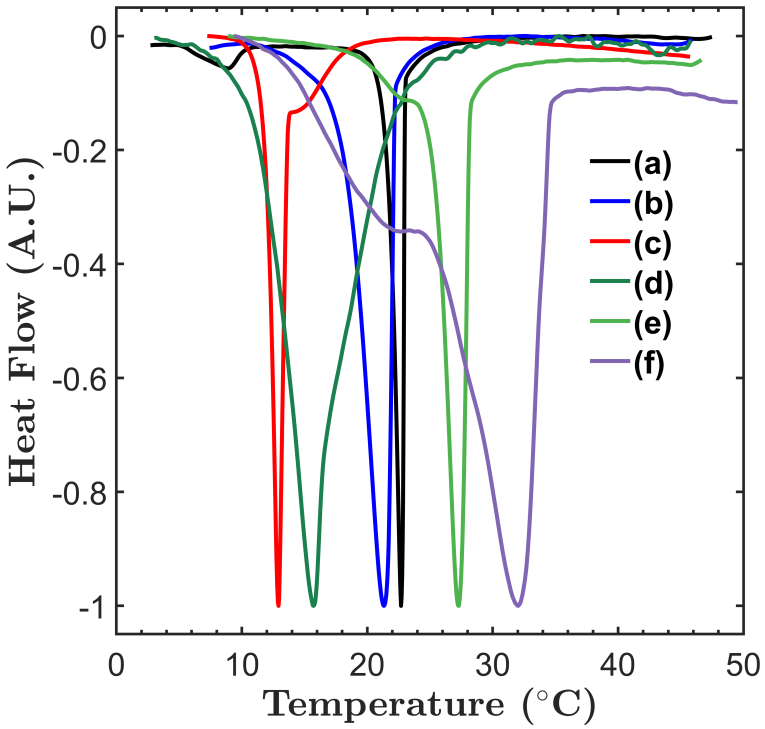

FIGURE 3.3: Differential scanning calorimetry (DSC) cooling curves of DMPC with and without alcohols. a) DMPC b) DMPC:ethanol (1:30) c) DMPC: pentanol (1:3) d) DMPC: octanol (1:0.5) e) DMPC: decanol (1:0.5) f) DMPC: dodecanol (3:1). Alcohols with $C_n = 2 - 8$ reduce T_m and $C_n = 10 - 12$ increase T_m.

3.3.2 Bending rigidity of DMPC membranes in the presence of alcohols

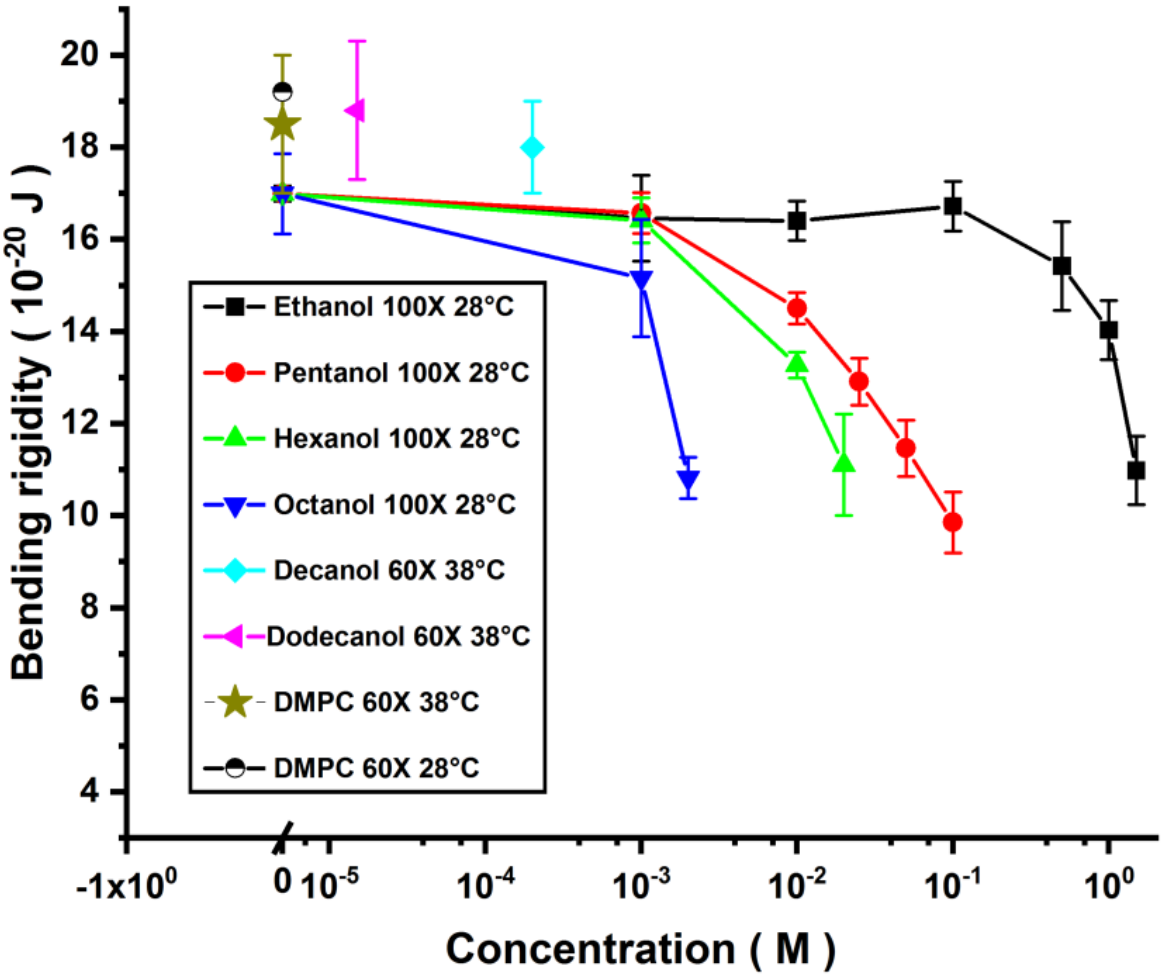

FIGURE 3.4: Variation of the bending rigidity modulus of DMPC bilayers with alcohol concentration in the interior and exterior solutions of the vesicles.

We have measured the bending rigidity of DMPC lipid bilayers in the presence of alcohols of varying chain length (C_n) at different concentrations (m). The κ values obtained are tabulated in table 3.3 and plotted in figure 3.4. From ethanol to octanol, as we vary the concentration at a fixed temperature of 28$\pm$1 °C, a reduction in κ is observed. As the chain length increases, a lower concentration of alcohol is enough to observe a comparable reduction in κ. Interestingly, near the saturation concentration all of them reduced κ by approximately the same amount. Both decanol and dodecanol, at 38 $\pm$ 1 °C, at saturation concentrations, did not alter the bending rigidity. To confirm the presence of decanol and dodecanol in the bilayer, we have measured the transition temperature of vesicles and found them to be 28.0 °C and 34.5 °C, respectively. This observation confirms their presence in the vesicles. The cross over in the trend, from a decrease in κ to a lack of influence, occurs between octanol and decanol. In a simulation study by Griepernau et al.[7] such a change is predicted at octanol. We have observed the change at decanol instead of octanol. To our knowledge, this is the first systematic experimental study in this direction.

System	m (M)	T (°C)	Magnification	Bending rigidity (10^{-20} J)
DMPC	0	28	100X	16.9 ± 0.8
DMPC	0	28	60X	19.2 ± 1.9
DMPC	0	38	60X	18.5 ± 1.5
DMPC+Ethanol	0.001	28	100X	16.5 ± 0.9
	0.01	28	100X	16.4 ± 0.4
	0.1	28	100X	16.7 ± 0.5
	0.5	28	100X	15.4 ± 1.0
	1.0	28	100X	14.0 ± 0.6
	1.5	28	100X	11.0 ± 0.7
DMPC+Pentanol	0.001	28	100X	16.6 ± 0.4
	0.01	28	100X	13.5 ± 1.3
	0.025	28	100X	12.9 ± 0.5
	0.05	28	100X	11.5 ± 0.6
	0.1	28	100X	9.9 ± 0.7
DMPC+Hexanol	0.001	28	100X	16.4 ± 0.5
	0.01	28	100X	14.4 ± 1.0
	0.02	28	100X	11.1 ± 1.1
DMPC+ Octanol	0.001	28	100X	15.2 ± 1.3
	0.002	28	100X	10.8 ± 0.5
DMPC+ Decanol	0.00023	38	60X	18.0 ± 1.0
DMPC+ Dodecanol	20×10^{-6}	38	60X	18.8 ± 1.5

TABLE 3.3: Bending rigidity values of DMPC membrane for different concentrations (m) and chain lengths of alcohols (C_n).

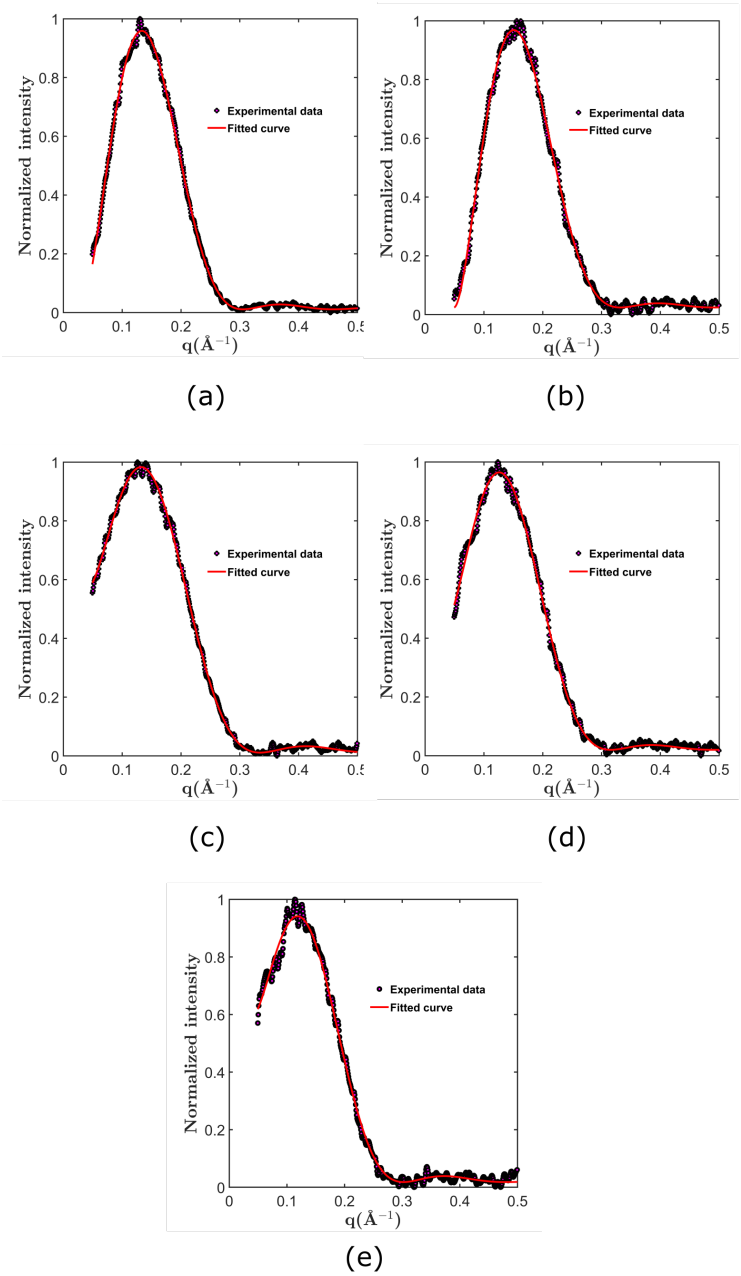

FIGURE 3.5: SAXS profiles of DMPC SUVs dispersion containing alcohols of different chain lengths. The solid lines are fits to equation 3.1. a) DMPC, 10 w/w %, 30 °C b) DMPC:ethanol (1:30 molar ratio), 10 w%, 30 °C c) DMPC:pentanol (1:3 molar ratio), 10 w%, 30 °C d) DMPC:octanol (1:0.5 molar ratio), 10 w%, 30 °C e) DMPC:decanol (1:0.5 molar ratio), 5 w%, 38 °C. Values of the model parameters obtained from the fit are listed in table 3.4

3.3.3 Bilayer thickness in presence of the alcohols

As discussed in section 1.4, various theoretical models of lipid membranes suggest that κ depends on the bilayer thickness. In order to check if the observed changes in κ of DMPC membranes in the presence of alcohols is related to changes in the bilayer thickness, we have obtained DMPC bilayer thickness in the presence of ethanol, pentanol, hexanol, and octanol at 30 °C and decanol at 38 °C. Typical fits of equation 3.1 to the experimental data are shown in figure 3.5. The obtained membrane thickness values are given in table 3.4. Alcohols with C_n = 2-8 reduce the bilayer thickness. In the case of decanol at 38 °C, after considering temperature, the bilayer thickness is very close to that of pure DMPC. These results confirm that changes in κ are correlated with changes in the bilayer thickness, in agreement with theoretical expectations. However, a quantitative comparison with theoretical predictions is not possible, since alcohol concentration in the bilayer in the two experiments need not be comparable.

Composition	T (°C)	σ_C (Å)	σ_H (Å)	$\bar{\rho}$	Z_H (Å)	$d_{HH} = 2Z_H$ (Å)
DMPC (Gel phase)	8	3.4 ± 0.1	2.3 ± 0.1	-0.8 ± 0.05	19.4 ± 0.2	38.8
DMPC	30	4.8 ± 0.1	2.4 ± 0.1	-0.9 ± 0.05	16.8 ± 0.2	33.6
DMPC	50	5.8 ± 0.1	2.7 ± 0.1	-0.9 ± 0.05	15.7 ± 0.2	31.4
Ethanol (1:30)	30	3.9 ± 0.1	2.4 ± 0.1	-0.9 ± 0.05	15.5 ± 0.2	31.0
Pentanol (1:3)	30	5.9 ± 0.1	2.4 ± 0.1	-0.9 ± 0.05	14.8 ± 0.2	29.6
Octanol (1:0.5)	30	5.7 ± 0.1	2.6 ± 0.1	-1.0 ± 0.05	15.9 ± 0.2	31.8
Decanol (1:0.5)	38	6.6 ± 0.1	2.6 ± 0.1	-0.9 ± 0.05	16.3 ± 0.2	32.6

TABLE 3.4: Membrane model parameters obtained from fitting the scattering data to 3.1. The alcohols used and their relative molar concentrations (lipid:alcohol) are mentioned.

We have estimated the alcohol content in the membrane (n'_A) in GUV dispersions employed in shape fluctuation analysis, using the values of the alcohol partition coefficients reported in the literature, which are given in table 3.5. In the literature the partition coefficients have been defined in terms of mole fraction, molality ratio and molarity ratio. To make comparison easy, we have converted all the values into mole fractions. As to be expected, the partition coefficient increases very strongly with increasing chain length of the alcohol. Using the values in second column we have estimated the alcohol content of the membrane for each value of the alcohol concentration in the solution. We have thus deduced the dependence of κ on the alcohol content in the membrane, from the observed dependence of κ on the alcohol concentration in the solution. This is presented in figure 3.6. κ is found to decrease sharply with increasing alcohol content of the membrane. However, no clear trend is observed in the ability of the alcohols to soften the membrane as a function of their chain length. At present we do not know if this results from inconsistencies in the values of the partition coefficients used in the calculation, arising from the fact that they have been obtained for different alcohols using different experimental techniques. We are not aware of any systematic measurement of the partition coefficient for all the alcohols studied here using the same experimental technique.

Alcohol	Partition coefficient	K	C_A (M)	$\frac{n_L}{n'_A}$in GUV	$\frac{n_L}{n_A}$in SUV	$\frac{n_L}{n'_A}$ in SUV
Ethanol	$K = 19$ [26]	19	1.5	1 : 1.17	1:10	1 : 1
			1.0	1 : 0.55		
			0.5	1 : 0.21		
			0.1	1 : 0.036		
			0.01	1 : 0.0034		
			0.001	1 : 0.00034		
Pentanol	K_m=5.02 [27]	188.3	0.1	1 : 0.34	1 : 3	1 : 1.4
			0.05	1 : 0.17		
			0.025	1 : 0.085		
			0.01	1 : 0.034		
			0.001	1 : 0.0034		
Hexanol	$K = 839$ [28]	839	0.020	1 : 0.43	-	-
			0.010	1 : 0.18		
			0.001	1 : 0.015		
Octanol	$K = 1.81 \times 10^4$ [28]	1.81×10^4	0.002	1 : 1.87	1:0.5	1 : 0.5
			0.001	1 : 0.48		
Decanol	$K_c = 3.9 \times 10^3$ [29]	1.42×10^5	0.23×10^{-3}	1 : 0.63	1:0.5	1 : 0.5
Dodecanol	$K_c = 6.9 \times 10^4$ [29]	2.53×10^6	20×10^{-6}	1 : 1.08	-	-

TABLE 3.5: Alcohol content in the membrane in GUV and SUV dispersion, estimated from the reported values of alcohol partition coefficients. Here K, K_m, K_c are partition coefficients defined in terms of mole fraction, molality ratio and molarity ratio, respectively. To make comparison easy, we have converted partition coefficients into mole fraction. C_A is the alcohol concentration in the solution used in GUV experiments. n_L is the lipid content in GUV or SUV samples. n_A is the total alcohol in the SUV dispersion. Alcohol content in the membrane is n'_A.

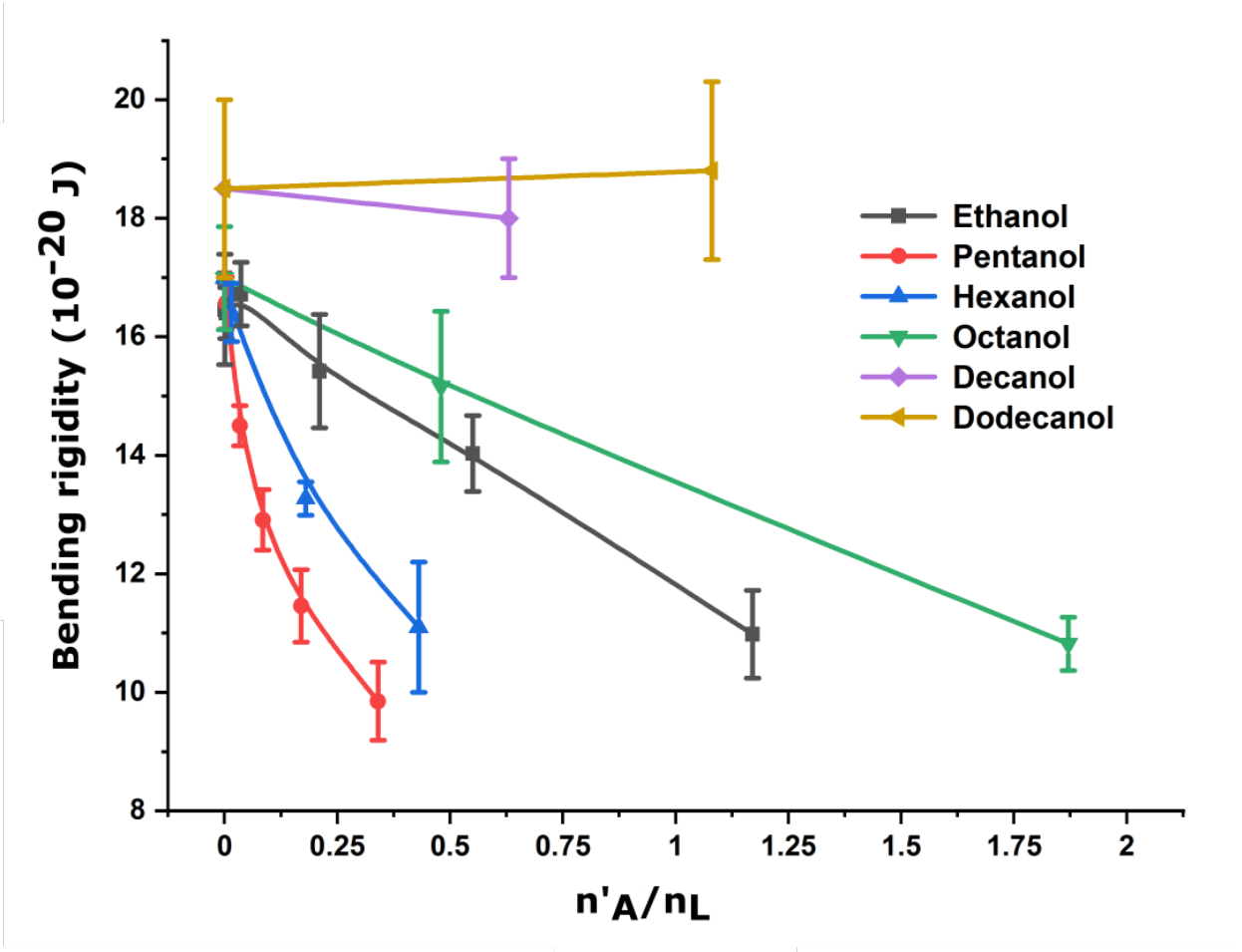

FIGURE 3.6: Variation of Bending rigidity with alcohol content of the membrane. Alcohol to lipid molar ratio in the GUV is obtained from the bulk alcohol concentration using values of partition coefficients taken from the literature and given in table 3.5.

3.4 Conclusions

We have carried out a systematic study on the influence of shorter and longer chain alcohols on DMPC lipid bilayers. Three techniques, namely vesicle fluctuation analysis, DSC, and SAXS, are used in the study. All the observations coherently confirm that alcohols with chain length lower than decanol disrupt the DMPC bilayer. This is reflected in lowering of T_m, bending rigidity, and thickness. In the literature, as alcohol chain length increases, a crossover from thinning to thickening of the bilayer is reported. In this study we do not observe the thickening of the bilayer for longer chain alcohols. However, in the case of decanol we find the bilayer thickness to be unaffected by the presence of the alcohol. The observed changes in the bilayer thickness are correlated with changes in κ, in agreement with theoretical predictions.

Bibliography

[1] Ingram LO, Buttke TM. Effects of alcohols on micro-organisms. In: Adv. Microb. Physiol.. vol. 25. Elsevier; 1985. p. 253–300.

[2] Harold FM. Antimicrobial agents and membrane function. In: Adv. Microb. Physiol.. vol. 4. Elsevier; 1969. p. 45–104.

[3] Pringle MJ, Brown KB, Miller KW. Can the lipid theories of anesthesia account for the cutoff in anesthetic potency in homologous series of alcohols? Mol Pharmacol. 1981;19(1):49–55.

[4] Klacsová M, Bulacu M, Kučerka N, Uhríková D, Teixeira J, Marrink S, et al. The effect of aliphatic alcohols on fluid bilayers in unilamellar DOPC vesicles—A small-angle neutron scattering and molecular dynamics study. Biochim Biophys Acta Biomembr. 2011;1808(9):2136–2146.

[5] Petrenko VI, Klacsova M, Beskrovnyy AI, Uhrikova D, Balgavy P. Interaction of long-chain n-alcohols with fluid DOPC bilayers: a neutron diffraction study. Gen Physiol Biophys. 2010;29(4):355.

[6] Pope J, Walker L, Dubro D. On the ordering of N-alkane and N-alcohol solutes in phospholipid bilayer model membrane systems. Chem Phys Lipids. 1984;35(3):259–277.

[7] Griepernau B, Leis S, Schneider MF, Sikor M, Steppich D, Böckmann RA. 1-Alkanols and membranes: a story of attraction. Biochim Biophys Acta Biomembr. 2007;1768(11):2899–2913.

[8] Ingólfsson HI, Andersen OS. Alcohol's effects on lipid bilayer properties. Biophys J. 2011;101(4):847–855.

[9] Westerman P, Pope J, Phonphok N, Doane J, Dubro D. The interaction of n-alkanols with lipid bilayer membranes: a 2H-NMR study. Biochim Biophys Acta Biomembr. 1988;939(1):64–78.

[10] Kondela T, Gallová J, Hauß T, Barnoud J, Marrink SJ, Kučerka N. Alcohol interactions with lipid bilayers. Molecules. 2017;22(12):2078.

[11] Kondela T, Gallová J, Hauß T, Ivankov O, Kučerka N, Balgavỳ P. Effect of alkan-1-ols on the structure of dopc model membrane. Eur Pharm J. 2017;64(2):4–8.

[12] Patra M, Salonen E, Terama E, Vattulainen I, Faller R, Lee BW, et al. Under the influence of alcohol: the effect of ethanol and methanol on lipid bilayers. Biophys J. 2006;90(4):1121–1135.

[13] Ly HV, Longo ML. The influence of short-chain alcohols on interfacial tension, mechanical properties, area/molecule, and permeability of fluid lipid bilayers. Biophysical Journal. 2004;87(2):1013–1033.

[14] Safinya C, Sirota E, Roux D, Smith G. Universality in interacting membranes: the effect of cosurfactants on the interfacial rigidity. Physical review letters. 1989;62(10):1134.

[15] Foret L, Würger A. Discontinuous bending rigidity and cosurfactant adsorption of amphiphile layers. Physical review letters. 2001;86(26):5930.

[16] Angelova M, Soléau S, Méléard P, Faucon F, Bothorel P. Preparation of giant vesicles by external AC electric fields. Kinetics and applications. In: Trends in colloid and interface science VI. Springer; 1992. p. 127–131.

[17] Pabst G, Rappolt M, Amenitsch H, Laggner P. Structural information from multilamellar liposomes at full hydration: full q-range fitting with high quality x-ray data. Phys Rev E. 2000;62(3):4000.

[18] Pabst G, Katsaras J, Raghunathan VA, Rappolt M. Structure and interactions in the anomalous swelling regime of phospholipid bilayers. Langmuir. 2003;19(5):1716–1722.

[19] Schneider CA, Rasband WS, Eliceiri KW. NIH Image to ImageJ: 25 years of image analysis. Nature methods. 2012;9(7):671–675.

[20] Schindelin J, Rueden CT, Hiner MC, Eliceiri KW. The ImageJ ecosystem: An open platform for biomedical image analysis. Molecular reproduction and development. 2015;82(7-8):518–529.

[21] Bhatia T, Husen P, Brewer J, Bagatolli LA, Hansen PL, Ipsen JH, et al. Preparing giant unilamellar vesicles (GUVs) of complex lipid mixtures on demand: Mixing small unilamellar vesicles of compositionally heterogeneous mixtures. Biochimica et Biophysica Acta (BBA)-Biomembranes. 2015;1848(12):3175–3180.

[22] Pabst G, Katsaras J, Raghunathan VA, Rappolt M. Structure and interactions in the anomalous swelling regime of phospholipid bilayers. Langmuir. 2003;19(5):1716–1722.

[23] Kučerka N, Liu Y, Chu N, Petrache HI, Tristram-Nagle S, Nagle JF. Structure of fully hydrated fluid phase DMPC and DLPC lipid bilayers using X-ray scattering from oriented multilamellar arrays and from unilamellar vesicles. Biophysical journal. 2005;88(4):2626–2637.

[24] Pringle MJ, Miller KW. Differential effects on phospholipid phase transitions produced by structurally related long-chain alcohols. Biochemistry. 1979;18(15):3314–3320.

[25] Kamaya H, Matubayasi N, Ueda I. Biphasic effect of long-chain n-alkanols on the main-phase transition of phospholipid vesicle membranes. The Journal of Physical Chemistry. 1984;88(4):797–800.

[26] Nizza DT, Gawrisch K. A layer model of ethanol partitioning into lipid membranes. General physiology and biophysics. 2009;28(2):140.

[27] McCreery M, Hunt W. Physico-chemical correlates of alcohol intoxication. Neuropharmacology. 1978;17(7):451–461.

[28] Rowe ES. Lipid chain length and temperature dependence of ethanol-phosphatidylcholine interactions. Biochemistry. 1983;22(14):3299–3305.

[29] Franks N, Lieb W. Partitioning of long-chain alcohols into lipid bilayers: implications for mechanisms of general anesthesia. Proceedings of the National Academy of Sciences. 1986;83(14):5116–5120.

Chapter 4

Phase behaviour of DMPC-decanol membranes

4.1 Introduction

Fluid-fluid coexistence in lipid membranes is a topic of much current interest due to its implications for the functioning of cell membranes[1–10]. At present, only ternary systems consisting of cholesterol and two lipids with widely different chain-melting transition temperatures (T_m) are known unambiguously to exhibit such a phase behavior[5,6]. However, there have been indications from spectroscopy experiments that some binary systems, such as PC lipid - cholesterol[11], PC-PC lipid[12], PE-PC lipid[13], and PA-PC lipid[14] systems may also exhibit fluid-fluid phase separation. But such a phase behaviour has not been confirmed using other experimental techniques.

It may be noted here that cholesterol does not induce phase coexistence in these ternary mixtures. Instead, it converts the fluid-gel coexistence present in the binary lipid system, over a temperature range in between the T_m of the two lipids, to a fluid-fluid coexistence region. It is also known that the average size of the fluid domains in the bilayer can be controlled by adding a third lipid species that reduces the interfacial line tension of the domains[7,8,10]. Given its ramifications for the functioning of cell membranes, it is important to understand the conditions under which fluid-fluid coexistence can be produced in lipid membranes. The first step towards this goal is to identify different model membrane systems that exhibit this behavior. It will then be possible to understand the various physical mechanisms at play, some of which could be of biological significance. The present study describes one such system, consisting of dimyristoyl phosphatidyl choline (DMPC) and 1-decanol.

Interaction of 1-alkanols with lipid membranes has been studied extensively, using a variety of experimental techniques as well as computer simulations, motivated mainly by their anesthetic properties[15–25]. Although a large fraction of these studies has focussed on the influence of short-chain alcohols on various membrane properties, the effect of both short- and long-chain alcohols on the phase behavior of lipid bilayers has also been investigated[15,19,21–25]. These studies show that short-chain alcohols make the lipid chains more disordered in the fluid phase, resulting in lower values of the bilayer thickness, bending rigidity modulus κ and T_m, compared to the pure lipid. Long-chain alcohols have the opposite effect on the fluid phase; they increase chain order, leading to higher bilayer thickness, κ and T_m. Results from the previous chapter are in agreement with these conclusions.

In this chapter, we show that 1-decanol induces fluid-fluid coexistence in dimyristoylphosphatidylcholine (DMPC) membranes. Presence of this two-phase region just above the T_m of the membrane is established using a variety of experimental techniques and different bilayer morphologies. Below T_m, a ripple phase is observed, which has a modulation wavelength more than twice the typical wavelength observed in the ripple phase of pure DMPC[26]. This phase transforms into a gel ($L_{\beta'}$) phase at lower temperatures.

4.2 Materials and Methods

The material details are the same as those given in chapter 3.

4.2.1 Preparation of giant unilamellar vesicles (GUVs)

GUVs are prepared using the electroformation method described in chapter 2 and chapter 3.

4.2.2 Preparation of small unilamellar vesicles (SUVs)

The ultrasonication method is used for the preparation of SUVs[27]. A 1 mg/ml stock solution of DMPC and rhodamine-DHPE is prepared in chloroform, with a dye to lipid concentration of 0.25 mol%. A thin film of the lipid is deposited on the inner wall of a glass vial using a rotary evaporator. A 10 mM PBS buffer solution is added to the vial to obtain a lipid concentration of 1 mg/ml. The solution is vortexed for 2-3 min and subsequently sonicated for an hour to obtain a SUV suspension.

4.2.3 Preparation of supported lipid bilayers (SLBs)

In order to prepare SLBs, glass coverslips are first cleaned with ethanol and then with chloroform. They are subsequently washed with deionized water. After drying the coverslips at 45 °C for 4-5 hours, they are plasma-cleaned for 10 min to make them hydrophilic. About 200 μl of the SUV solution is spread over the coverslip in order to form bilayers. Excess lipid is removed by gentle washing with 10 mM PBS buffer. SLBs are incubated with decanol saturated PBS solution at 60 °C for at least 10 hours prior to observations.

4.2.4 FRAP experiments

FRAP experiments are carried out using a confocal microscope with a 40X objective (Leica SP8). A 563 nm laser is used for bleaching. The fluorescence intensity from the bleached area is fitted to a two-dimensional Gaussian profile, and the integrated intensity of the bleached region, $I(t)$, at time t is determined. The intensity recovery curve is fitted to a single exponential function, $I(t) = I_o(1 - \exp(-t/\tau))$, where I_o is the intensity at large t, to obtain the recovery time constant τ. A nonlinear least-square fitting routine (MATLAB2018a) is used to fit the data. The diffusion coefficient (D) is estimated using the relation,[28] $D = 0.224\ \omega^2/\tau_{1/2}$, where, ω is the radius of the bleached area, and $\tau_{1/2} = \ln(2)\tau$, is the half time of recovery. ω is determined following the procedure described in ref. 28.

4.2.5 X-ray diffraction on aligned bilayer stack

Appropriate amounts of DMPC and decanol are dissolved in deionized water to give a 10 w% lipid solution. A homogeneous solution is obtained by following the protocol described in the literature[29], which consists of repeated vortexing of the solution followed by temperature cycling between 10 °C and 45 °C. The solution is further equilibrated at 45 °C for 3 days before carrying out the experiments.

For x-ray studies, about 15 μl of the solution is coated on a cylindrical glass substrate and dried for 3-4 hours. The sample is then kept in a closed humidity chamber for 12 hours at 35 °C before data collection. This procedure results in aligned multilayers of DMPC-decanol on the glass substrate. The relative humidity is maintained close to saturation by keeping a small beaker of water in the chamber and the temperature is maintained by water circulation. A small fan is used to maintain uniform temperature and humidity within the chamber. The relative humidity and temperature near the sample are monitored using a thermo-hygrometer (Testo 610). X-rays of 1.54 Å wavelength from a Genix 3D source (Xenocs) operating at 50 kV and 0.6 mA are used in this study. An image plate detector (MAR345) with a 0.1 mm pixel size is used to record the diffraction patterns with a typical acquisition time of 30 min. Intensity (I) vs. scattering wavevector (q) plots are obtained by integrating the images over the azimuthal angle.

The transbilayer electron density profiles (EDPs) are determined from the diffraction data by the Fourier reconstruction method described in the literature[30]. The electron density profile, ρ(z), along the bilayer normal is given by,

$$\rho(z) = \sum_{h=1}^{n} \alpha_h |F_h| \cos(q_h z), \tag{4.1}$$

where h is the index of the peak, $|F_h|$ its magnitude and α_h its phase. $q_h = h(2\pi/d)$, where d is the lamellar periodicity. In order to determine the magnitudes of the peaks, their intensities, $I_h = |F_h|^2$, are first obtained by finding the area under each peak and then applying the appropriate geometric correction, which in the present case is a factor proportional to h. Since the bilayer is symmetric with respect to the midplane, $\alpha_h = \pm 1$. The phases are determined by trial and error.

4.2.6 Differential scanning calorimetry (DSC)

The procedure followed for DSC experiments is the same as that described in chapter 3.

4.3 Results

4.3.1 Fluorescence microscopy

DMPC GUVs suspended in a decanol saturated aqueous solution show a homogeneous state from 45 °C to 30 °C (figure 4.1(left-top)) and exhibit thermal shape fluctuations. Upon decreasing the temperature below 30 °C, dark domains appear on the GUVs. These domains coalesce over time to form larger domains (figure 4.1(middle)). Vesicles that are elliptical in the high-temperature fluid phase take on a cylindrical shape in the two-phase region, with fluorescence confined to their end caps (figure 4.1(left-bottom)). These bright end caps are found to exhibit thermal undulations, whereas the dark cylindrical body does not. Vesicles of various shapes are formed in the phase

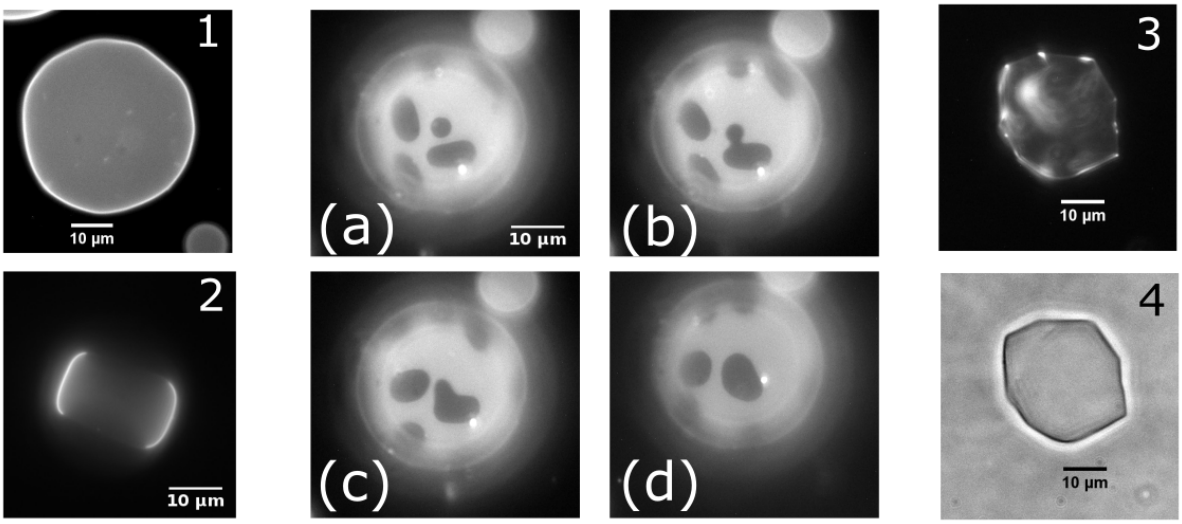

FIGURE 4.1: 1 Left (top): A DMPC GUV suspended in a decanol saturated aqueous solution exhibiting a single fluid phase with thermal undulations at 30 °C. Middle (a)–(d): Time-lapse images showing the coalescence of dark domains at 28 °C, over a duration of 4 min. 2 Left (bottom): A cylindrical vesicle observed in the two-phase region at 24 °C. Fluorescence microscopy (3 right, top) and phase contrast microscopy (4 right, bottom) images of a GUV with faceted shape observed in the gel phase at 23.5 °C

coexisting regime as shown in figure 4.2. On cooling down to 23.5 °C, these vesicles acquire very irregular faceted shapes with the dye expelled into narrow boundaries between the facets (figure 4.1(right-top)). These transformations are reversible on heating. For the corresponding video, please click here.

Fluorescence microscopy observations are also carried out on supported lipid bilayers (SLBs). SLBs formed from DMPC exhibit spatially uniform fluorescence at 30 °C (figure 4.3(a)). Upon incubating them in decanol saturated PBS buffer, small dot-like features are observed as shown in figure 4.3(b). These coalesce in time, leading to larger domains (figure 4.3(c)). The rate of domain coalescence is found to be slower in SLBs compared to GUVs. Further, these domains do not disappear even on heating the SLBs to 45 °C.

4.3.2 FRAP

In order to carry out the FRAP experiment, a DMPC SLB is incubated with decanol saturated PBS buffer solution for about 12 hours at 60 °C. It is then transferred to an observation chamber maintained at 40 °C. At this temperature, the bilayer is found to exhibit two-phase coexistence, as shown in figure 4.3 (c). FRAP experiments are carried out in both the coexisting phases, and the fluorescence recovery curves are given in figure 4.4 (a). It may be noted here that fluorescence intensity from the dark phase was sufficient for these experiments. Values of the diffusion coefficient (D) obtained are presented in table 4.1. In the bright phase D = 4.8 $\pm$ 0.6 $\mu m^2/s$ and in the dark phase D = 3.6 $\pm$ 0.6 $\mu m^2/s$. On lowering the temperature to 30 °C, fluorescence recovery in the dark region is almost completely hindered, whereas, in the bright phase, the recovery is only slightly slower than that at 40 °C. At this temperature D = 3.8 $\pm$ 0.6 $\mu m^2/s$ in the bright phase, but it was not possible to estimate D in the dark phase (table 4.1). FRAP experiments are also carried out on DMPC SLBs in a PBS buffer solution without decanol for comparison (table 4.1). All values

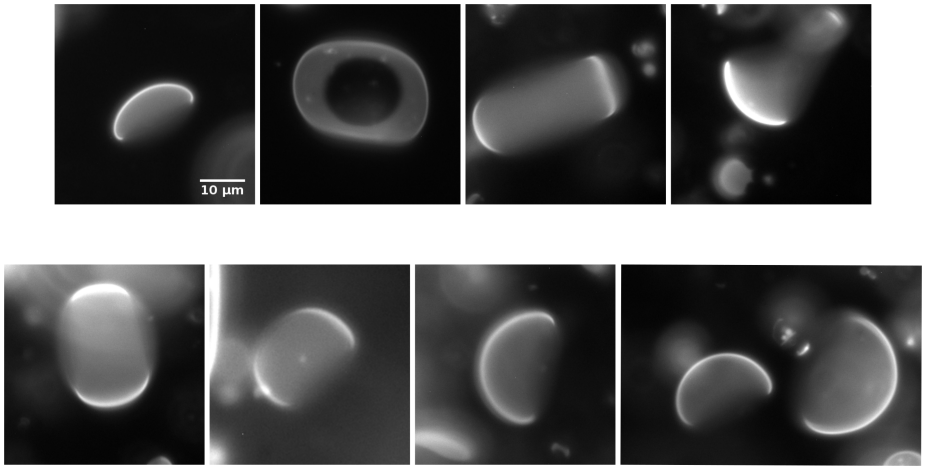

FIGURE 4.2: Images of some non-spherical GUV shapes observed in the two-phase coexistence region at 28 °C. Note that the dark regions in all the GUVs have a smaller curvature compared to the bright region. The bright regions of the GUVs show thermal shape fluctuations, indicating that they are in the fluid phase. Magnification is the same in all the images.

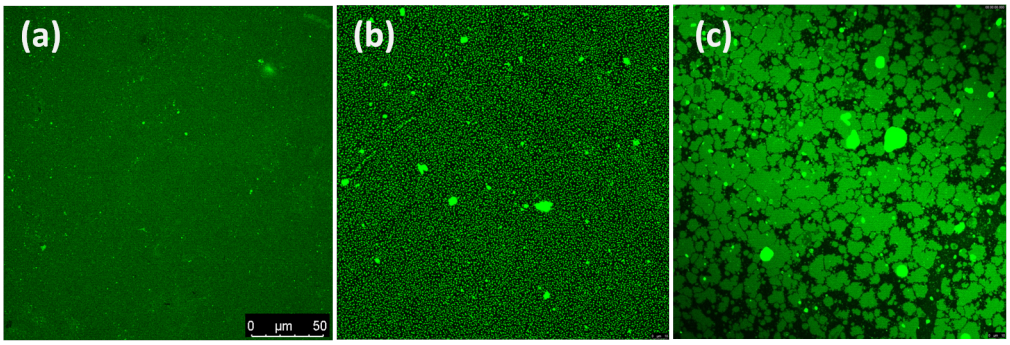

FIGURE 4.3: (a) DMPC SLB in water exhibiting uniform fluorescence. The appearance of dark domains soon after the addition of decanol saturated PBS buffer at 30 °C (b) and after incubation for 2 hours at 45 °C (c). Magnification is the same in all the images.

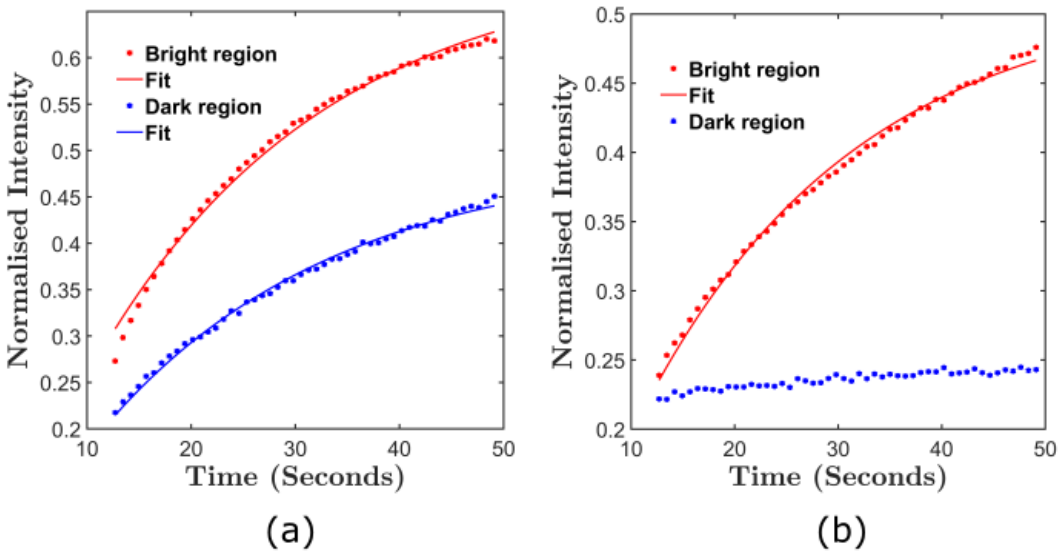

FIGURE 4.4: Typical recovery curves in the dark and bright regions of a DMPC SLB in equilibrium with a decanol saturated PBS buffer solution at 40 °C (a) and at 30 °C (b) Solid lines are fits to a single exponential function.

of D are averaged over at least 15 measurements. It may be noted here that values of D obtained here are comparable to those reported in the literature for DMPC SLBs[31,32].

TABLE 4.1: Values of diffusion coefficient obtained from FRAP experiments in the bright and dark phases of DMPC SLBs in the presence of decanol in the fluid state.

T (°C)	D ($\mu m^2/s$)		
	Dark phase	Bright phase	DMPC
40	3.6 ± 0.3	4.8 ± 0.6	5.0 ± 0.6
30	-	3.8 ± 0.6	3.6 ± 0.6

4.3.3 SAXS and WAXS

Small-angle x-ray scattering (SAXS) and wide-angle x-ray scattering (WAXS) patterns of aligned 1:0.5 molar ratio DMPC-decanol multilayers recorded at 98 % relative humidity are shown in figures 4.5(a) and 4.5(b), respectively. The SAXS pattern at 30.4 °C corresponds to a lamellar phase with a periodicity, d, of 5.22 nm. At this temperature, no sharp peaks are observed in the WAXS pattern. Upon cooling the sample to 26.2 °C, the SAXS pattern shows the coexistence of two lamellar phases with d = 5.27 nm and 5.64 nm. At this temperature also there are no sharp peaks in the WAXS pattern. On cooling down to 25.5 °C, additional weak peaks appear in the SAXS pattern very close to the lamellar peaks, and a single peak appears in the WAXS pattern corresponding to a spacing of 0.42 nm. Similar patterns are observed at 24.7 °C and 23.9 °C. On cooling down to 22.7 °C, the weak peaks disappear, and only a set of lamellar peaks corresponding to a periodicity of 5.45 nm is observed. Concomitantly, the WAXS pattern changes and shows a very sharp peak followed by a broader one. Identical SAXS and WAXS patterns are observed at 19.2 °C and 17.5 °C. The sequence of diffraction patterns is reversible on heating.

A similar sequence of SAXS and WAXS patterns are observed in the case of 1:0.25 DMPC-decanol multilayers, as shown in figure 4.6. For T $\geq$ 28.5 °C, a set of lamellar peaks is observed in the SAXS pattern and no sharp peaks in the wide-angle. At T = 26.8 °C and 25.5 °C, no sharp wide-angle peaks are seen, but two sets of lamellar peaks are present in the SAXS pattern. A wide-angle peak is observed between 24 °C and 18 °C, and the SAXS patterns show a set of lamellar peaks and additional weak peaks very close to them. At lower temperatures, the weak peaks disappear, and only a set of lamellar peaks remains. The corresponding WAXS patterns show a very sharp peak followed by a broad one.

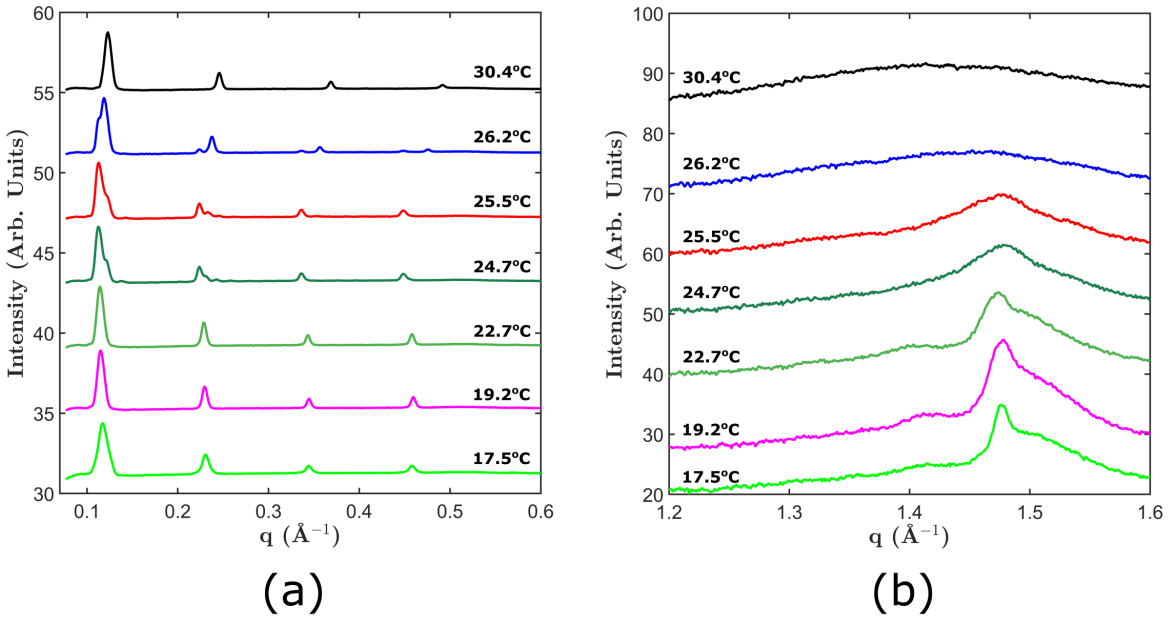

FIGURE 4.5: Small-angle (a) and wide-angle (b) scattering profiles from 1:0.5 DMPC-decanol multilayers at different temperatures.

The transbilayer electron density profiles, calculated from the SAXS data, are shown in figure 4.7. Values of different parameters used for Fourier reconstruction of EDP are listed in table 4.2. The phases of reflections obtained are in agreement with those reported in the literature for DMPC multilayers[33]. The lamellar periodicities, d, and the separation between the head group peaks in the EDPs, d_{HH}, are also given.

4.3.4 Differential scanning calorimetry (DSC)

Figure 4.8 shows DSC data for pure DMPC and DMPC-decanol bilayers of 1:0.25 and 1:1 molar compositions. DSC curve of pure DMPC in excess water conditions shows two peaks at around 8 °C and 23 °C, corresponding to the pre- and main-transitions, respectively[26]. The main transition temperature (T_m) shifts to higher values with increasing decanol concentration, and the corresponding peaks become broader. T_m = 23.6 °C and 25.8 °C in the 1:0.25 and 1:1 samples, respectively. An additional broad peak is observed at around 18 °C in the 1:0.25 sample but is absent in the 1:1 sample.

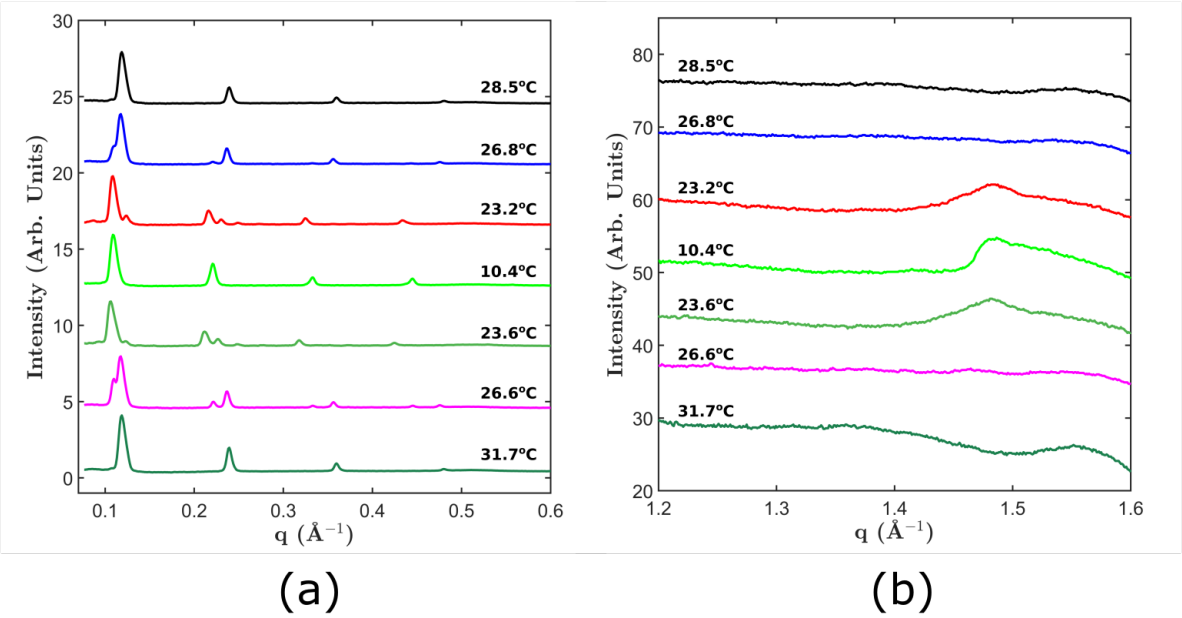

FIGURE 4.6: SAXS (a) and WAXS (b) patterns obtained from a 1:0.25 DMPC-decanol sample at a few temperatures on cycling the temperature from high to low and back to high, showing thermal reversibility of the phase behavior.

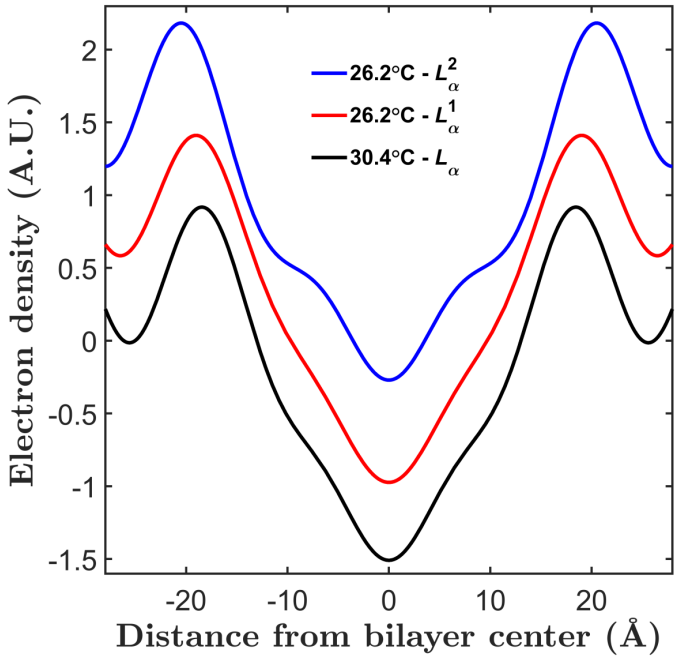

FIGURE 4.7: Transbilayer electron density profiles of 1:0.5 DMPC-decanol membranes in different phases determined from the SAXS data. The maxima correspond to the headgroup regions and the minimum to the midplane of the bilayer. The separation, d_{HH}, between the two maxima is a measure of the bilayer thickness.

4.4 Discussions

The uniform fluorescence intensity and thermal shape fluctuations of DMPC GUVs suspended in a decanol saturated aqueous solution show that the bilayer is in the L_α phase above 30 °C (figure

TABLE 4.2: Observed relative magnitudes ($|F_h|$) and estimated phases (α_h) of different diffraction peaks used for the Fourier reconstruction of EDPs of different phases of 1:0.5 DMPC-decanol bilayers, and the corresponding values of lamellar periodicity (d) and bilayer thickness (d_{HH}).

h	α_h	$\lvert F_h \rvert$		
		30.4 °C	26.2 °C	
		L_α	L_α^1	L_α^2
1	-1	1.00	1.00	1.00
2	-1	0.35	0.37	0.26
3	+1	0.25	0.22	0.27
4	-1	0.21	0.17	0.28
d (nm)		5.10 ± 0.02	5.23 ± 0.02	5.54 ± 0.02
d_{HH} (nm)		3.69 ± 0.02	3.82 ± 0.02	4.09 ± 0.02

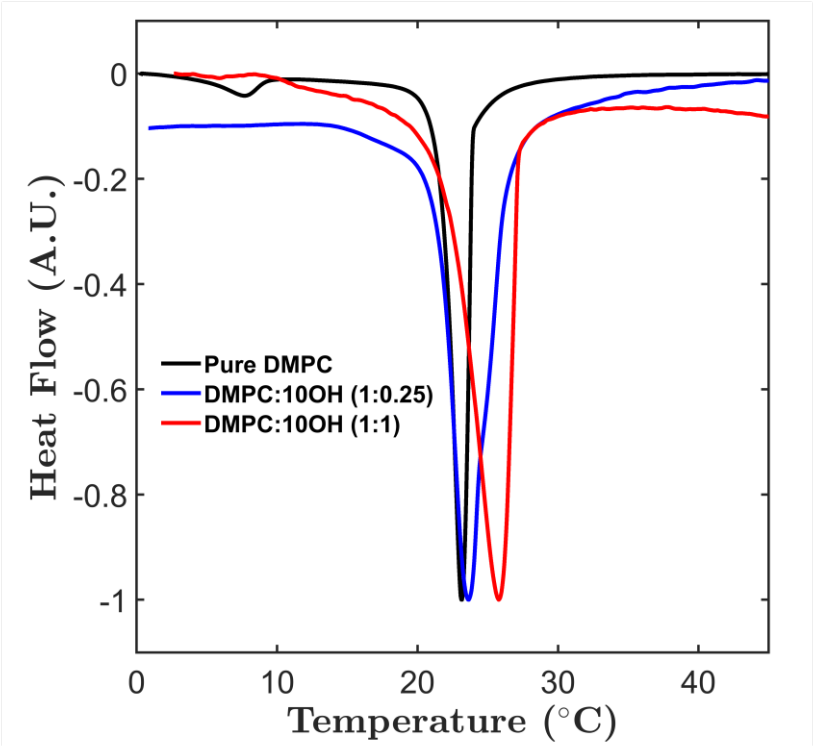

FIGURE 4.8: Normalized DSC curves for pure DMPC and DMPC-decanol samples of 1:0.25 and 1:1 molar composition. Lipid concentration in all samples is 10 w%.

4.1). The observed coalescence of dark domains that appear on cooling from this phase below 30 °C clearly establishes that both the coexisting phases are in the fluid state. We label the bright and dark coexisting phases as L_α^1 and L_α^2, respectively.

Observation of cylindrical vesicles in the two-phase region with the bright L_α^1 phase forming their end caps is similar to what has been reported in the case of vesicles made from raft mixtures in the liquid-ordered (L_o) - liquid-disordered (L_d) coexistence region[34]. This shape results from the minimization of the interfacial tension and the bending energy of the bilayer. The central part of the vesicle that has a lower curvature is occupied by the L_o phase, which has a much higher bilayer bending rigidity modulus, κ, compared to the L_d phase[35]. The present observations, therefore, suggest that κ of the L_α^2 phase is higher than that of the L_α^1 phase. On further cooling,

the bilayer is converted into a gel phase, and the vesicles take on irregular faceted shapes, with the dye molecules expelled into narrow domain boundaries. Such faceted vesicles have been observed in the gel phase in earlier studies[36]. Thus the observations on GUVs provide irrefutable evidence for fluid-fluid coexistence in DMPC bilayers in the presence of decanol over a temperature range of about 5 °C.

Results of FRAP experiments on SLBs corroborate the coexistence of two fluid phases in the present system. The value of D obtained in the bright phase at 40 °C is comparable to that found for DMPC SLBs at this temperature. In the dark phase, D is lower by a factor of about 1.3. This is consistent with the reduction in D observed on incorporating long-chain alcohols in DMPC bilayers, both in experiments and computer simulations[23]. These observations indicate that the bright (L_α^1) and dark (L_α^2) phases are decanol-poor and decanol-rich, respectively. A slight reduction in D is observed in the bright phase on cooling down to 30 °C, similar to that found in pure DMPC. On the other hand, at this temperature, fluorescence recovery in the dark phase becomes too slow, and it is not possible to estimate D. This drastic reduction in D is consistent with the dark phase being in a gel phase at this temperature.

The ability of the present system to form two coexisting fluid phases is further confirmed by the results of x-ray scattering experiments. Both the 1:0.5 and 1:0.25 DMPC-decanol samples show a single lamellar phase at high temperatures. This can be identified as the fluid L_α phase in the absence of any sharp wide-angle peaks. On cooling, the coexistence of two fluid lamellar phases is seen in both cases, whose periodicities differ by about 0.3 nm. This region extends over a temperature range of about 2 °C. Intensities of the two sets of lamellar peaks have been determined from these SAXS patterns, and the trans-bilayer electron density profiles (EDPs) of the two coexisting phases have been calculated following the procedure described earlier. From these EDPs, shown in figure 4.7, it is clear that the difference in the periodicities (d) of these two phases can be almost entirely accounted for by the difference in their bilayer thickness (d_{HH}). The phase with thinner bilayers (L_α^1) has a d_{HH} of 3.8 nm, which is very close to that reported for DMPC[37], whereas in the other (L_α^2) phase, d_{HH} = 4.1 nm. Computer simulations have shown that the insertion of long-chain alcohols such as 1-decanol increases the bilayer thickness of DMPC[23]. Thus, the x-ray data support our earlier conclusion based on diffusion data that the L_α^1 and L_α^2 phases are decanol-poor and decanol-rich, respectively.

TABLE 4.3: The observed (d_o) and calculated (d_c) values of the spacings of the different reflections in the ripple phase of the 1:0.5 DMPC-decanol multilayers at 25.5°C are shown. The lattice parameters of the ripple phase are: d = 5.57 nm, ripple wave length (λ) = 38.72 nm and γ = 103.2°.

h	k	d_o (nm)	d_c (nm)
1	0	5.57	5.57
1	1	5.32	5.34
1	2	5.08	5.06
2	0	2.79	2.79
2	2	2.69	2.67
2	4	2.55	2.53
3	0	1.86	1.86
3	3	1.77	1.78
4	0	1.39	1.39

The phase occurring below the L_{α}^{1}-L_{α}^{2} coexistence region exhibits a wide-angle peak and many weak peaks in the small-angle region. The SAXS peaks can be indexed on an oblique lattice corresponding to a ripple ($P_{\beta'}$) phase (table 4.3). The wavelength (λ) of the bilayer height modulations in this phase is about 39 nm in the 1:0.5 sample at 25.5 °C, which is much higher than the wavelength of about 15 nm typically observed in the ripple phase of pure DMPC[26]. The temperature range of this phase is broader in the 1:0.25 sample compared to the 1:0.5 sample. This decanol induced ripple phase is very similar to the meta stable ripple phase observed by Rappolt et al.[38] in pure DPPC membranes.The phase observed on cooling from the ripple phase is the gel ($L_{\beta'}$) phase, characterized by a tilt of the lipid molecules with respect to the bilayer normal. The presence of chain tilt can be deduced from the occurrence of a sharp wide-angle peak followed by a broad peak[39].

Our DSC data show that the main-transition of DMPC shifts to higher temperatures with increasing decanol concentration in the bilayer, in agreement with earlier studies[19]. The peaks also broaden in the presence of decanol, as would be expected in a two-component system. The presence of a broad peak at around 18 °C in the DSC curve of the 1:0.25 sample most probably corresponds to the pre-transition, since the SAXS data show the presence of the ripple phase down to this temperature on cooling. The absence of this peak in the DSC curve of the 1:1 sample is also consistent with the SAXS data, which shows that the pre-transition temperature increases much faster than the main-transition temperature with increasing decanol concentration. We do not see any indication of the formation of the fluid-fluid coexistence region in the DSC data, which is not surprising since the enthalpy change at such a transition is negligible compared to that at the fluid-gel transition.

We have used three different bilayer morphologies in the present study, namely, GUVs, SLBs and multilayers. It is important to note that fluid-fluid coexistence is found in all of them, in spite of some differences between these morphologies described below. Although GUVs and SLBs are made up of single lipid bilayers, the proximity of the substrate in SLBs is known to lead to differences in the phase behavior[40]. Interactions with the substrate are not relevant in GUVs and multilayers, but they differ in the degree of hydration. GUVs are dispersed in water and hence are fully hydrated. Multilayers are in equilibrium with a water-saturated environment, which usually leads to a slightly lower level of hydration, resulting in small shifts in the transition temperatures from those at full hydration[41], but the phase behavior remains qualitatively the same[42].

In addition to the above, the three bilayer morphologies used here also differ in the way decanol is added to the bilayers. Decanol is introduced into GUVs and SLBs by incubating them in a saturated aqueous solution of decanol, since the DMPC concentration in these samples is extremely small. The solubility limit of decanol in water is 0.24 mM[43] and the partition coefficient of decanol, expressed as a ratio of molar concentration, between a fluid lipid bilayer and water is 3.9×10^{3}[44]. From this, the decanol to lipid molar ratio in the bilayer can be estimated to be about 0.4. This ratio in the samples used for DSC was 0.25 and 1, and in the multilayers used for x-ray studies was 0.25 and 0.5. Thus the concentration of decanol in all the samples probed using different techniques is expected to be comparable. Therefore, it is not clear if the observed differences in the temperature range of L_{α}^{1}-L_{α}^{2} coexistence and in the phase behavior at lower temperatures arise from differences in the decanol content of the different types of samples, or if factors such as interaction with the substrate and levels of hydration also play a role.

As mentioned earlier, computer simulations have shown that long-chain alcohols increase chain order and hence the bilayer thickness in lipids with saturated as well as unsaturated chains[23,24]. This effect is analogous to that of cholesterol, which has been studied extensively[45]. In the case of lipid-cholesterol binary systems fluid-fluid coexistence has been inferred using spectroscopy techniques[11,12]. However, this has not been confirmed with other experimental techniques, such as x-ray scattering or fluorescence microscopy. Recent experiments and computer simulations suggest instead the occurrence of dynamic compositional heterogeneities in these systems[46,47]. Observation of fluid-fluid coexistence in the present system, therefore, points to interesting differences in the interactions within the membrane, which are yet to be elucidated. Further studies are clearly required for a better understanding of the mechanism responsible for this behavior.

4.5 Conclusion

We have established the occurrence of fluid-fluid phase separation in DMPC membranes containing 1-decanol using a variety of experimental techniques. Although earlier studies have shown that incorporation of long-chain alcohols, such as 1-decanol, in lipid bilayers leads to an increase in chain order, the possibility of fluid-fluid coexistence in these systems has not been hitherto envisaged. The mechanism driving the observed phase separation is presently unclear.

Bibliography

[1] Simons K, Ikonen E. Functional rafts in cell membranes. nature. 1997;387(6633):569–572.

[2] Lingwood D, Simons K. Lipid rafts as a membrane-organizing principle. science. 2010;327(5961):46–50.

[3] Simons K, Sampaio J. Cold Spring Harbor Perspect. Biol. 2011;3:a004697.

[4] Sezgin E, Levental I, Mayor S, Eggeling C. The mystery of membrane organization: composition, regulation and roles of lipid rafts. Nature reviews Molecular cell biology. 2017;18(6):361.

[5] Veatch SL, Soubias O, Keller SL, Gawrisch K. Critical fluctuations in domain-forming lipid mixtures. Proceedings of the National Academy of Sciences. 2007;104(45):17650–17655.

[6] Bagatolli L, Kumar PS. Phase behavior of multicomponent membranes: Experimental and computational techniques. Soft Matter. 2009;5(17):3234–3248.

[7] Heberle F, Feigenson G. Cold Spring Harbor Perspect. Biol. 2011;3:a004630.

[8] Heberle FA, Petruzielo RS, Pan J, Drazba P, Kucˇerka N, Standaert RF, et al. Bilayer thickness mismatch controls domain size in model membranes. Journal of the American Chemical Society. 2013;135(18):6853–6859.

[9] Sodt AJ, Sandar ML, Gawrisch K, Pastor RW, Lyman E. The molecular structure of the liquid-ordered phase of lipid bilayers. Journal of the American Chemical Society. 2014;136(2):725–732.

[10] Nickels JD, Cheng X, Mostofian B, Stanley C, Lindner B, Heberle FA, et al. Mechanical properties of nanoscopic lipid domains. Journal of the American Chemical Society. 2015;137(50):15772–15780.

[11] Collado MI, Goñi FM, Alonso A, Marsh D. Domain formation in sphingomyelin/cholesterol mixed membranes studied by spin-label electron spin resonance spectroscopy. Biochemistry. 2005;44(12):4911–4918.

[12] Marsh D. Liquid-ordered phases induced by cholesterol: a compendium of binary phase diagrams. Biochimica et Biophysica Acta (BBA)-Biomembranes. 2010;1798(3):688–699.

[13] Wu SH, McConnell HM. Phase separations in phospholipid membranes. Biochemistry. 1975;14(4):847–854.

[14] Ito T, Ohnishi SI. Ca2+-induced lateral phase separations in phosphatidic acid-phosphatidylcholine membranes. Biochimica et Biophysica Acta (BBA)-Biomembranes. 1974;352(1):29–37.

[15] Lee A. Interactions between anesthetics and lipid mixtures. Normal alcohols. Biochemistry. 1976;15(11):2448–2454.

[16] Pringle MJ, Miller KW. Differential effects on phospholipid phase transitions produced by structurally related long-chain alcohols. Biochemistry. 1979;18(15):3314–3320.

[17] Rowe ES. Lipid chain length and temperature dependence of ethanol-phosphatidylcholine interactions. Biochemistry. 1983;22(14):3299–3305.

[18] Simon S, McIntosh T. Interdigitated hydrocarbon chain packing causes the biphasic transition behavior in lipid/alcohol suspensions. Biochimica et Biophysica Acta (BBA)-Biomembranes. 1984;773(1):169–172.

[19] Kamaya H, Matubayasi N, Ueda I. Biphasic effect of long-chain n-alkanols on the main-phase transition of phospholipid vesicle membranes. The Journal of Physical Chemistry. 1984;88(4):797–800.

[20] Pope J, Dubro D. The interaction of n-alkanes and n-alcohols with lipid bilayer membranes: a 2H-NMR study. Biochimica et Biophysica Acta (BBA)-Biomembranes. 1986;858(2):243–253.

[21] Westerman P, Pope J, Phonphok N, Doane J, Dubro D. The interaction of n-alkanols with lipid bilayer membranes: a 2H-NMR study. Biochimica et Biophysica Acta (BBA)-Biomembranes. 1988;939(1):64–78.

[22] Aagaard TH, Kristensen MN, Westh P. Packing properties of 1-alkanols and alkanes in a phospholipid membrane. Biophysical chemistry. 2006;119(1):61–68.

[23] Griepernau B, Leis S, Schneider MF, Sikor M, Steppich D, Böckmann RA. 1-Alkanols and membranes: a story of attraction. Biochimica Et Biophysica Acta (BBA)-Biomembranes. 2007;1768(11):2899–2913.

[24] Kondela T, Gallová J, Hauß T, Barnoud J, Marrink SJ, Kučerka N. Alcohol interactions with lipid bilayers. Molecules. 2017;22(12):2078.

[25] Kondela T, Gallová J, Hauß T, Ivankov O, Kučerka N, Balgavỳ P. Effect of alkan-1-ols on the structure of dopc model membrane. European Pharmaceutical Journal. 2017;64(2):4–8.

[26] Wack DC, Webb WW. Synchrotron x-ray study of the modulated lamellar phase P β'in the lecithin-water system. Physical Review A. 1989;40(5):2712.

[27] Bhatia T, Husen P, Brewer J, Bagatolli LA, Hansen PL, Ipsen JH, et al. Preparing giant unilamellar vesicles (GUVs) of complex lipid mixtures on demand: Mixing small unilamellar vesicles of compositionally heterogeneous mixtures. Biochimica et Biophysica Acta (BBA)-Biomembranes. 2015;1848(12):3175–3180.

[28] Kang M, Day CA, Kenworthy AK, DiBenedetto E. Simplified equation to extract diffusion coefficients from confocal FRAP data. Traffic. 2012;13(12):1589–1600.

[29] Pabst G, Katsaras J, Raghunathan VA, Rappolt M. Structure and interactions in the anomalous swelling regime of phospholipid bilayers. Langmuir. 2003;19(5):1716–1722.

[30] Zhang R, Suter RM, Nagle JF. Theory of the structure factor of lipid bilayers. Physical Review E. 1994;50(6):5047.

[31] Tamm LK. Lateral diffusion and fluorescence microscope studies on a monoclonal antibody specifically bound to supported phospholipid bilayers. Biochemistry. 1988;27(5):1450–1457.

[32] Scomparin C, Lecuyer S, Ferreira M, Charitat T, Tinland B. Diffusion in supported lipid bilayers: Influence of substrate and preparation technique on the internal dynamics. The European Physical Journal E. 2009;28(2):211–220.

[33] Petrache HI, Tristram-Nagle S, Nagle JF. Fluid phase structure of EPC and DMPC bilayers. Chemistry and physics of lipids. 1998;95(1):83–94.

[34] Yanagisawa M, Imai M, Taniguchi T. Periodic modulation of tubular vesicles induced by phase separation. Physical Review E. 2010;82(5):051928.

[35] Usery RD, Enoki TA, Wickramasinghe SP, Nguyen VP, Ackerman DG, Greathouse DV, et al. Membrane bending moduli of coexisting liquid phases containing transmembrane peptide. Biophysical journal. 2018;114(9):2152–2164.

[36] Hirst LS, Ossowski A, Fraser M, Geng J, Selinger JV, Selinger RL. Morphology transition in lipid vesicles due to in-plane order and topological defects. Proceedings of the National Academy of Sciences. 2013;110(9):3242–3247.

[37] Nagle JF, Tristram-Nagle S. Structure of lipid bilayers. Biochimica et Biophysica Acta (BBA)-Reviews on Biomembranes. 2000;1469(3):159–195.

[38] Rappolt M, Rapp G. Structure of the stable and metastable ripple phase of dipalmitoylphosphatidylcholine. European biophysics journal. 1996;24(6):381–386.

[39] Sun WJ, Suter R, Knewtson M, Worthington C, Tristram-Nagle S, Zhang R, et al. Order and disorder in fully hydrated unoriented bilayers of gel-phase dipalmitoylphosphatidylcholine. Physical Review E. 1994;49(5):4665.

[40] Alessandrini A, Facci P. Phase transitions in supported lipid bilayers studied by AFM. Soft matter. 2014;10(37):7145–7164.

[41] Katsaras J. Adsorbed to a rigid substrate, dimyristoylphosphatidylcholine multibilayers attain full hydration in all mesophases. Biophysical journal. 1998;75(5):2157–2162.

[42] Smith G, Sirota E, Safinya C, Plano R, Clark NA. X-ray structural studies of freely suspended ordered hydrated DMPC multimembrane films. The Journal of chemical physics. 1990;92(7):4519–4529.

[43] Barton AF. Alcohols with Water: Solubility Data Series. Elsevier; 2013.

[44] Franks N, Lieb W. Partitioning of long-chain alcohols into lipid bilayers: implications for mechanisms of general anesthesia. Proceedings of the National Academy of Sciences. 1986;83(14):5116–5120.

[45] Róg T, Pasenkiewicz-Gierula M, Vattulainen I, Karttunen M. Ordering effects of cholesterol and its analogues. Biochimica et Biophysica Acta (BBA)-Biomembranes. 2009;1788(1):97–121.

[46] Armstrong CL, Marquardt D, Dies H, Kučerka N, Yamani Z, Harroun TA, et al. The observation of highly ordered domains in membranes with cholesterol. PLoS One. 2013;8(6):e66162.

[47] Javanainen M, Martinez-Seara H, Vattulainen I. Nanoscale membrane domain formation driven by cholesterol. Scientific reports. 2017;7(1):1–10.

Chapter 5

Tension induced phase separation in an unsaturated lipid membrane containing hydroxycholesterol

5.1 Introduction

Membrane tension plays a crucial role in various cellular processes such as morphogenesis, endocytosis, exocytosis, fission and fusion[1–6]. Understanding the influence of tension on model lipid bilayers is important to elucidate cell membrane response to tension. A few studies exist in the literature with focus on the influence of tension on the phase behavior of lipid bilayers, using ternary raft mixtures[7–11]. These studies show that the boundaries of the fluid-fluid coexistence region are shifted by the tension in the bilayer. In a two-component DPPC: DOPC bilayer, Chen et al.[12] have studied the influence of tension on the fluid-gel phase transition. The main transition temperature is found to decrease on increasing the tension.

Hydroxycholesterols are oxidized derivatives of cholesterol and are known to exhibit cytotoxic and pro-apoptotic activities. They are involved in biological processes such as cholesterol homeostasis and autophagy. They interact with lipid bilayers and alter their physiochemical properties differently compared to cholesterol[13–15]. Kamal and Madhukar observed a fluid-fluid phase coexistence in some of the saturated lipid- hydroxycholesterol systems, namely 1,2-dipalmitoyl -sn-glycero- 3- phosphocholine (DPPC) : 27-hydroxycholesterol, 1,2-dimyristoyl-sn-glycero-3- phosphocholine (DMPC) : 27-hydroxycholesterol, DMPC:25-hydroxycholesterol and 1,2-dilauroyl- sn-glycero-3- phosphocholine (DLPC):25- hydroxycholesterol[16,17]. No such fluid-fluid phase coexistence is observed in the unsaturated lipid and hydroxycholesterol system, namely 1-palmitoyl-2-oleoyl-glycero-3-phosphocholine (POPC) : 27-hydroxycholesterol and POPC : 25- hydroxycholesterol. In this chapter, we report the observation of a novel tension induced fluid-fluid phase coexistence in the POPC:27-hydroxycholesterol system.

In the POPC:27-Hydroxycholesterol system, we also observed illumination induced fluid-fluid phase separation when high light intensities are used for dye excitation. In the literature, some three-component systems, for example, DOPC:sphingomyelin (SM):cholesterol[18,19] and POPC:SM:cholesterol[19], have been shown to exhibit a similar behaviour. In the present study, care was taken to suppress this artifact by reducing the intensity of excitation light.

In this chapter, we report the observation of tension induced fluid-fluid phase coexistence in

two-component POPC:27- hydroxycholesterol giant unilamellar vesicles. Tension was applied either by micropipette aspiration or by creating an osmotic pressure difference between the interior and exterior of the GUV. We have measured the threshold tension needed to induce transition from uniform phase to fluid-fluid phase coexistence by employing the micropipette aspiration technique[20,21].

5.2 Materials

1-palmitoyl-2-oleoyl-glycero-3-phosphocholine (POPC), 1,2-dipalmitoyl -sn- glycero- 3- phosphocholine (DPPC), 1,2-dioleoyl-sn-glycero-3-phosphocholine (DOPC), cholesterol and 27- hydroxycholesterol are purchased from Avanti polar lipids. Rhodamine b 1, 2-dihexadecanoyl-sn-glycero-3-phosphoethanolamine, triethylammonium salt (rhodamine DHPE) and 1,1′- dioctadecyl- 3,3,3′,3′-tetramethyl indo carbocyanine perchlorate (DiI) are obtained from Invitrogen bioservices. 25-hydroxycholesterol and bovine serum albumin (BSA) are obtained from Sigma Aldrich. All chemicals are used as received.

Glass capillaries (model G -1) with 0.6 mm inner diameter and 1 mm outer diameter and capillary holder are obtained from Narishige scientific instruments. Flaming micropipette puller (model P-97) from Sutter instruments is used to pull micropipettes to less than 10 µm inner diameter. Micro-forge (model MF-900) from Narishige is used to cut and fire polish the micropipette opening. VEXTA stepping motor (model PK245-01 AA) is used to adjust water beaker height in steps of 5 µm. The height of the beaker is controlled through computer interfacing. A manual micromanipulator from Leica is employed to position the micropipette. Olympus IX 70 microscope is used for vesicle observations.

5.3 Methods

5.3.1 Vesicle preparation and observation

The procedure followed for vesicle preparation is described in the previous chapter. For room temperature micropipette aspiration experiments, a chamber is made by pasting a silane coated coverslip at the bottom of a circular Teflon spacer and partially covering by another coverslip on the top to allow the micropipette to enter. 50 mM solutions of sucrose and glucose are used as interior and exterior mediums of the vesicles respectively. A typical differential interference contrast image of an aspirated vesicle is shown in figure 5.1.

5.3.2 Micro-pipette aspiration experiment

The Micro-pipette aspiration technique was developed by Mitchison and Swann[22] for studying the response of sea urchin egg to suction pressure. In a pioneering work by Evans and Needham[20,23,24] this technique was used to measure the bending rigidity, area expansion modulus, lysis tension and permeability to water of lipid bilayer[25,26]. Later several groups used this as a tool to control tension in GUVs[11,12,27]. By combining this technique with optical tweezers nanotube pulling experiments are conducted[28,29].

The experimental setup consists of a water column placed on a height adjustable stage, a micro pipette inserted into pipette holder which is fixed to a micro manipulator, and a semi flexible tube to connect the water reservoir to the pipette as shown in figure 5.2. The principle of the technique is simple. By varying the relative height between the reservoir and the micropipette tip, the suction pressure at the micro pipette tip is controlled. When the reservoir is at lower (higher) height than the tip, water flows in (flows out). Along with the water, the GUV also tries to enter the pipette and makes a seal at the tip as shown in figure 5.1. By varying the suction pressure, we can control the tension (σ) in the vesicle and correspondingly the protrusion length inside the pipette changes.

The glass capillaries are pulled to reduce the diameter gradually from millimetre to micron size. The shape profile of pipette tip is controlled by varying the pulling parameters. By using the micro-forge, we cut the pipette tip at a typical inner radius of 5-10 µm. A smooth edge at the pipette tip is obtained by fire polishing using a micro forge. In our setup, the micro pipette enters the observation chamber at an angle. To have most of the pipette tip in focus, we bend the pipette at an angle between 30°- 45°a few millimeters away from the tip by heating with a micro-forge. Just before conducting the experiment, we treat the pipette with a 2 mg/ml BSA solution to avoid vesicle sticking to the inner surface of the pipette. The treatment is done by aspirating the protein solution into the capillary and then discharging it after a few minutes. The unbound protein is removed by aspirating and ejecting water a few times. The pipette is filled with a 50mM glucose solution from the back side with the help of a thin needle attached to a syringe. We follow the procedure described by Henriksen et al.[21] and Heinrich et al.[30].

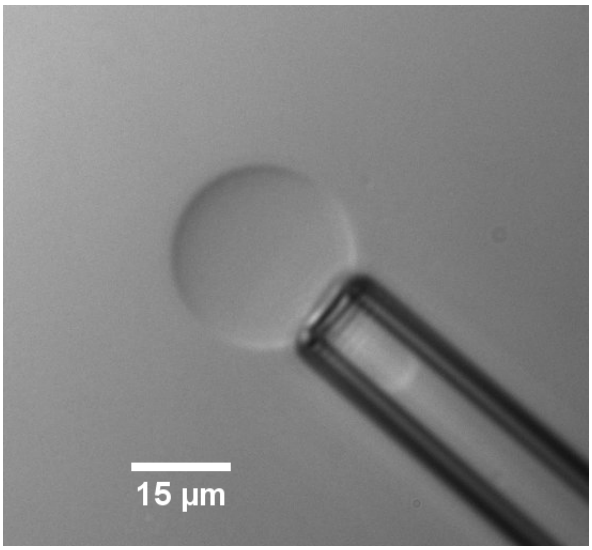

FIGURE 5.1: A typical differential interference contrast (DIC) image of SOPC vesicle. 50 mM sucrose and glucose solutions are used as interior and exterior media respectively, for vesicles.

The tension (σ) in the membrane is calculated from the applied hydrostatic pressure difference (Δp) by using the following Laplace's equation[20,23,25].

$$\sigma = \frac{\Delta p R_1}{2(1 - \frac{R_1}{R_2})} \tag{5.1}$$

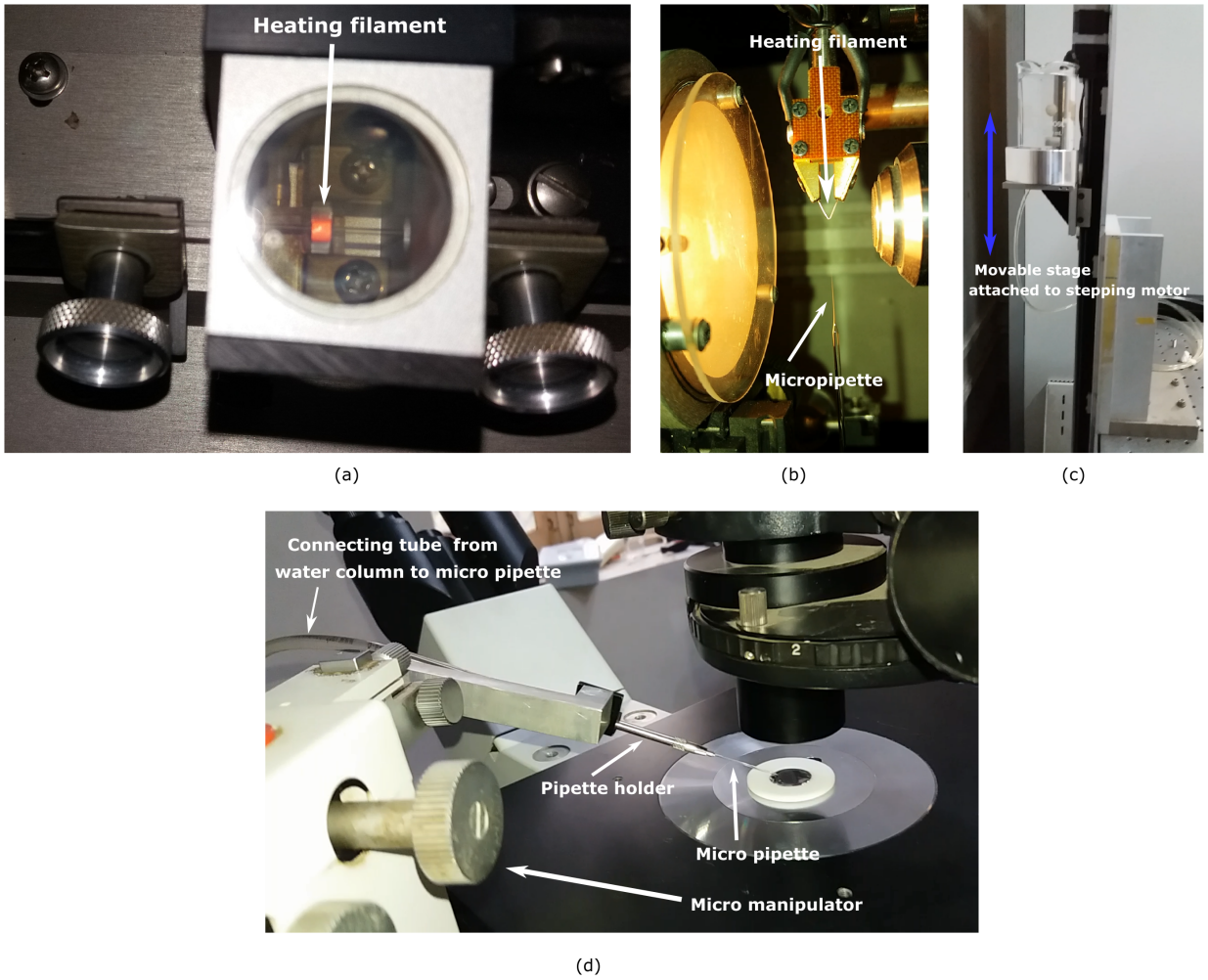

FIGURE 5.2: a) Micro pipette puller b) Micro-forge c) Water column on 1-D movable stage d) Typical experimental set up for micro pipette aspiration.

$$\Delta p = \Delta h \rho g$$

where Δh is the height difference between the reference position of water column, at which no flow occurs at the pipette tip to the current position , ρ is the water density =997 kg/m^3, g is the acceleration due to gravity = 9.8 m/s^2. R_1 and R_2 are pipette inner radius and vesicle radius respectively.

5.4 Results

5.4.1 Illumination induced fluid-fluid phase coexistence

POPC:27- hydroxycholesterol: rhodamine-DHPE (79.5:20:0.5 molar ratio) vesicles, under continuous illumination with high-intensity light, showed a transition from a uniformly bright phase to a coexistence of bright and dark domains as shown in figure 5.3. These dark domains showed diffusion and coalescence, which confirms that both dark and bright domains are in a fluid phase. If low-intensity light is used, dark domains appeared at much later times. This illumination induced phase separation is irreversible once it appears. Even if the illumination is stopped for 10 minutes, vesicles did not revert back to a uniform phase. During this phase transition, we have

not observed any change in undulations and shape of the vesicle, which are sensitive to the tension in the membrane. This observation clearly distinguishes tension induced phase separation discussed in the following sections from illumination induced phase separation. The intensity of light is lowered by using objectives with lower magnification. As the magnification increases, the light gets focused to a smaller beam waist at the focus. So higher light intensities at focus are obtained by using objectives in the order 40X, 60X, and 100X. If a 100X objective is used for illuminating vesicles, domains appeared within seconds. When we use a 60X objective, it took a few minutes for the domains to appear. In the case of a 40X objective, no domains appeared even until the bleaching of the dye.

We have observed this phase transition with two different dyes, namely rhodamine DHPE and DiI. The system POPC:27- hydroxycholesterol: rhodamine DHPE (79.5:20:0.5 molar ratio) showed fluid-fluid coexistence very quickly in around 10 seconds under illumination with a 100X objective. The POPC:27-hydroxysterol: DiI (79.5:20:0.5 molar ratio) showed domains in a few minutes under the same conditions. When 60X and 40X objectives are used to observe POPC:27-hydroxysterol: DiI vesicles, the illumination induced phase transition is not observed. So, for the rest of the experiments, to avoid the illumination induced phase transition, we have used DiI for staining the membrane and low-intensity light for dye excitation.

We have not observed illumination induced phase transition in POPC: 25-hydroxycholesterol: rhodamine-DHPE (79.5:20:0.5 molar ratio) vesicles.

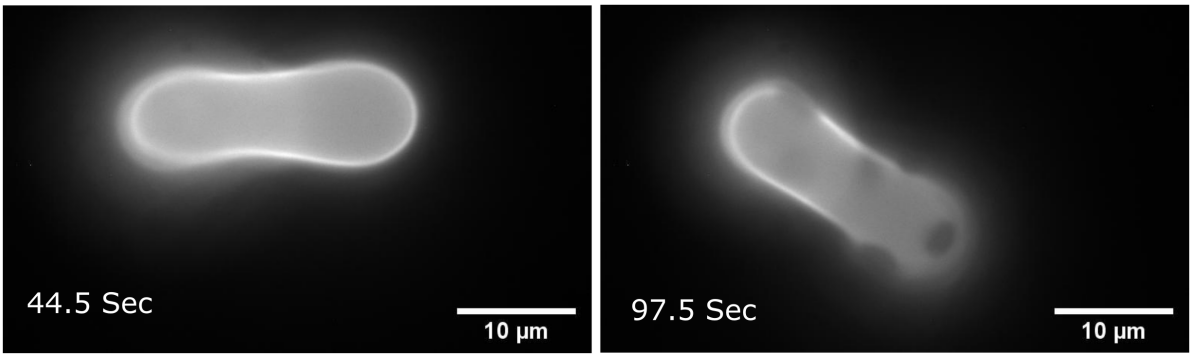

FIGURE 5.3: POPC:27-hydroxysterol: rhodamine DHPE (79.5:20:0.5 molar ratio) vesicle showing an irreversible transition from a uniform phase to a fluid-fluid coexistence under illumination with a 100X objective. For the corresponding video, please click here

5.4.2 Osmotic pressure induced fluid-fluid coexistence

Vesicles of POPC:27- hydroxysterol:DiI in 79.5:20:0.5 molar ratio, under osmotic pressure, showed a transition from a uniform phase to a fluid-fluid coexistence region. The vesicles are prepared in 50 mM sucrose solution and then transferred to water at room temperature. In time, an oscillatory phase behaviour is observed as shown in figure 5.4. The dark domains showed diffusion and coalescence as shown in figure 5.5 which confirms that both dark and bright phases are in liquid phase. During a cycle from uniform phase to fluid-fluid coexistence and back to uniform phase, it is observed that the vesicle spends more time in the fluid-fluid coexistence state compared to the uniform phase.

This osmotic pressure induced phase transition is observed over a temperature range from 12 °C to 42 °C. We could not extend the temperature range due to experimental limitations.

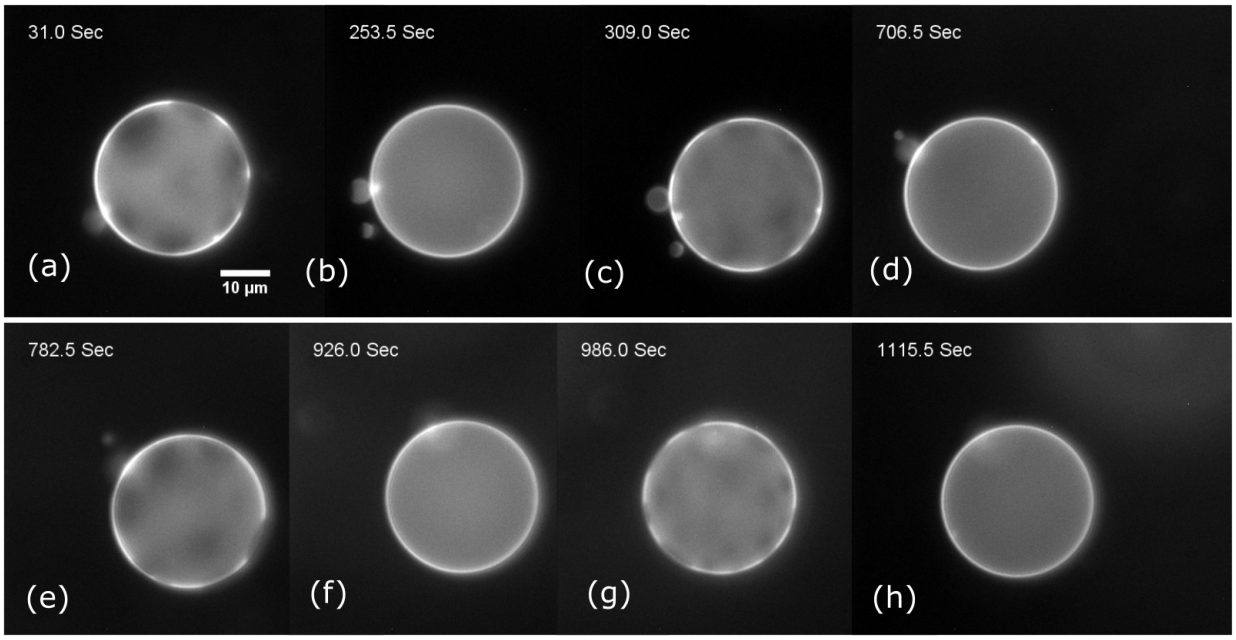

FIGURE 5.4: A POPC:27-hydroxysterol:DiI (79.5:20:0.5 molar ratio) vesicle showing an oscillatory behavior of tension-induced phase transition under a hypotonic environment from a uniform phase to fluid-fluid coexistence at 27 ± 2 °C. The vesicles are prepared in a 50 mM sucrose solution and then dropped in water. The magnification is the same for all the images. For the corresponding video, please click here

5.4.3 Tension induced fluid-fluid coexistence

By employing the micropipette aspiration technique, influence of tension on phase transition of POPC:27-hydroxysterol:DiI (79.5:20:0.5 molar ratio) vesicles was studied. Under tension, vesicles showed a reversible phase transition from uniform phase to fluid-fluid coexistence as shown in figure 5.6. As suction pressure is increased, the length of protrusion inside the pipette is also increases. The tension in the membrane is calculated from the suction pressure by using equation 5.1. As tension is increased above a threshold, dark domains appeared. Coalescence of dark domains is observed. As we lower the suction pressure, a phase transition from fluid-fluid coexistence to uniform phase is observed. It confirms that the observed phase transition is purely a tension induced phenomena.

The threshold tension needed to induce the phase transition for 39 vesicles is represented in figure 5.7 as a histogram. The threshold tension is found to be in the range of 1.5-7.5 ± 0.2 mN/m. Response of a lipid bilayer in the fluid phase consists of two regimes; undulation dominated regime for $\sigma < 0.5$ mN/m and area expansion regime for $\sigma > 0.5$ mN/m[20,23,25]. In the undulation dominated regime, as tension increases, the amplitudes of the undulations reduce, and the hidden area in undulations becomes visible as increased length of the protrusion. On further increasing the tension, lipid bilayer area directly expands, and its thickness reduces[31]. The obtained threshold tension needed to induce phase separation is in the area expansion regime.

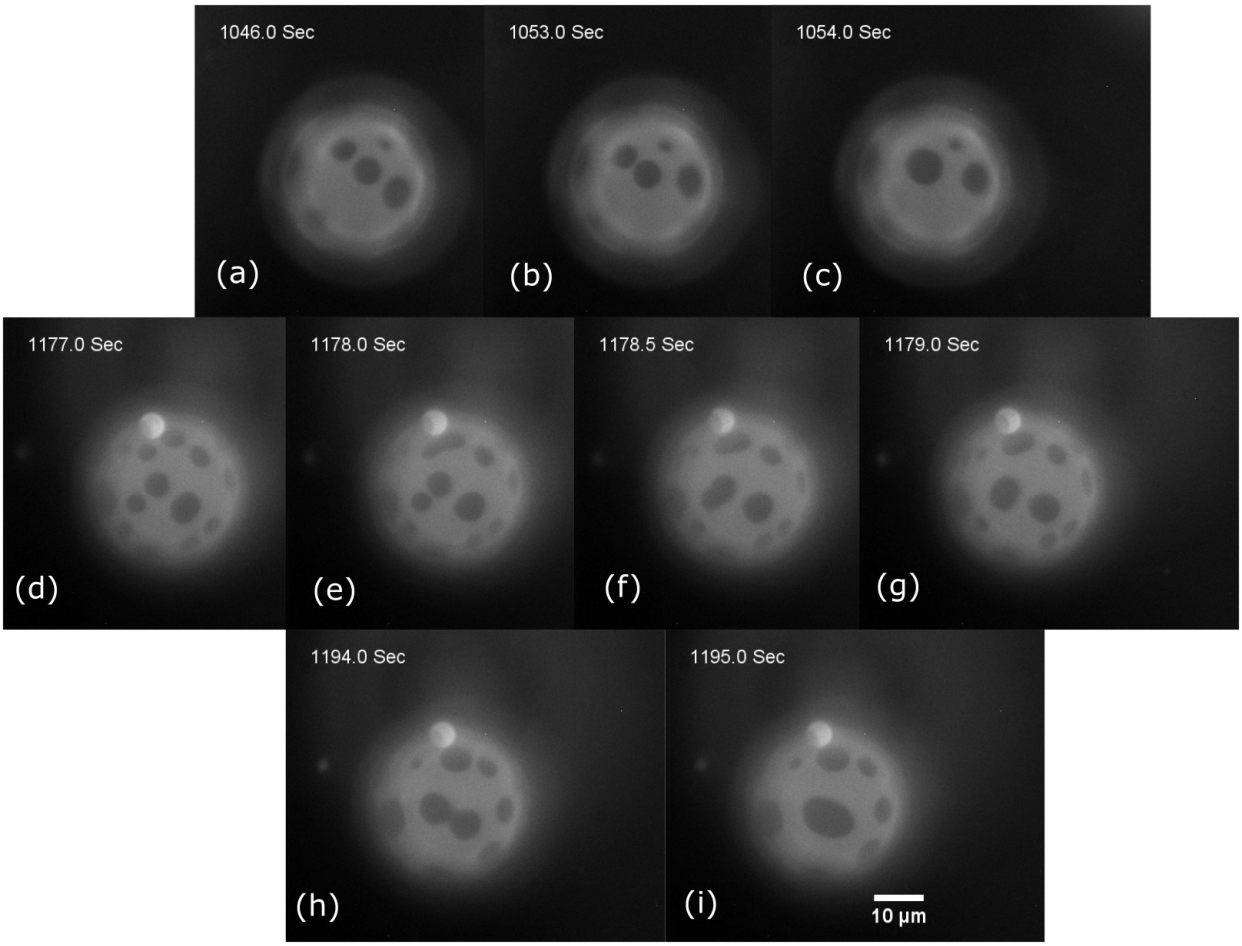

FIGURE 5.5: In the osmotic pressure induced fluid-fluid coexistence, domain diffusion and coalescence is observed. Figures (a,b,c), (d,e,f,g,h,i) correspond to two different domain merging events on the same vesicle. The scale bar is the same for all the images. These images and the images in 5.4 are part of the same video.

We have not found any correlation between the vesicle diameter and the threshold tension as shown in figure 5.8.

We have not observed any phase transition under osmotic stress in DOPC:27 -hydroxysterol: DiI (79.5:20:0.5 molar ratio), POPC: cholesterol: DiI (79.5:20:0.5 molar ratio) and POPC: 25-hydroxy sterol: rhodamine DHPE (79.5:20:0.5 molar ratio) systems. In micro pipette aspiration experiment, at high tension, no phase transition is observed in POPC: 25- hydroxysterol: rhodamine DHPE (79.5:20:0.5 molar ratio) vesicles. Under illumination with high intensity light, no dark domains are observed in POPC: 25-hydroxysterol: rhodamine DHPE (79.5:20:0.5 molar ratio) vesicles.

5.5 Discussion

We have observed a phase transition from uniform fluid phase to fluid-fluid coexistence in three different conditions, namely under illumination, under osmotic pressure and upon application of tension in giant unilamellar vesicles of POPC:27-hydroxysterol:dye system at 79.5:20:0.5 molar ratio.

In the literature, illumination induced fluid-fluid coexistence is reported in POPC:SM: cholesterol and DOPC:SM: cholesterol and a few more systems[18,19]. Zhao et al.[19] proposed that this

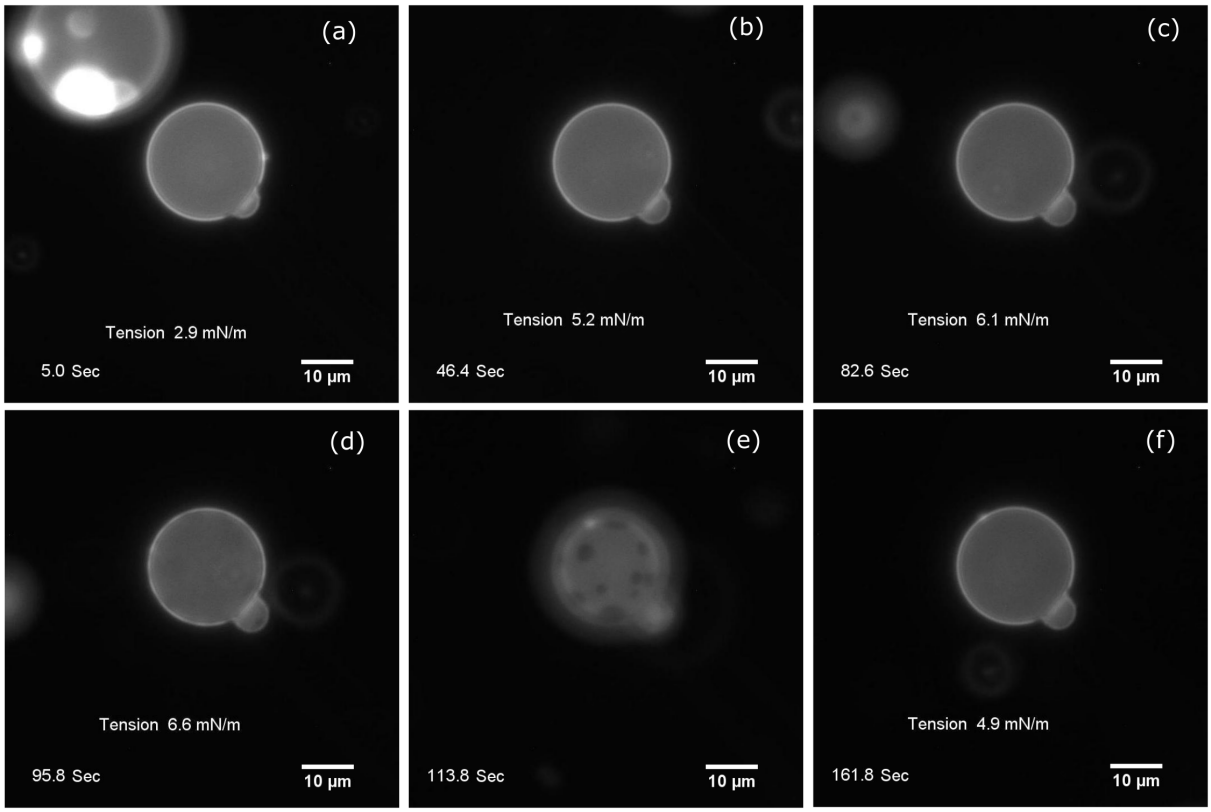

FIGURE 5.6: Fluorescence microscopy images of an aspirated POPC:27-hydroxysterol:DiI (79.5:20:0.5 molar ratio) GUV at lower tension exhibiting a uniform phase (a,b,c) and at higher tension exhibiting dark domains indicating two-phase coexistence (d,e). In image (e) top part of the vesicle is focused at same tension as in (d). The dark domains are found to diffuse and coalesce, confirming that both phases are in the fluid state. This phase transition is found to be reversible with tension, as shown in figure (f). The vesicle radius is 11.7 µm and the pipette radius is 3.4 µm. For the corresponding video, please click here

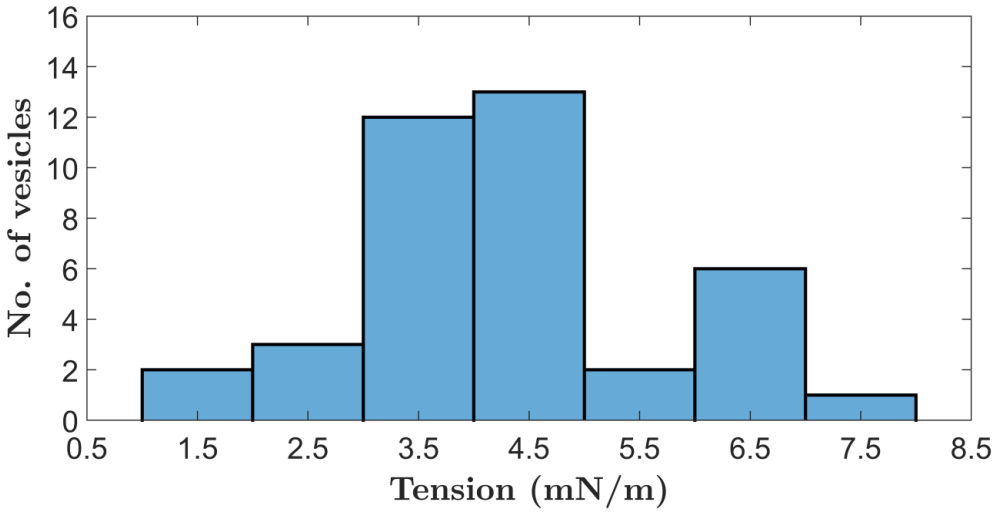

FIGURE 5.7: Histogram of the threshold tension in the membrane required to induce fluid-fluid coexistence in POPC:27- hydroxysterol:DiI vesicles. A total of 39 vesicles were considered to obtain this plot.

phase separation is induced by chemicals produced in the dye excitation process, and it is neither

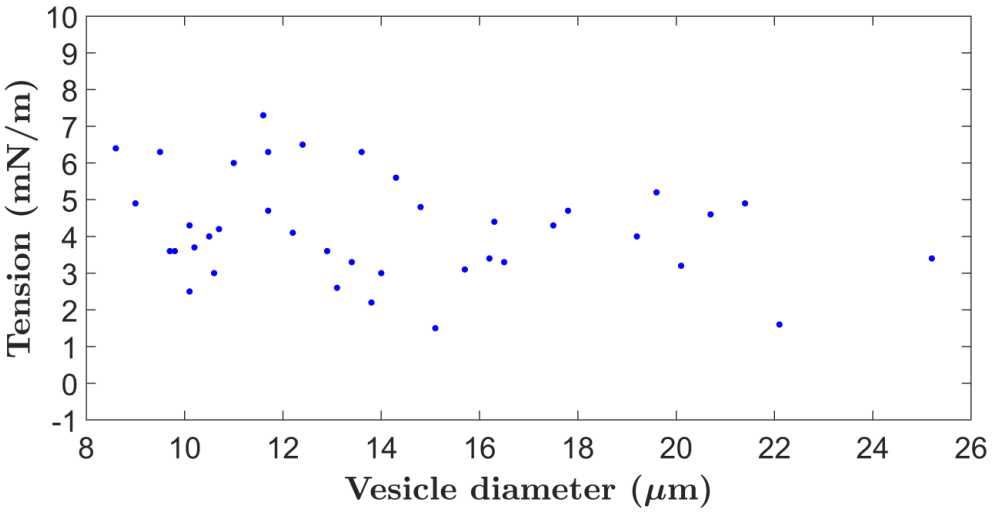

FIGURE 5.8: Vesicle diameter vs threshold tension needed to induce fluid-fluid coexistence. No correlation is found between them.

dependent on the vesicle preparation method nor temperature. Bouvrais et al.[32] observed an illumination induced phase transition in POPC membranes containing Rh-DPPE. They hypothesized that this originated from oxygen radical formation due to non-radiative de-excitation of the dye, which is inversely proportional to the quantum yield of the dye. To our knowledge, there have not been any systematic studies in the literature on elucidating this phenomenon. Our present observations are very similar to those of Ayuyan et al.[18], and Zhao et al.[19].

We have decoupled the light-induced and the osmotic pressure or the tension induced phase separation by reducing the intensity of light and using a suitable dye. Under osmotic stress, a phase transition from fluid phase to fluid-fluid coexistence occurring in an oscillatory manner is observed. Similar observations have been reported by Ayuyan et al.[10] and Oglecka et al.[9] in a three-component POPC:SM: cholesterol system. They have given the following explanation for the oscillatory phase behaviour. In a hypotonic environment, water permeates into the vesicle. As a result, volume of the vesicle and membrane tension increases. Above a threshold tension, a membrane pore forms and some amount of fluid gets ejected through it. As a result, volume of the vesicle and the membrane tension reduce and the pore gets sealed. Although the osmotic pressure inside the vesicle decreases, it is still higher than that in the outside solution. Hence this process repeats until isotonic conditions are reached. The whole process in a step by step manner was observed by Oglecka et al.[9]. During the above processes, similar to our observations, a phase transition cycle from uniform phase to fluid-fluid coexistence is also observed, and it is attributed to a combined effect of tension in the membrane and the osmotic pressure.

With the micropipette aspiration technique, we could vary the tension in a controlled manner without osmotic pressure. A tension induced reversible phase transition from fluid phase to fluid-fluid phase coexistence is observed. To our knowledge, this is the first observation of such a phase behaviour in a two-component membrane.

We attribute the spread in measured threshold tension between 1.5-7.5 ± 0.2 mN/m to variations of hydroxysterol concentration from vesicle to vesicle, but further studies are required to confirm this hypothesis.

Bibliography

[1] Raucher D, Sheetz MP. Cell spreading and lamellipodial extension rate is regulated by membrane tension. J Cell Biol. 2000;148(1):127–136.

[2] Houk AR, Jilkine A, Mejean CO, Boltyanskiy R, Dufresne ER, Angenent SB, et al. Membrane tension maintains cell polarity by confining signals to the leading edge during neutrophil migration. Cell. 2012;148(1-2):175–188.

[3] Apodaca G. Modulation of membrane traffic by mechanical stimuli. Am J Physiol Renal Physiol. 2002;282(2):F179–F190.

[4] Rossy J, Laufer JM, Legler DF. Role of mechanotransduction and tension in T cell function. Front Immunol. 2018;9:2638.

[5] Diz-Muñoz A, Fletcher DA, Weiner OD. Use the force: membrane tension as an organizer of cell shape and motility. Trends Cell Biol. 2013;23(2):47–53.

[6] Sitarska E, Diz-Muñoz A. Pay attention to membrane tension: Mechanobiology of the cell surface. Curr Opin Cell Biol. 2020;66:11–18.

[7] Hamada T, Kishimoto Y, Nagasaki T, Takagi M. Lateral phase separation in tense membranes. Soft Matter. 2011;7(19):9061–9068.

[8] Wongsirojkul N, Shimokawa N, Opaprakasit P, Takagi M, Hamada T. Osmotic-Tension-Induced Membrane Lateral Organization. Langmuir. 2020;36(11):2937–2945.

[9] Oglęcka K, Rangamani P, Liedberg B, Kraut RS, Parikh AN. Oscillatory phase separation in giant lipid vesicles induced by transmembrane osmotic differentials. elife. 2014;3:e03695.

[10] Ayuyan AG, Cohen FS. Raft composition at physiological temperature and pH in the absence of detergents. Biophysical journal. 2008;94(7):2654–2666.

[11] Portet T, Gordon SE, Keller SL. Increasing membrane tension decreases miscibility temperatures; an experimental demonstration via micropipette aspiration. Biophysical journal. 2012;103(8):L35–L37.

[12] Chen D, Santore MM. Large effect of membrane tension on the fluid–solid phase transitions of two-component phosphatidylcholine vesicles. Proceedings of the national academy of sciences. 2014;111(1):179–184.

[13] Olkkonen VM, Béaslas O, Nissilä E. Oxysterols and their cellular effectors. Biomolecules. 2012;2(1):76–103.

[14] Luu W, Sharpe LJ, Capell-Hattam I, Gelissen IC, Brown AJ. Oxysterols: old tale, new twists. Annu Rev Pharmacol Toxicol. 2016;56:447–467.

[15] Griffiths WJ, Wang Y. Oxysterol research: a brief review. Biochem Soc Trans. 2019;47(2):517–526.

[16] Arif Kamal M. Influence of some membrane active biomolecules on the phase behavior of model lipid membranes,PhD thesis, Jawaharlal Nehru University; 2012.

[17] Madhukar S. Influence of some sterols and nucleotides on the structure of self-assembled amphiphilic systems,PhD thesis, Jawaharlal Nehru University, New Delhi; 2019.

[18] Ayuyan AG, Cohen FS. Lipid peroxides promote large rafts: effects of excitation of probes in fluorescence microscopy and electrochemical reactions during vesicle formation. Biophysical journal. 2006;91(6):2172–2183.

[19] Zhao J, Wu J, Shao H, Kong F, Jain N, Hunt G, et al. Phase studies of model biomembranes: macroscopic coexistence of Lα+ Lβ, with light-induced coexistence of Lα+ Lo phases. Biochimica et Biophysica Acta (BBA)-Biomembranes. 2007;1768(11):2777–2786.

[20] Evans E, Rawicz W. Entropy-driven tension and bending elasticity in condensed-fluid membranes. Phys Rev Lett. 1990;64(17):2094.

[21] Henriksen JR, Ipsen JH. Measurement of membrane elasticity by micro-pipette aspiration. Eur Phys J E Soft Matter. 2004;14(2):149–167.

[22] Mitchison J, Swann M. The mechanical properties of the cell surface. J exp Biol. 1954;31(3):443–460.

[23] Evans E, Needham D. Physical properties of surfactant bilayer membranes: thermal transitions, elasticity, rigidity, cohesion and colloidal interactions. The Journal of Physical Chemistry. 1987;91(16):4219–4228. Available from: https://doi.org/10.1021/j100300a003.

[24] Rawicz W, Olbrich KC, McIntosh T, Needham D, Evans E. Effect of chain length and unsaturation on elasticity of lipid bilayers. Biophysical journal. 2000;79(1):328–339.

[25] Evans E, Rawicz W. Elasticity of "Fuzzy" Biomembranes. Phys Rev Lett. 1997 Sep;79:2379–2382. Available from: https://link.aps.org/doi/10.1103/PhysRevLett.79.2379.

[26] Olbrich K, Rawicz W, Needham D, Evans E. Water Permeability and Mechanical Strength of Polyunsaturated Lipid Bilayers. Biophysical Journal. 2000;79(1):321–327. Available from: https://www.sciencedirect.com/science/article/pii/S0006349500762941.

[27] Tian A, Johnson C, Wang W, Baumgart T. Line Tension at Fluid Membrane Domain Boundaries Measured by Micropipette Aspiration. Phys Rev Lett. 2007 May;98:208102. Available from: https://link.aps.org/doi/10.1103/PhysRevLett.98.208102.

[28] Sorre B, Callan-Jones A, Manneville JB, Nassoy P, Joanny JF, Prost J, et al. Curvature-driven lipid sorting needs proximity to a demixing point and is aided by proteins. Proceedings of the National Academy of Sciences. 2009;106(14):5622–5626. Available from: https://www.pnas.org/content/106/14/5622.

[29] Sorre B, Callan-Jones A, Manzi J, Goud B, Prost J, Bassereau P, et al. Nature of curvature coupling of amphiphysin with membranes depends on its bound density. Proceedings of the National Academy of Sciences. 2012;109(1):173–178. Available from: https://www.pnas.org/content/109/1/173.

[30] Heinrich V, Rawicz W. Automated, high-resolution micropipet aspiration reveals new insight into the physical properties of fluid membranes. Langmuir. 2005;21(5):1962–1971.

[31] Reddy AS, Warshaviak DT, Chachisvilis M. Effect of membrane tension on the physical properties of DOPC lipid bilayer membrane. Biochimica et Biophysica Acta (BBA)-Biomembranes. 2012;1818(9):2271–2281.

[32] Bouvrais H, Pott T, Bagatolli LA, Ipsen JH, Méléard P. Impact of membrane-anchored fluorescent probes on the mechanical properties of lipid bilayers. Biochimica et Biophysica Acta (BBA)-Biomembranes. 2010;1798:1333–1337.

Chapter 6

Conclusions

This thesis deals with studies on mechanical properties, phase transitions, and structure of lipid bilayers in the presence of shorter and longer chain alcohols and oxysterol. These systems are probed with a variety of experimental techniques, such as vesicle fluctuation analysis, small-angle x-ray scattering (SAXS), fluorescence and phase-contrast microscopy, fluorescence recovery after photobleaching (FRAP), differential scanning calorimetry (DSC) and micropipette aspiration. Various membrane morphologies are used in these studies, namely, multilamellar vesicles (MLV), small unilamellar vesicles (SUV), giant unilamellar vesicles (GUV), supported bilayers, and aligned bilayer stacks.

Chapter 2 discusses the implementation of vesicle fluctuation analysis (VFA) technique. Experimental parameters and protocols are optimized for obtaining bending rigidity (κ) and tension (σ) of the membrane. The effects of various experimental parameters such as magnification, camera exposure time on the spectrum are studied.

In chapter 3, the effect of shorter and longer chain alcohols, namely, ethanol, pentanol, hexanol, octanol, decanol and dodecanol, on the bending rigidity and thickness (d_{HH}) of DMPC bilayers in the fluid phase, is discussed. A change in the influence of alcohols on the membrane is observed between octanol and decanol. Alcohols from ethanol to octanol reduce the main phase transition temperature (T_m), bending rigidity and thickness of the bilayer. Both decanol and dodecanol increase T_m and show no influence on κ and d_{HH}. In the literature, it is shown that short-chain alcohols reduce the packing density of lipids which results in thinning of the lipid bilayer. On the other hand, long-chain alcohols enhance the packing density of lipids which results in the thickening of the membrane. Our observations are in good agreement with the literature.

The influence of 1-decanol on the phase behaviour of DMPC bilayers is discussed in chapter 4. The DMPC-decanol system shows a transition from a uniform fluid phase to a gel phase on cooling, with a narrow fluid-fluid coexistence region in between. The occurrence of fluid-fluid coexistence is confirmed using various membrane platforms such as giant unilamellar vesicles (GUVs), supported lipid bilayers (SLBs) and aligned bilayer stacks. It is observed that decanol rich fluid phase is thicker and less diffusive than the decanol poor fluid phase. More experimental and simulation studies are needed to understand the differences between the two fluid phases, the influence of concentration of decanol on these phases, the influence of alcohol chain length and lipid chain length on fluid-fluid coexistence.

Chapter 5 discusses the observation of a novel tension-induced fluid-fluid phase coexistence. We find that fluid-fluid coexistence can be induced in a reversible manner in an unsaturated POPC

lipid bilayer containing 27-hydroxycholesterol on applying tension. A similar transition is observed by applying tension in vesicles by changing the osmolarity of the solution. Further systematic studies are necessary to understand the mechanisms responsible for the observed phase behaviour.

There is much interest in the literature on fluid-fluid phase coexistence or raft domains in model membranes due to their role in the functioning of cell membranes. Fluid-fluid phase coexistence is observed in 3 component systems with two lipids and cholesterol. In these 3 component raft mixtures, cholesterol is not inducing rafts but converting fluid - gel phase coexistence to fluid-fluid phase coexistence. Even after innumerable studies there is lack of understanding on what type of systems show fluid-fluid phase coexistence and the interactions involved in stabilizing the phase coexistence.

In this thesis, we have reported observation of temperature and membrane tension induced fluid-fluid phase coexistence in PC lipid + alcohol, and PC lipid + hydroxycholesterol binary component membrane systems. These observations should motivate further studies on binary component systems by choosing molecules with diverse structures. Since both alcohol and hydroxycholesterol are less correlated in structure, the interactions involved in stabilizing fluid-fluid phase coexistence may come from different origins. Some of those interactions may be pertinent in understanding proposed raft domains in cell membranes.